AD-A131 852 MECHANICAL BEHAVIOR OF SEA ICE(U) COLD REGIONS RESEARCH   1/2
             AND ENGINEERING LAB HANOVER NH M MELLOR JUN 83
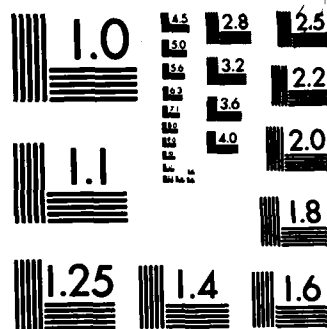UNCLASSIFIED CRREL-MONO-83-1

                                              F/G 8/12   NL

CRREL
MONOGRAPH 83-1

Mechanical behavior of sea ice

US Army Corps
of Engineers
Cold Regions Research &
Engineering Laboratory

For conversion of SI metric units to U.S./British customary units of measurement consult ASTM Standard E380, Metric Practice Guide, published by the American Society for Testing and Materials, 1916 Race St., Philadelphia, Pa. 19103.
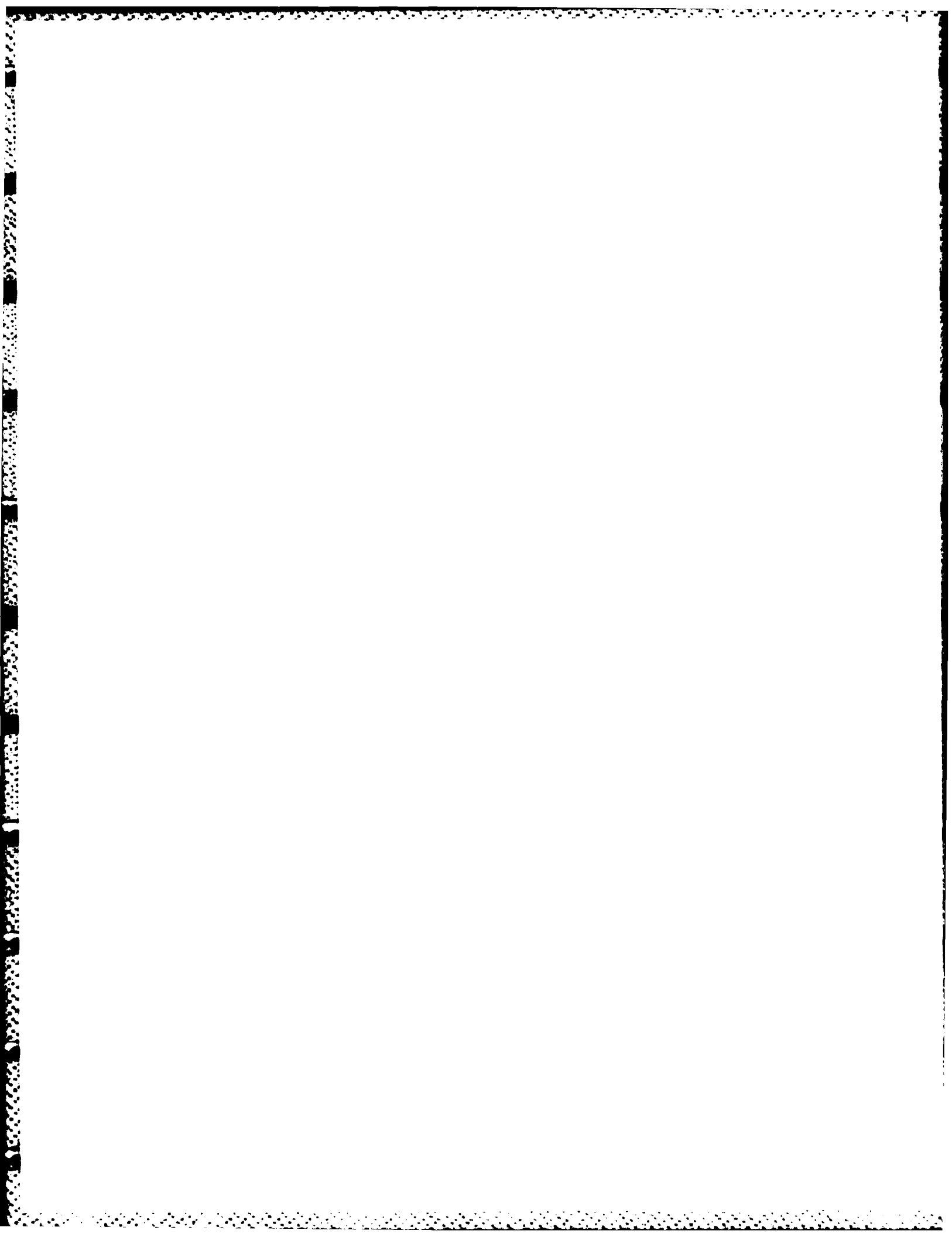
Monograph 83-1

June 1983

Mechanical behavior of sea ice

Malcolm Mellor

REPORT DOCUMENTATION PAGE		READ INSTRUCTIONS BEFORE COMPLETING FORM
1. REPORT NUMBER Monograph 83-1	**2. GOVT ACCESSION NO.** AD-A131 852	**3. RECIPIENT'S CATALOG NUMBER**
4. TITLE (and Subtitle) MECHANICAL BEHAVIOR OF SEA ICE		**5. TYPE OF REPORT & PERIOD COVERED**
		6. PERFORMING ORG. REPORT NUMBER
7. AUTHOR(s) Malcolm Mellor		**8. CONTRACT OR GRANT NUMBER(s)**
9. PERFORMING ORGANIZATION NAME AND ADDRESS U.S. Army Cold Regions Research and Engineering Laboratory Hanover, New Hampshire 03755		**10. PROGRAM ELEMENT, PROJECT, TASK AREA & WORK UNIT NUMBERS**
11. CONTROLLING OFFICE NAME AND ADDRESS U.S. Army Cold Regions Research and Engineering Laboratory Hanover, New Hampshire 03755		**12. REPORT DATE** June 1983
		13. NUMBER OF PAGES 102
14. MONITORING AGENCY NAME & ADDRESS(if different from Controlling Office)		**15. SECURITY CLASS. (of this report)** Unclassified
		15a. DECLASSIFICATION/DOWNGRADING SCHEDULE

16. DISTRIBUTION STATEMENT (of this Report)

Approved for public release; distribution unlimited.

17. DISTRIBUTION STATEMENT (of the abstract entered in Block 20, if different from Report)

18. SUPPLEMENTARY NOTES

19. KEY WORDS (Continue on reverse side if necessary and identify by block number)

Elastic properties	Sea ice
Fracture (mechanics)	Strain (mechanics)
Ice	Strength (mechanics)
Mechanical properties	Stresses
Rheology	

20. ABSTRACT (Continue on reverse side if necessary and identify by block number)

The first part of the report provides an introduction to the mechanics of deformable solids, covering the basic ideas of stress and strain, rheology, equilibrium equations, strain/displacement relations, constitutive equations, and failure criteria. Fracture mechanics and fracture toughness are also reviewed briefly. The second part of the report summarizes available data on the mechanical properties of freshwater ice and saline ice, accounting for the influences of strain rate and loading rate, temperature, porosity, salinity, and grain size. Boundary value problems are not dealt with, but there is

DD FORM 1473 EDITION OF 1 NOV 65 IS OBSOLETE

20. Abstract (cont'd)

discussion of some miscellaneous topics, including thermal strains, behavior
of brash ice, and pressure ridges. The report was written as a study text for
a NATO Advanced Study Institute on Sea/Ice/Air Interactions, and was intended
to be used in conjunction with companion texts on related topics.

PREFACE

This Monograph was prepared as a study text and reference source for a NATO Advanced Study Institute by Dr. Malcolm Mellor, Research Physical Scientist, Experimental Engineering Division, U.S. Army Cold Regions Research and Engineering Laboratory.

The report was technically reviewed by Dr. Gordon F.N. Cox of CRREL and by two anonymous referees.

This report was written during the summer of 1981, and since that time several significant pieces of research have been published or completed. The review does not cover all results which appeared after the end of 1981.

CONTENTS

ILLUSTRATIONS

MECHANICAL BEHAVIOR OF SEA ICE

Malcolm Mellor

INTRODUCTION

This review deals with properties of sea ice that are relevant to
mechanical behavior on a fairly small scale. The main concern is with
polycrystalline ice that is more or less intact. This sets the lower lim:
of scale not far below 0.1 m, and the upper limit around 10 m. However,
the discussion is extended to cover the behavior of fragmented ice over
broader areas. The latter discussion is intended to bridge the gap between
this review, which relates to small-scale natural processes and engineering
problems, and companion reviews, which deal with the mechanics of sea ice
over very large areas.

Part I is a selective summary of the basic theory which is applicable
to ice mechanics. This theory defines the various mechanical properties
that have to be measured, and it provides a framework for the solution of
practical (boundary value) problems. Since ice displays a wide range of
behavioral characteristics, from elasticity and brittle fracture to ductil-
ity and plastic yielding, it is important to have a good appreciation for
the various theories that might apply in different ranges of behavior.

Part II summarizes measured values for common mechanical properties.
Most of the data are derived from field tests or laboratory tests on fairly
small specimens (minimum linear dimension typically < 0.1 m for lab speci-
mens, or < 2 m for in-situ field tests). The summary is selective, and it
does not include some older data which are judged to be erroneous or mis-
leading. A great deal of the information refers to ice that is non-saline,
and this calls for a word of explanation.

By convention, the term "sea ice" covers all types of ice formed by
direct freezing of seawater, but it does not cover icebergs (i.e. glacier
ice), or freshwater ice flushed into the sea by rivers. First-year sea ice
is a very complicated substance — an anisotropic crystalline solid con-
taining bubbles of air, pockets and films of brine, and sometimes solid
salts. However, not all sea ice is significantly saline, or even aniso-
tropic. Multi-year ice, which is of great concern in ice navigation and
offshore structural engineering, may be of very low salinity and without
significant anisotropy where large masses are concerned. It is therefore
useful to regard sea ice not as a unique and exotic material, but simply as
a variant of freshwater ice. The complications introduced by salinity and

structure are important, but not to the extent that sea ice need be regarded as something wholly different from freshwater ice. In Part II of this review, the mechanical properties of sea ice are discussed in relation to the properties of freshwater ice. This is largely a matter of practicality, since non-saline has been studied in more detail than sea ice. However, there is another justification, in that the effects of salinity have to be referred to a zero salinity state, the effects of porosity have to refer to a zero porosity datum, and anisotropy has to be compared with isotropy.

Part III discusses the mechanical behavior of ice that has been fragmented, either by natural processes or by human activities. The discussion covers brash ice and ice rubble, but it does not deal with mush ice (which is somewhat like saturated snow), or with pack ice (broad expanses of ice floes).

Ideally, a review such as this ought to conclude with a major section on the application of the theory and the measured properties to the solution of boundary value problems. However, during this assignment there was insufficient time to complete such a task.

PART I. GENERAL BACKGROUND TO THE
MECHANICS OF DEFORMABLE SOLIDS

Ice mechanics is concerned largely with the interactions of forces and deformations. When a force acts on a material it deforms, and the deformation may culminate in rupture of the material. We have to consider: 1) force, 2) deformation, and 3) the property of the material which controls the relation between force and deformation.

STRESSES, STRAINS AND THEIR TIME DERIVATIVES

Force and stress

Force (P) is the product of mass times acceleration, and it has the dimensions MLT^{-2}, where these symbols represent respectively mass, length and time. Traditional engineering units include pounds force and kilograms force, which should properly be abbreviated as "lbf" and "kgf" as a reminder that they are units of force, not mass. The distinction is important for non-gravitational inertial forces, where pounds and kilograms have to be divided by the gravitational acceleration g. In physics, and in engineering research, dynes or newtons are more likely to be used as units of force.

Stress (σ) is force per unit area, so that it has dimensions $ML^{-1}T^{-2}$. Traditional engineering units include pounds per square inch (lbf/in.^{2} or, in archaic notation, psi), and kilograms per square centimetre (kgf/cm^2). The metric units in common use for ice mechanics research are dynes/cm^2, newtons/m^2 (or pascals), and bars, where 10^6 dynes/cm^2 = 1 bar = 0.1 MN/m^2 = 0.1 MPa = 1.02 kgf/cm^2 = 14.5 lbf/in^2. Stresses may be either: 1) normal stresses, produced by tensile or compressive forces acting perpendicular to the faces of cubic elements, or 2) shear stresses, produced by tangential forces acting parallel to the surfaces of cubic elements. In a three-dimensional stress field, the stress system can also be resolved into: 1) an isotropic component, or bulk stress, which tends only to change the volume of an element, and 2) a deviatoric component, which tends to change the shape of an element.

Displacement and strain

Displacement (u) is the movement of one point relative to another, resulting in increase or decrease of a linear dimension. The physical dimension of displacement is L, and typical units are inches, feet, miles, millimetres, metres, etc.

Strain (ϵ) is displacement per unit length, and it is therefore dimensionless. Although there are no units for strain, engineers sometimes use implied multiples, e.g. "microinches per inch," a number which is

strain $\times 10^6$, or "percent strain," a number which is strain $\times 10^2$. Where strain is displacement per unit of length in the direction of displacement, it is referred to as a normal strain. Where the strain is displacement per unit of length in a direction perpendicular to the direction of displacement, it is referred to as a shear strain. In a three-dimensional strain field the strain can be resolved into: 1) an isotropic component, or volumetric strain, representing change in volume (and density) of an element, and 2) a deviatoric component, representing change in the shape of an element.

Variation of force, stress, displacement and strain with respect to time

Loading rate is the rate of change of force with time, dP/dt. It has dimensions MLT^{-3}, and units such as lbf/min or N/s.

Stress rate is the rate of change of stress with time, $d\sigma/dt$ or $\dot{\sigma}$. The dimensions are $ML^{-1} T^{-3}$, and typical units are lbf/in.^{2}-s, bar/s, or Pa/s.

Velocity is the rate of change of displacement with time, du/dt or $\dot{u}$. Dimensions are LT^{-1} and typical units are ft/s, knots, m/s, etc.

Strain rate is the rate of change of strain with time, $d\epsilon/dt$ or $\dot{\epsilon}$. Dimensions are T^{-1} and typical units are s^{-1}, yr^{-1}.

Acceleration (f) is the rate of change of velocity with time, or the second derivative of displacement with respect to time, d^2u/dt^2 or $\ddot{u}$. Dimensions are LT^{-2} and typical units are ft/s^2 or m/s^2.

Strain acceleration is the rate of change of strain rate with time, or the second derivative of strain with respect to time, $d^2\epsilon/dt^2$ or $\ddot{\epsilon}$. Dimensions are T^{-2}, and typical units s^{-2}.

RHEOLOGICAL PROPERTIES OF MATERIALS

The relationships between stress, strain and time for typical engineering materials can seem fairly simple, for example if stress is directly proportional to strain. However, this is true only for very restricted ranges of stress, strain and temperature, and over a sufficiently broad range of conditions virtually all materials experience time-dependent inelastic deformations. To introduce some of the more complicated aspects of rheology, it is convenient to first consider simple mechanisms, or models, which have stress/strain/time characteristics similar to those displayed by deformable solids.

Elasticity

Linear elasticity means that stress is directly proportional to strain (Fig. 1), and the coefficient of proportionality is called the elastic modulus. For one-dimensional stress and strain, the ratio of stress to strain, σ/ϵ, is called Young's modulus E, and the relationship is known as Hooke's Law. The elastic modulus has the dimensions of a stress, i.e.

4

LINEAR ELASTICITY
(Hooke's Law)

Spring

$\varepsilon = \frac{a}{b}$

LINEAR VISCOSITY
(Newtonian Viscosity)

Dashpot

$\eta = \frac{a}{b}$

IDEAL PLASTICITY
(Saint-Venant)

Yield Point, $\sigma = k$

Block with Dry Friction
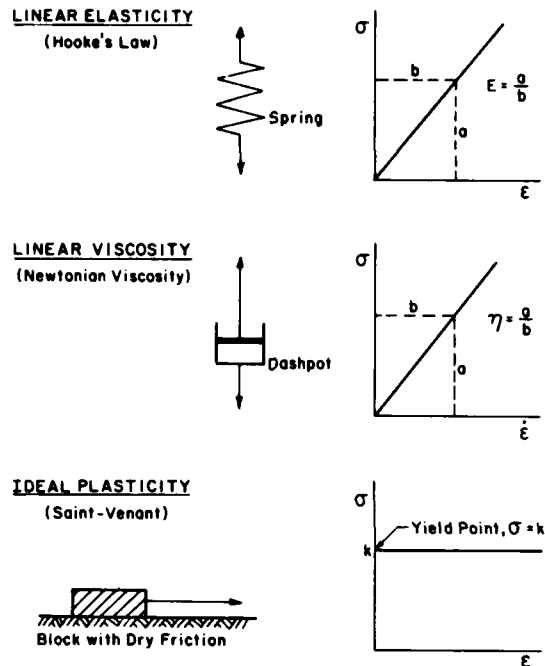
Figure 1. Simple rheological responses and models.

$ML^{-1} T^{-2}$. In a rheological model, linear elasticity is represented by a spring of modulus E, so that $\sigma = E\varepsilon$.

Viscosity

Linear viscosity, which is also referred to as Newtonian viscosity, means that stress σ is proportional to strain rate $\dot{\varepsilon}$ (Fig. 1). The coefficient of proportionality η is the viscosity, or viscosity coefficient, and it has dimensions $ML^{-1} T^{-1}$. In a rheological model, viscosity is represented by a dashpot. In the dashpot, force and velocity are proportional and we can cut the corner a little by letting the dashpot represent proportionality between stress σ and strain rate $\dot{\varepsilon}$, i.e. $\sigma = \eta \, d\varepsilon/dt = \eta \, \dot{\varepsilon}$. It is worth pointing out at this stage that viscosity is frequently <u>nonlinear</u>, i.e. stress is a function of strain rate, but is not directly proportional. However, introduction of nonlinear viscosity into simple rheological models destroys their value as learning tools.

Plasticity

Ideal plasticity, or rigid-plastic behavior, means that there is no strain in the material until a critical yield stress k is reached, after which the material strains indefinitely at indeterminate speed (Fig. 1). The name Saint-Venant is sometimes associated with ideal plastic behavior. In a rheological model, plasticity is represented by a block lying on a plane, with dry friction between the block and the plane. The upper limit of the static friction force is assumed equal to the kinetic friction force, so that it can represent a simple yield stress k. With $\sigma < k$, $\varepsilon = 0$; with $\sigma = k$, $\varepsilon \to \infty$.

5

Combinations of rheological properties

We can take it as an axiom that all real materials possess all rheo-
logical properties, but the relative significance of any component will
vary with the physical environment, the stress state, and the time scale of
events. For example, a material will be predominantly elastic with low
deviatoric stress, high rates of stress or strain, short load-duration, and
low temperature (relative to the melting point). The same material may be
predominantly viscous, or plastic, with high deviatoric stress, low rates
of stress or strain, long load duration, and high homologous temperature.

The real difficulties arise when the conditions are such that two or
more types of rheological behavior are of comparable significance. To
explore situations of this kind we can look first at some two-element rheo-
logical models and then at three- and four-element models. There is, of
course, no limit to the number of elements that can be built into a model,
but at some stage refinements become pointless. A model consisting of
linear elements is not truly representative of real materials, and its
chief merit is as a simple device for visualizing rheologic responses.

RHEOLOGICAL MODELS

Two-element models for linear viscoelasticity

(a) The Maxwell model. This model consists of a spring and a dashpot
in series, and it is easy to see how it behaves when constant force, or
constant stress, is applied (Fig. 2). For constant stress σ across the
system, the stress/strain relation for the spring is

$$\sigma = E\epsilon_s$$

where ϵ_s is the strain in the spring. The stress/strain-rate relation
for the dashpot is

$$\sigma = \eta \, \dot{\epsilon}_D$$

where $\dot{\epsilon}_D$ is the strain rate of the dashpot. The total strain of the
system at time t is the sum of the strain in the spring and the accumulated
strain in the dashpot:

$$\epsilon = \epsilon_s + \epsilon_D$$

or, differentiating with respect to time,

$$\dot{\epsilon} = \dot{\epsilon}_s + \dot{\epsilon}_D.$$

Since

$$\dot{\epsilon}_s = (1/E)\ \dot{\sigma}$$

and

$$\dot{\epsilon}_D = (1/\eta)\ \sigma$$

the overall strain rate is

$$\dot{\epsilon} = (1/E)\ \dot{\sigma} + (1/\eta)\ \sigma$$

$$= \left(\frac{1}{E}\ \frac{d}{dt} + \frac{1}{\eta}\right)\ \sigma \quad .$$

The required solution of this differential equation for constant stress applied at time $t = 0$, $\epsilon = 0$, is

$$\epsilon = \sigma\left(\frac{1}{E} + \frac{1}{\eta}\ t\right) \ .$$

(b) <u>The Kelvin-Voigt model</u>. This model consists of a spring and dashpot in parallel. When constant force, or constant stress, is applied across this system, the spring extends to its equilibrium length, but at a decelerating rate, i.e. the spring is damped (Fig. 2). The strain is the same for the spring and the dashpot, but stress is different in the two elements. In the spring

$$\sigma_s = E\epsilon$$

and in the dashpot

$$\sigma_D = \eta\ \dot{\epsilon} \ .$$

Overall,

$$\sigma = \sigma_s + \sigma_D$$

$$= E\epsilon + \eta\ \dot{\epsilon}$$

$$= \left(E + \eta\ \frac{d}{dt}\right)\epsilon \ .$$

The required solution for stress applied at $t = 0$, $\epsilon = 0$ is

$$\epsilon = \frac{\sigma}{E}\left(1 - e^{-(E/\eta)t}\right) \ .$$

LINEAR VISCO-ELASTIC
(Maxwell)

$\dot\epsilon = \sigma/\eta$

$\epsilon = \sigma/E$

$\sigma = $ Constant

LINEAR VISCO-ELASTIC
(Kelvin-Voigt)

$\epsilon = \sigma/E$

$\sigma = $ Constant

ELASTIC-PLASTIC
(Prandtl)

VISCOUS-PLASTIC

VISCO-PLASTIC
(Bingham)

ELASTIC-VISCO-PLASTIC

Elastic up to $\sigma = k$
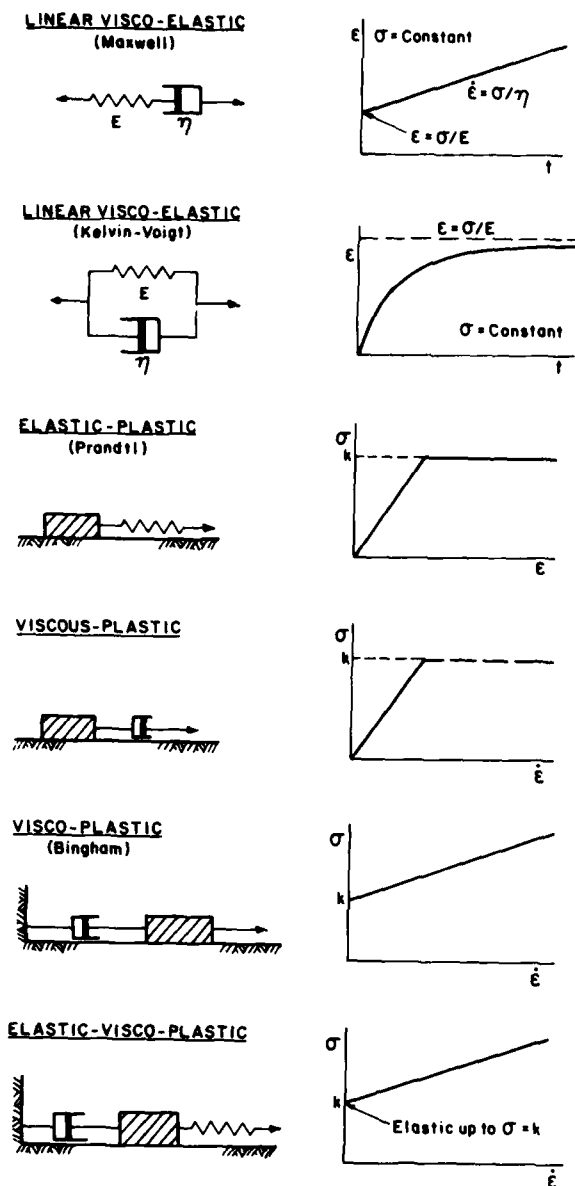
Figure 2. Two-element rheological
models.

Two-element models for elastoplastic and viscoplastic behavior

(a) Elastic-plastic model. This model, sometimes associated with the
name of Prandtl, consists of a spring and a friction block in series (Fig.
2). For $\sigma < k$, $\sigma = E\epsilon$, but when $\sigma = k$, $\epsilon = \sigma/E + \epsilon_{plas}$, where ϵ_{plas} is
the indeterminate plastic strain.

(b) Viscous-plastic model. The simplest viscous-plastic model is a
series combination of a dashpot and a friction block. For $\sigma < k$, $\sigma = \eta\dot\epsilon$,
while at $\sigma = k$, $\dot\epsilon \geq (1/\eta)k$.

8

(c) <u>Viscoplastic model</u>. This model, sometimes associated with the name Bingham, consists of a dashpot and a friction block connected in such a way that the dashpot cannot move until the block slips (Fig. 2). If $\sigma \geq k$,

$$\sigma = k + \eta \, \dot{\varepsilon} \, .$$

Multi-element models

Perhaps the most useful multi-element model for introducing general viscoelastic response is one known as the Burgers' model. It consists of a Maxwell model in series with a Kelvin-Voigt model (Fig. 3). The general differential equation can be derived by considering constant stress across the model. Using subscripts M and K to denote respectively the Maxwell and Kelvin-Voigt units, and using additional subscripts S and D for spring and dashpot respectively, the overall strain is

$$\varepsilon = \varepsilon_{MS} + \varepsilon_{MD} + \varepsilon_K \, .$$

In the Maxwell spring

$$\sigma = E_M \, \varepsilon_{MS}$$

and in the Maxwell dashpot

$$\sigma = \eta_M \, \dot{\varepsilon}_{MD} \, .$$

In the Kelvin-Voigt unit

$$\sigma = E_K \, \varepsilon_K + \eta_K \, \dot{\varepsilon}_K \, .$$

After suitable differentiation, these relations give the general differential equation

$$\ddot{\sigma} + \left(\frac{E_M}{\eta_M} + \frac{E_M}{\eta_K} + \frac{E_K}{\eta_K}\right) \dot{\sigma} + \frac{E_M \, E_K}{\eta_M \, \eta_K} \sigma = E_M \, \ddot{\varepsilon} + \frac{E_M \, E_K}{\eta_M} \, \dot{\varepsilon} \, .$$

This equation can be solved for various sets of initial conditions and boundary conditions to give relations of special interest. In Figure 3, solutions are given for constant stress, for constant strain rate, and for constant stress rate.

9

Figure 3. Summary of basic rheological relations.

THREE-DIMENSIONAL STRESS AND STRAIN

The preceding ideas are easy to understand in one-dimensional or simple two-dimensional situations, but three-dimensional systems are a little more complicated.

External forces acting on a body

The external forces acting on a body may include surface forces and body forces. Surface forces, or surface tractions, are distributed over area. Body forces are distributed over volume. They are typically gravity, inertia, or magnetic forces.

In considering the forces on an element, it may be permissible to neglect body forces, since they diminish with the cube of a linear dimension, whereas surface forces diminish with the square of a linear dimension.

Components of stress

Any system of stress can be resolved into a set of orthogonal components. If we define an element with respect to the axes of a cartesian coordinate system, the stress acting on that element can be resolved into nine components, which reduce by symmetry to six components.

We can denote all stress components by σ, differentiating between normal and shear stresses only by the subscripts, as in Figure 4. Normal stresses which act in a tensile sense are considered positive.

The first subscript indicates the direction of the normal to the plane on which the stress acts; the second subscript gives the direction in which the stress acts. For a normal stress, first and second subscripts are alike. For a shear stress, the two subscripts are different.

a. In x, y, z notation.   b. In 1, 2, 3 notation.
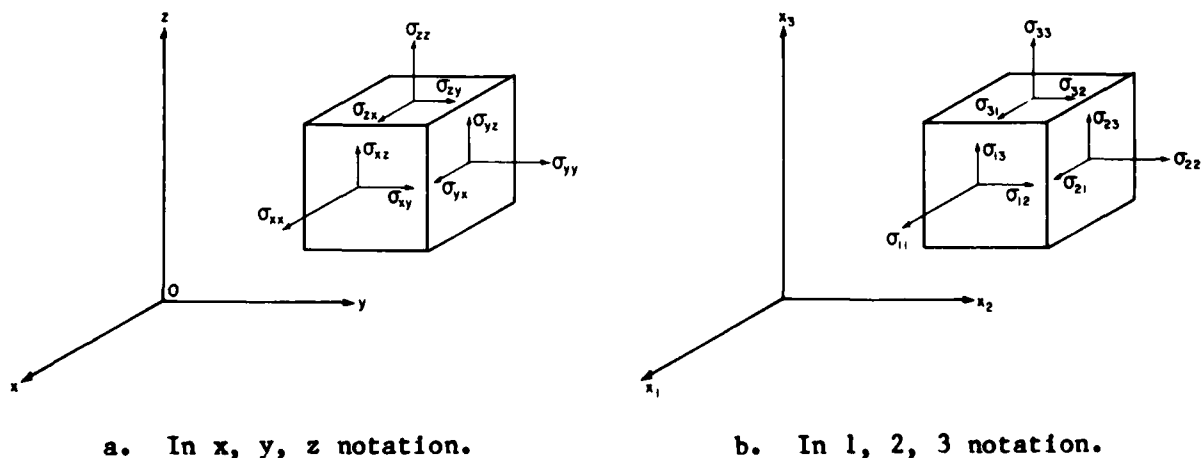
Figure 4. Components of stress.

We can set out these stress components in a matrix, which has nine components:

$$
\begin{vmatrix}
\sigma_{xx} & \sigma_{xy} & \sigma_{xz} \\
\sigma_{yx} & \sigma_{yy} & \sigma_{yz} \\
\sigma_{zx} & \sigma_{zy} & \sigma_{zz}
\end{vmatrix}
$$

Note that, from consideration of the equilibrium of the element, $\sigma_{xy} = \sigma_{yx}$, $\sigma_{xz} = \sigma_{zx}$, $\sigma_{yz} = \sigma_{zy}$. This reduces the number of independent components to six, and the matrix is now symmetrical about the diagonal terms.

Now, we can make the above notation more compact in the following way. If, instead of x, y, z, we use the labels x_1, x_2, x_3 for the coordinate axes, we can then replace the subscripts x, y, z with the numerals 1, 2, 3, as in Figure 4b.

Our stress matrix becomes

$$
\begin{vmatrix}
\sigma_{11} & \sigma_{12} & \sigma_{13} \\
\sigma_{21} & \sigma_{22} & \sigma_{23} \\
\sigma_{31} & \sigma_{32} & \sigma_{33}
\end{vmatrix}.
$$

This we call the __stress__ __tensor.__ It can be written more compactly as

$$
\sigma_{ij}
$$

where i,j = 1, 2, 3, i.e. if we write down in order all the possible combinations (permutations) of the values 1, 2 and 3 for i and j, we obtain all the terms of the stress tensor.

The stress tensor is a symmetric tensor of the second rank, or second order. As a matter of interest, vectors and tensors have the following numbers of components:

Scalar, S   1 component

Vector V_i 3 components   (first rank tensor)

Tensor II T_{ij} 9 components

Tensor III T_{ijk} 27 components

Tensor IV T_{ijkf} 81 components

The number of subscripts gives the order or rank, while 3 raised to a power equal to rank gives number of components.

Strain

In considering strain, it is convenient to assume that strains will be small and homogeneous.

Infinitesimal strain. These are strains sufficiently small that powers higher than the first can be neglected, e.g. squares and products of strains are negligible.

Homogeneous strain. Strain is homogeneous if planes remain plane, and parallel planes remain parallel.

Components of strain

Any system of strain can be resolved into nine orthogonal components, with normal and shear strains corresponding to the components of stress.

We shall assume for a start that there is <u>no rigid-body rotation</u> relative to the reference axes, i.e. only deformation of the body.

When a body is <u>deformed</u>, the <u>displacement</u> of each point P can be expressed in terms of three components of displacement, u, v, w, in the directions x, y, z, respectively (Fig. 5).

The <u>gradients</u> of u, v, w with respect to x, y, z are <u>strains</u>.

For simplicity we can derive the strain components in two dimensions only (Fig. 6):

$$\frac{1}{2}\gamma_{xy} = \epsilon_{xy} = \epsilon_{12} = \frac{1}{2}\left(\frac{\partial u}{\partial y} + \frac{\partial v}{\partial x}\right)$$

$$\frac{1}{2}\gamma_{yz} = \epsilon_{yz} = \epsilon_{23} = \frac{1}{2}\left(\frac{\partial v}{\partial z} + \frac{\partial w}{\partial y}\right)$$

$$\frac{1}{2}\gamma_{zx} = \epsilon_{zx} = \epsilon_{31} = \frac{1}{2}\left(\frac{\partial w}{\partial x} + \frac{\partial u}{\partial z}\right).$$

Now we can write the strain tensor:

$$\epsilon_{ij} = \begin{vmatrix} \epsilon_{11} & \epsilon_{12} & \epsilon_{13} \\ \epsilon_{21} & \epsilon_{22} & \epsilon_{23} \\ \epsilon_{31} & \epsilon_{32} & \epsilon_{33} \end{vmatrix}.$$

Or, in terms of the displacement gradients,

$$\epsilon_{ij} = \frac{1}{2}\left(\frac{\partial u_i}{\partial x_j} + \frac{\partial u_j}{\partial x_i}\right).$$

13
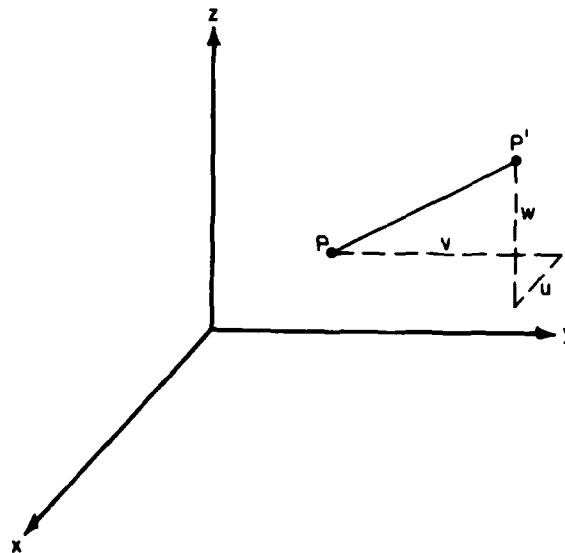
Figure 5. Displacement of a point.
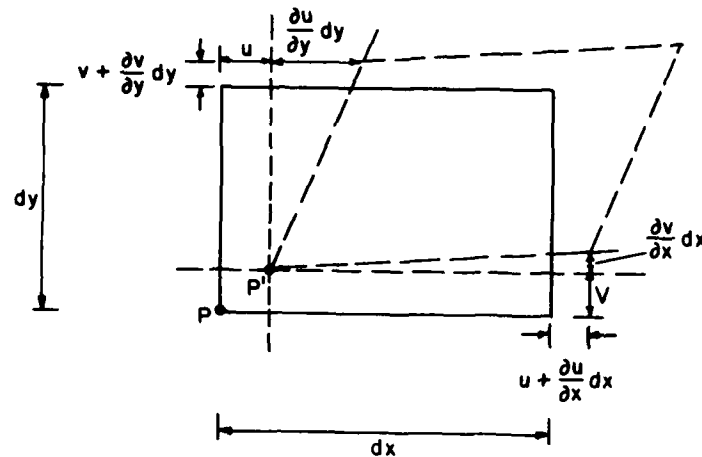
Figure 6. Displacement gradients and strains.

That is,

$$
\begin{vmatrix}
\varepsilon_{11} & \varepsilon_{12} & \varepsilon_{13} \\
\varepsilon_{21} & \varepsilon_{22} & \varepsilon_{23} \\
\varepsilon_{31} & \varepsilon_{32} & \varepsilon_{33}
\end{vmatrix}
=
\begin{vmatrix}
\dfrac{\partial u_1}{\partial x_1} & \dfrac{1}{2}\left(\dfrac{\partial u_1}{\partial x_2} + \dfrac{\partial u_2}{\partial x_1}\right) & \dfrac{1}{2}\left(\dfrac{\partial u_1}{\partial x_3} + \dfrac{\partial u_3}{\partial x_1}\right) \\
\dfrac{1}{2}\left(\dfrac{\partial u_2}{\partial x_1} + \dfrac{\partial u_1}{\partial x_2}\right) & \dfrac{\partial u_2}{\partial x_2} & \dfrac{1}{2}\left(\dfrac{\partial u_2}{\partial x_3} + \dfrac{\partial u_3}{\partial x_2}\right) \\
\dfrac{1}{2}\left(\dfrac{\partial u_3}{\partial x_1} + \dfrac{\partial u_1}{\partial x_3}\right) & \dfrac{1}{2}\left(\dfrac{\partial u_3}{\partial x_2} + \dfrac{\partial u_2}{\partial x_3}\right) & \dfrac{\partial u_3}{\partial x_3}
\end{vmatrix} .
$$

Rotation. Referring back to the diagram for strain derivation, it will be seen that if $(\partial u/\partial y)dy \neq (\partial v/\partial x)dx$, the element undergoes rotation as well as pure deformation.

14

Change in length in x-direction $= \left(u + \dfrac{\partial u}{\partial x}\, dx\right) - u = \dfrac{\partial u}{\partial x}\, dx$.

Unit change in x-direction $= \varepsilon_{xx} = \dfrac{\partial u}{\partial x}$.

Similarly, $\varepsilon_{yy} = \dfrac{\partial v}{\partial y}$.

Change in angle in the x-y plane at P, or γ_{xy}, is

$$\gamma_{xy} = \frac{\partial u}{\partial y} + \frac{\partial v}{\partial x} .$$

By identical considerations for the yz and zx planes we obtain the remaining components:

$$\varepsilon_{xx} = \frac{\partial u}{\partial x} , \qquad \varepsilon_{yy} = \frac{\partial v}{\partial y} , \qquad \varepsilon_{zz} = \frac{\partial w}{\partial z}$$

$$\gamma_{xy} = \gamma_{yx} = \frac{\partial u}{\partial y} + \frac{\partial v}{\partial x}$$

$$\gamma_{yz} = \gamma_{zy} = \frac{\partial v}{\partial z} + \frac{\partial w}{\partial y}$$

$$\gamma_{zx} = \gamma_{xz} = \frac{\partial w}{\partial x} + \frac{\partial u}{\partial z} .$$

γ_{xy}, γ_{yx}, γ_{zx} are the components of shear strain according to the classical, or engineering, definitions. In order to utilize the tensor system we adopt a slightly different form for the shear strains. We denote all strain components by ε, and replace subscripts x, y, z by 1, 2, 3, as in the case of stress, getting:

$$\varepsilon_{xx} = \varepsilon_{11} = \frac{\partial u}{\partial x}$$

$$\varepsilon_{yy} = \varepsilon_{22} = \frac{\partial v}{\partial y}$$

$$\varepsilon_{zz} = \varepsilon_{33} = \frac{\partial w}{\partial z}$$

$$\frac{1}{2}\gamma_{xy} = \varepsilon_{xy} = \varepsilon_{12} = \frac{1}{2}\left(\frac{\partial u}{\partial y} + \frac{\partial v}{\partial x}\right)$$

$$\frac{1}{2}\gamma_{yz} = \varepsilon_{yz} = \varepsilon_{23} = \frac{1}{2}\left(\frac{\partial v}{\partial z} + \frac{\partial w}{\partial y}\right)$$

$$\frac{1}{2}\gamma_{zx} = \varepsilon_{xx} = \varepsilon_{31} = \frac{1}{2}\left(\frac{\partial w}{\partial x} + \frac{\partial u}{\partial z}\right) .$$

Now we can write the strain tensor:

$$\varepsilon_{ij} = \begin{vmatrix} \varepsilon_{11} & \varepsilon_{12} & \varepsilon_{13} \\ \varepsilon_{21} & \varepsilon_{22} & \varepsilon_{23} \\ \varepsilon_{31} & \varepsilon_{32} & \varepsilon_{33} \end{vmatrix}.$$

Defining a displacement gradient tensor $e_{ij} = \dfrac{\partial u_i}{\partial x_j}$

$$e_{ij} = \frac{\partial u_i}{\partial x_j} = \frac{1}{2}\left(\frac{\partial u_i}{\partial x_j} + \frac{\partial u_j}{\partial x_i}\right) + \frac{1}{2}\left(\frac{\partial u_i}{\partial x_j} - \frac{\partial u_j}{\partial x_i}\right)$$

$\dfrac{1}{2}\left(\dfrac{\partial u_i}{\partial x_j} + \dfrac{\partial u_j}{\partial x_i}\right) = \varepsilon_{ij}$ is a symmetric tensor, with $\varepsilon_{ij} = \varepsilon_{ji}$

$\dfrac{1}{2}\left(\dfrac{\partial u_i}{\partial x_j} - \dfrac{\partial u_j}{\partial x_i}\right) = \omega_{ij}$ is an antisymmetric, or skew symmetric, tensor, with $\omega_{ij} = -\omega_{ji}$; ω_{ij} is the rotation tensor. Diagonal terms = 0.

TRANSFORMATION EQUATIONS

Rotation of reference directions for stress components

Having defined the components of stress and strain with respect to a given set of coordinate axes, we have to consider now the resolution, or transformation, of stress and strain into a different set of directions (Fig. 7).
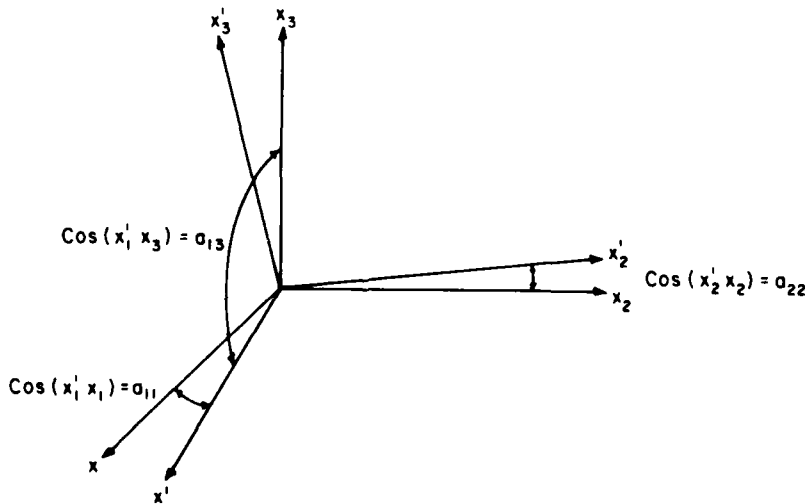
Figure 7. Rotation of axes.

16

Denoting the direction cosine by a, the transformation matrix is:

	x_1	x_2	x_3	old directions
x'_1	a_{11}	a_{12}	a_{13}	
x'_2	a_{21}	a_{22}	a_{23}	
new directions x'_3	a_{31}	a_{32}	a_{33}	

From a consideration of the equilibrium of the tetrahedron (Fig. 8), with p_x, p_y, p_z as cartesian components of stress on the oblique plane, it can be shown that:

$$\sigma_{nn} = a_{nx}p_x + a_{ny}p_y + a_{nz}p_z$$

$$= a_{nx}\left(a_{nx}\sigma_{xx} + a_{ny}\sigma_{yx} + a_{nz}\sigma_{zx}\right)$$

$$+ a_{ny}\left(a_{nx}\sigma_{xy} + a_{ny}\sigma_{yy} + a_{nz}\sigma_{zy}\right)$$

$$+ a_{nz}\left(a_{nx}\sigma_{xz} + a_{ny}\sigma_{yz} + a_{nz}\sigma_{zz}\right)$$

$$= \sigma_{xx}a_{nx}^2 + \sigma_{yy}a_{ny}^2 + \sigma_{zz}a_{nz}^2$$

$$+ 2\sigma_{xy}a_{nx}a_{ny} + 2\sigma_{yz}a_{ny}a_{nz} + \sigma_{zx}a_{nz}a_{nx}$$

and similarly

$$\sigma_{ns} = \sigma_{xx}a_{nx}a_{sx} + \sigma_{yy}a_{ny}a_{sy} + \sigma_{zz}a_{nz}a_{sz}$$

$$+ \left(a_{nx}a_{sy} + a_{ny}a_{sx}\right)\sigma_{xy} + \left(a_{nx}a_{sz} + a_{nz}a_{sx}\right)\sigma_{xz} + \left(a_{ny}a_{sz} + a_{nz}a_{sy}\right)\sigma_{yz}.$$
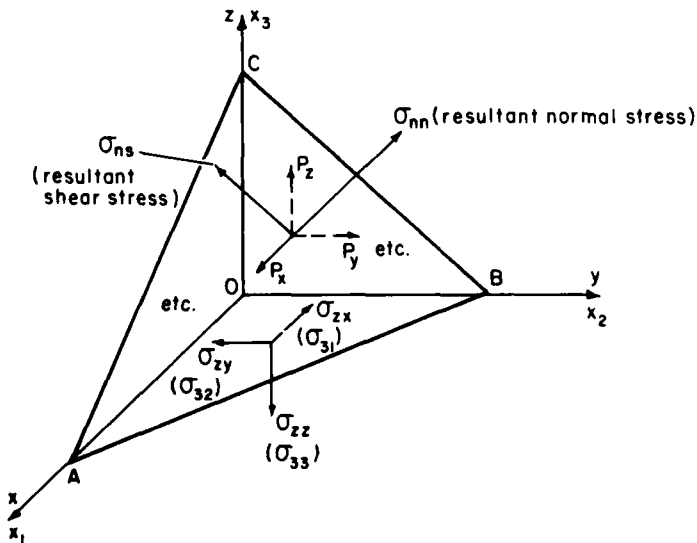
Figure 8. Resultant stresses on a tetrahedral plane.

17

If we now introduce into our tensor notation a __summation convention__, such that all terms containing a repeated suffix are summed, we can write the above equations in compact form:

$$\sigma_{nn} = a_{ni} \, a_{nj} \, \sigma_{ij}$$

$$\sigma_{ns} = a_{ni} \, a_{sj} \, \sigma_{ij}$$

If n and s are the x' and y' axes of the transformed system, the complete transformation is given by

$$\sigma_{ns} = a_{ni} \, a_{sj} \, \sigma_{ij}$$

Principal directions

By a suitable rotation of the axes x, y, z to a new set of directions x', y', z', the shear components of the transformed system can be made to disappear while the normal components reach extreme values. These new normal components are called __principal stresses__, and the planes on which they act are __principal planes__.

Suppose the plane ABC in Figure 8 has been rotated so as to coincide with a principal plane. Thus $\sigma_{ns} = 0$, and σ_{nn} is a minimum, which we shall just denote as σ.

Then

$$\sigma \, a_{nx} = p_x = a_{nx} \sigma_{xx} + a_{ny} \sigma_{yx} + a_{nz} \sigma_{zx}$$

$$\sigma \, a_{ny} = p_y = a_{nx} \sigma_{xy} + a_{ny} \sigma_{yy} + a_{nz} \sigma_{zy}$$

$$\sigma \, a_{nz} = p_z = a_{nx} \sigma_{xz} + a_{ny} \sigma_{yz} + a_{nz} \sigma_{zz} \, .$$

That is,

$$\left(\sigma_{xx} - \sigma \right) a_{nx} + \sigma_{yx} \, a_{ny} + \sigma_{zx} \, a_{nz} = 0$$

$$\sigma_{xy} \, a_{nx} + \left(\sigma_{yy} - \sigma \right) a_{ny} + \sigma_{zy} \, a_{nz} = 0$$

$$\sigma_{xz} \, a_{nz} + \sigma_{tz} \, a_{ny} + \left(\sigma_{zz} - \sigma \right) a_{nz} = 0 \, .$$

Since the direction cosines cannot all be zero (the condition for orthogonality is $a^2_{nx} + a^2_{ny} + a^2_{nz} = 1$), the determinant of their coefficients must equal zero, i.e.

$$\sigma^3 - \left(\sigma_{xx} + \sigma_{yy} + \sigma_{zz} \right) \sigma^2 + \left(\sigma_{xx} \sigma_{yy} + \sigma_{yy} \sigma_{zz} + \sigma_{zz} \sigma_{xx} - \sigma^2_{xy} - \sigma^2_{yz} - \sigma^2_{zx} \right) \sigma$$

$$- \left(\sigma_{xx} \sigma_{yy} \sigma_{zz} - \sigma_{xx} \sigma^2_{yz} - \sigma_{yy} \sigma^2_{xz} - \sigma_{zz} \sigma^2_{xy} + 2 \, \sigma_{xy} \sigma_{yz} \sigma_{xz} \right) = 0 \, .$$

There are three real roots of this cubic equation in σ: σ_1, σ_2, σ_3. These are the principal stresses. They depend <u>only</u> on the state of stress at a point, and not on the system of coordinates. Thus the <u>coefficients</u> of the cubic equation are the same for <u>any coordinate system</u>, i.e. they are <u>invariant</u> with rotation of the reference. The <u>first</u>, <u>second</u> and <u>third</u> invariants of stress are:

$$I_1 = \sigma_{xx} + \sigma_{yy} + \sigma_{zz} = \sigma_1 + \sigma_2 + \sigma_3$$

$$I_2 = - \left(\sigma_{xx}\sigma_{yy} + \sigma_{yy}\sigma_{zz} + \sigma_{zz}\sigma_{xx}\right) + \sigma_{xy}^2 + \sigma_{yz}^2 + \sigma_{zx}^2$$

$$= - \left(\sigma_1\sigma_2 + \sigma_2\sigma_3 + \sigma_3\sigma_1\right)$$

$$I_3 = \sigma_{xx}\sigma_{yy}\sigma_{zz} - \sigma_{xx}\sigma_{yz}^2 - \sigma_{yy}\sigma_{zx}^2 - \sigma_{zz}\sigma_{xy}^2 + 2\,\sigma_{xy}\sigma_{yz}\sigma_{xz}$$

$$= \sigma_1\sigma_2\sigma_3 \,.$$

Strain transformations

There are corresponding transformation equations for strain. They are completely analogous to the stress transformations if we use the tensor components of shear strain ε_{xy}, etc., rather than γ_{xy}, etc. Principal strains are analogous to principal stresses, and we also have invariants of strain analogous to the stress invariants.

ISOTROPIC AND DEVIATORIC COMPONENTS OF STRESS AND STRAIN

Bulk stress and deviatoric stress

There is a particular scheme of stress resolution which is used a good deal in the consideration of flow laws and failure criteria. It has obvious physical significance.

<u>Bulk stress</u>, or volumetric stress, is that combination of stress components which tends to change the <u>volume</u> of an element. Bulk stress, σ, is

$$\bar{\sigma} = \frac{1}{3}\left(\sigma_{xx} + \sigma_{yy} + \sigma_{zz}\right) = \frac{1}{3}\left(\sigma_1 + \sigma_2 + \sigma_3\right)$$

i.e the average normal pressure. In the case of a fluid the bulk stress is the hydrostatic pressure ($\sigma_{xx} = \sigma_{yy} = \sigma_{zz}$).

Using the tensor rotation with the summation convention (adding terms formed from repeated suffixes):

$$\bar{\sigma} = \frac{1}{3}\,\sigma_{ii}$$

i.e

$$\bar{\sigma} = \frac{1}{3}(\sigma_{11} + \sigma_{22} + \sigma_{33}) .$$

We note that the bulk stress is equal to one-third of the first invariant of stress:

$$\bar{\sigma} = \frac{1}{3} I_1 .$$

Deviatoric stress (shear stress) tends to change the shape of an element. Deviators are denoted by primes. In tensor notation:

$$\sigma'_{ij} = \sigma_{ij} - \frac{1}{3} \delta_{ij} \sigma_{kk}.$$

Here we have introduced two new additions to the scheme of tensor notation. The symbol δ_{ij} is known as the Kronecker delta and it can take one of two values:

when $\quad i = j$, $\qquad \delta_{ij} = 1$

when $\quad i \neq j$, $\qquad \delta_{ij} = 0$.

The subscripts k are "dummy suffixes."

Examples of the application of this scheme are:

$$\sigma'_{11} = \sigma_{11} - \frac{1}{3}(\sigma_{11} + \sigma_{22} + \sigma_{33})$$

$$\sigma'_{12} = \sigma_{12} - 0 = \sigma_{12}.$$

A deviatoric stress is sometimes called a "reduced stress."

Bulk strain and deviatoric strain

Bulk strain and deviatoric strain are analogous to bulk stress and deviatoric stress respectively. Bulk strain, which is also called volumetric strain, or dilatation, is

$$\bar{\epsilon} = \epsilon_{xx} + \epsilon_{yy} + \epsilon_{zz} = \epsilon_1 + \epsilon_2 + \epsilon_3$$

or

$$\bar{\epsilon} = \epsilon_{ii} .$$

Note that there is a factor of 3 difference between the expressions for bulk stress and bulk strain.

Deviatoric strain (shear strain) is

$$\epsilon'_{ij} = \epsilon_{ij} - \frac{1}{3} \delta_{ij} \epsilon_{kk}$$

i.e., it corresponds to deviator stress in form.

Octahedral stresses

If we take axes parallel to the directions of principal stress, the directions of principal shear stress form a regular octahedron which has its corners on the principal axes (Fig. 9).

The direction cosines of the normals to the octahedral planes are $\pm 1/\sqrt{3}$.

The octahedral normal stress $\sigma_{n\ oct}$ is

$$\sigma_{n\ oct} = \frac{1}{3}(\sigma_1 + \sigma_2 + \sigma_3)$$

$$= \frac{1}{3} I_1 .$$
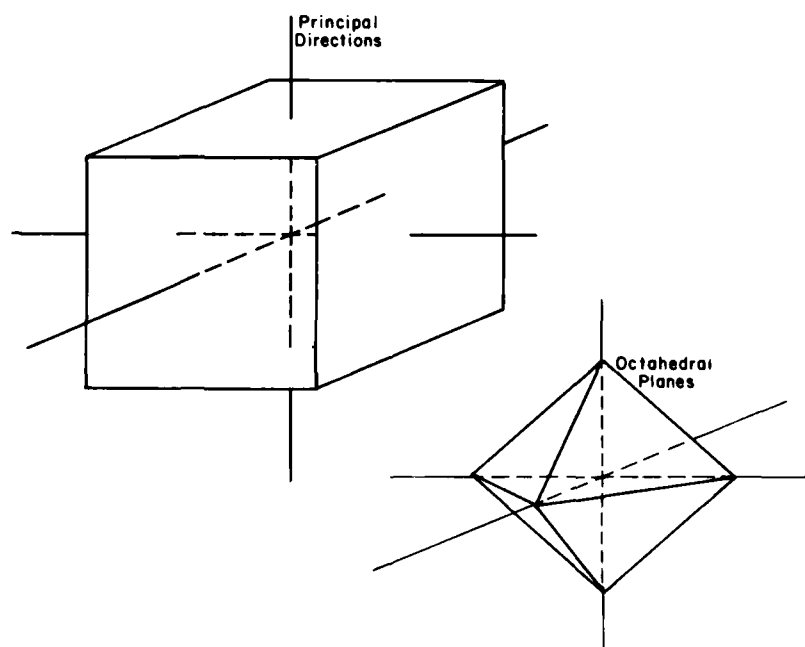
Figure 9. Octahedral planes.

21

The octahedral shear stress $\sigma_{s\ oct}$ is

$$\sigma_{s\ oct} = \frac{1}{3}[(\sigma_1 - \sigma_2)^2 + (\sigma_2 - \sigma_3)^2 + (\sigma_3 - \sigma_1)^2]^{1/2}$$

$$= \frac{\sqrt{2}}{3}[I_2^2 + 3I_2]^{1/2} \ .$$

If the principal directions are not immediately known, the octahedral stresses are

$$\sigma_{n\ oct} = \frac{1}{3}(\sigma_{xx} + \sigma_{yy} + \sigma_{zz})$$

$$\sigma_{s\ oct} = \frac{\sqrt{2}}{3}[\sigma_{xx}^2 + \sigma_{yy}^2 + \sigma_{zz}^2 + 3(\sigma_{xy}^2 + \sigma_{yz}^2 + \sigma_{zx}^2) - (\sigma_{xx}\sigma_{yy} + \sigma_{yy}\sigma_{zz} + \sigma_{zz}\sigma_{xx})]^{1/2} \ .$$

Invariants of stress and strain deviation

The components of stress deviation σ'_{ij} are formed by subtracting the mean stress from the normal components of stress, but not from the shear components. Thus the cartesian components of stress deviation are

$$\sigma'_{xx} = \sigma_{xx} - \overline{\sigma} \ , \qquad \sigma'_{yy} = \sigma_{yy} - \overline{\sigma} \ , \qquad \sigma'_{zz} = \sigma_{zz} - \overline{\sigma}$$

$$\sigma'_{xy} = \sigma_{xy} \ , \qquad \sigma'_{yz} = \sigma_{yz} \ , \qquad \sigma'_{zx} = \sigma_{zx} \ .$$

The principal stress deviations are

$$\sigma'_1 = \sigma_1 - \overline{\sigma} = \frac{1}{3}(2\sigma_1 - \sigma_2 - \sigma_3)$$

$$\sigma'_2 = \sigma_2 - \overline{\sigma} = \frac{1}{3}(2\sigma_2 - \sigma_1 - \sigma_3)$$

$$\sigma'_3 = \sigma_3 - \overline{\sigma} = \frac{1}{3}(2\sigma_3 - \sigma_1 - \sigma_2) \ .$$

The invariants of stress deviation are:

$$J_1 = \sigma'_{xx} + \sigma'_{yy} + \sigma'_{zz} = \sigma'_1 + \sigma'_2 + \sigma'_3 = 0$$

$$J_2 = -(\sigma'_{xx}\sigma'_{yy} + \sigma'_{yy}\sigma'_{zz} + \sigma'_{zz}\sigma'_{xx}) + \sigma_{xy}^2 + \sigma_{yz}^2 + \sigma_{zx}^2$$

$$= \frac{1}{6}[(\sigma_1 - \sigma_2)^2 + (\sigma_2 - \sigma_3)^2 + (\sigma_3 - \sigma_1)^2]$$

$$= \frac{1}{2}[\sigma_1'^2 + \sigma_2'^2 + \sigma_3'^2]$$

22

$$J_3 = \sigma'_{xx}\sigma'_{yy}\sigma'_{zz} + 2\,\sigma_{xy}\sigma_{yz}\sigma_{zx} - \left(\sigma'_{xx}\sigma^2_{yz} + \sigma'_{yy}\sigma^2_{zx} + \sigma'_{zz}\sigma^2_{xy}\right)$$

$$= \sigma'_1\,\sigma'_2\,\sigma'_3\ .$$

The octahedral shear stress can be expressed in terms of stress deviation as

$$\sigma_{s\ oct} = \left[2J_2/3\right]^{1/2}\ .$$

Components of strain deviation, denoted by the symbol e, are formed in exactly the same way as the components of stress deviation, i.e.

$$e_{xx} = \varepsilon_{xx} - \overline{e}\ ,\qquad e_{yy} = \varepsilon_{yy} - \overline{e}\ ,\qquad e_{zz} = \varepsilon_{zz} - \overline{e}$$

$$e_{xy} = \varepsilon_{xy}\ ,\qquad e_{yz} = \varepsilon_{yz}\ ,\qquad e_{zx} = \varepsilon_{zx}$$

$$e_1 = \varepsilon_1 - \overline{e}\ ,\qquad e_2 = \varepsilon_2 - \overline{e}\ ,\qquad e_3 = \varepsilon_3 - \overline{e}$$

where e is the mean normal strain:

$$\overline{e} = \left(\varepsilon_{xx} + \varepsilon_{yy} + \varepsilon_{zz}\right)/3 = \left(\varepsilon_1 + \varepsilon_2 + \varepsilon_3\right)/3\ .$$

The invariants of strain deviation are exactly analogous to the invariants of stress deviation.

ELASTICITY AND LINEAR VISCOSITY

Elastic constants

The basis for study of deformable solids is the theory of elasticity, which is usually introduced through consideration of an axial push or pull on a prismatic bar (Fig. 10). The material is assumed to be homogeneous, isotropic and linearly elastic, with axial stress proportional to axial strain

$$\sigma_{yy} = E\,\varepsilon_{yy}$$

and transverse strain proportional to axial strain

$$\varepsilon_{xx} = \varepsilon_{zz} = -\,\nu\,\varepsilon_{yy} = -\frac{\nu}{E}\,\sigma_{yy}$$

where E is Young's modulus and ν is Poisson's ratio. Because the material is <u>linearly</u> elastic, the principle of superposition can be applied in order to obtain the strains when stresses σ_{xx}, σ_{yy}, σ_{zz} are acting, e.g.

$$\epsilon_{xx} = \frac{\sigma_{xx}}{E} - \frac{\nu\sigma_{yy}}{E} - \frac{\nu\sigma_{zz}}{E} = \frac{1}{E}\left[\sigma_{xx} - \nu\left(\sigma_{yy} + \sigma_{zz}\right)\right] .$$

Shear stress and shear strain can be related more directly by the shear modulus, or modulus of rigidity, G:

$$\sigma_{xy} = 2G\,\epsilon_{xy} .$$

It can easily be shown, e.g. by expressing ϵ_{xy} and σ_{xy} in terms of principal stresses, that

$$G = \frac{E}{2(1+\nu)} .$$

Young's modulus and Poisson's ratio are to some extent accidents of history, and for some purposes it is more convenient to have direct relations between bulk stress and volumetric strain, and between deviatoric stress and deviatoric strain. For isotropic volumetric deformations the proportionality constant is the bulk modulus K, where

$$K = \frac{\text{bulk stress}}{\text{volumetric strain}} = \frac{\bar{\sigma}}{\bar{\epsilon}}$$

$$= \frac{\sigma_{11}}{3\,\epsilon_{11}} .$$

$$\epsilon_{axial} = \frac{\Delta L}{L_0} = \frac{\sigma}{E}$$

$$\frac{4F}{\pi D_0^2\, E}$$

$$\epsilon_{radial} = -\nu\,\epsilon_{axial}$$
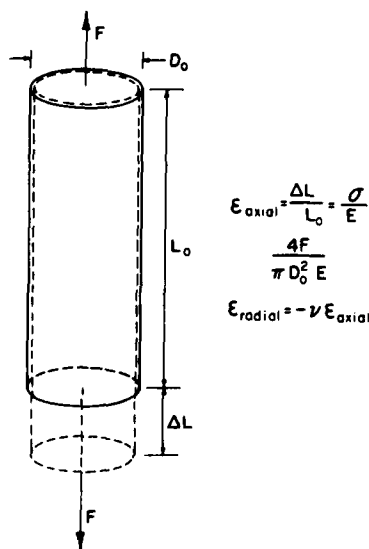
Figure 10. Axial elastic deformation of a bar.

Deviatoric components are related by the shear modulus G, with the general form of the relation expressable as

$$G = \frac{\sigma'_{ij}}{2\epsilon'_{ij}} \; .$$

Another constant, Lamé's constant λ, can be used in association with G. However, only two constants are required to specify the elastic properties of an isotropic material, and the choice of which two is largely a matter of convenience. The relations between the various elastic constants are:

$$K = \frac{E}{3(1 - 2\nu)} = \frac{2G(1 + \nu)}{3(1 - 2\nu)} = \frac{\lambda(1 + \nu)}{3\nu} = \frac{3\lambda + 2G}{3}$$

$$G = \frac{E}{2(1 + \nu)} = \frac{3K(1 - 2\nu)}{2(1 + \nu)} = \frac{\lambda(1 - 2\nu)}{2\nu} = \frac{3(K - \lambda)}{2}$$

$$\lambda = \frac{\nu E}{(1 + \nu)(1 - 2\nu)} = \frac{2G\nu}{(1 - 2\nu)} = \frac{3K\nu}{(1 + \nu)} = \frac{3K - 2G}{3}$$

$$\nu = \frac{E - 2G}{2G} = \frac{3K - E}{6K} = \frac{\lambda}{2(\lambda + G)} = \frac{\lambda}{3K - \lambda} = \frac{3K - 2G}{2(3K + G)} \; .$$

Solution of problems by theory of elasticity

Practical problems in elasticity are solved by solving certain sets of equations for appropriate boundary conditions. The sets of equations used are: 1) equilibrium equations, 2) strain/displacement relations, 3) compatibility equations, 4) stress/strain relations.

Equilibrium equations. The equilibrium equations are derived from Newton's laws. For static equilibrium the stress components in any direction sum to zero. In many engineering problems, body forces can be ignored, but in ice mechanics it is often necessary to include gravity body forces. The stress equilibrium equations with body forces included in the form of gravity forces are:

$$\frac{\partial \sigma_{ij}}{\partial x_j} + \rho g_i = 0$$

where ρ is the density of the material and g_i are components of the gravitational acceleration g.

In rectangular coordinates these equilibrium equations expand as:

$$\frac{\partial \sigma_{xx}}{\partial x} + \frac{\partial \sigma_{xy}}{\partial y} + \frac{\partial \sigma_{xz}}{\partial z} + \rho g_x = 0$$

$$\frac{\partial \sigma_{xy}}{\partial x} + \frac{\partial \sigma_{yy}}{\partial y} + \frac{\partial \sigma_{yz}}{\partial z} + \rho g_y = 0$$

25

$$\frac{\partial \sigma_{xz}}{\partial x} + \frac{\partial \sigma_{yz}}{\partial y} + \frac{\partial \sigma_{zz}}{\partial z} + \rho g_z = 0 .$$

The corresponding equations in cylindrical coordinates are:

$$\frac{\partial \sigma_{rr}}{\partial r} + \frac{1}{r} \frac{\partial \sigma_{r\theta}}{\partial \theta} + \frac{\partial \sigma_{rz}}{\partial z} + \frac{1}{r} \left(\sigma_{rr} - \sigma_{\theta\theta} \right) + \rho g_r = 0$$

$$\frac{\partial \sigma_{r\theta}}{\partial r} + \frac{1}{r} \frac{\partial \sigma_{\theta\theta}}{\partial \theta} + \frac{\partial \sigma_{\theta z}}{\partial z} + \frac{2}{r} \sigma_{r\theta} + \rho g_\theta = 0$$

$$\frac{\partial \sigma_{rz}}{\partial r} + \frac{1}{r} \frac{\partial \sigma_{\theta z}}{\partial \theta} + \frac{\partial \sigma_{zz}}{\partial z} + \frac{1}{r} \sigma_{rz} + \rho g_z = 0 .$$

Strain/displacement relations. The strain/displacement relations have already been derived and given as

$$\epsilon_{ij} = \frac{1}{2} \left(\frac{\partial u_i}{\partial x_j} + \frac{\partial u_j}{\partial x_i} \right) .$$

In rectangular coordinates these expand as:

$$\epsilon_{xx} = \frac{\partial u_x}{\partial x} \qquad\qquad \epsilon_{xy} = \frac{1}{2} \left(\frac{\partial u_x}{\partial y} + \frac{\partial u_y}{\partial x} \right)$$

$$\epsilon_{yy} = \frac{\partial u_y}{\partial y} \qquad\qquad \epsilon_{yz} = \frac{1}{2} \left(\frac{\partial u_y}{\partial z} + \frac{\partial u_z}{\partial y} \right)$$

$$\epsilon_{zz} = \frac{\partial u_z}{\partial z} \qquad\qquad \epsilon_{zx} = \frac{1}{2} \left(\frac{\partial u_z}{\partial x} + \frac{\partial u_x}{\partial z} \right) .$$

In cylindrical coordinates they expand as:

$$\epsilon_{rr} = \frac{\partial u_r}{\partial r} \qquad\qquad \epsilon_{r\theta} = \frac{1}{2} \left\{ \frac{1}{r} \frac{\partial u_r}{\partial \theta} + \frac{\partial u_\theta}{\partial r} - \frac{u_\theta}{r} \right\}$$

$$\epsilon_{\theta\theta} = \frac{u_r}{r} + \frac{1}{r} \frac{\partial u_\theta}{\partial \theta} \qquad\qquad \epsilon_{\theta z} = \frac{1}{2} \left\{ \frac{\partial u_\theta}{\partial z} + \frac{1}{r} \frac{\partial u_z}{\partial \theta} \right\}$$

$$\epsilon_{zz} = \frac{\partial u_z}{\partial z} \qquad\qquad \epsilon_{zr} = \frac{1}{2} \left\{ \frac{\partial u_z}{\partial r} + \frac{\partial u_r}{\partial z} \right\} .$$

Compatibility equations for strain. If the components of <u>displacement</u> are given, then the components of strain can be found by appropriate partial differentiation, as indicated above. If, however, it is the components of <u>strain</u> which are given, then certain restrictions must be placed upon the strains in order to ensure that there are only three values of

26

displacement, and that the displacement field is continuous. These restrictions are called the compatibility equations, or compatibility conditions.

The compatibility conditions for strain can be written in general form as

$$\frac{\partial^2 \epsilon_{ij}}{\partial x_k \partial x_\ell} + \frac{\partial^2 \epsilon_{k\ell}}{\partial x_i \partial x_j} = \frac{\partial^2 \epsilon_{ik}}{\partial x_j \partial x_\ell} + \frac{\partial^2 \epsilon_{j\ell}}{\partial x_i \partial x_k} .$$

This expression represents 81 equations, only 6 of which are independent. The independent equations are:

$$\frac{\partial^2 \epsilon_{xx}}{\partial y^2} + \frac{\partial^2 \epsilon_{yy}}{\partial x^2} = 2 \frac{\partial^2 \epsilon_{xy}}{\partial x \partial y}$$

$$\frac{\partial^2 \epsilon_{yy}}{\partial z^2} + \frac{\partial^2 \epsilon_{zz}}{\partial y^2} = 2 \frac{\partial^2 \epsilon_{yz}}{\partial y \partial z}$$

$$\frac{\partial^2 \epsilon_{zz}}{\partial x^2} + \frac{\partial^2 \epsilon_{xx}}{\partial z^2} = 2 \frac{\partial^2 \epsilon_{zx}}{\partial z \partial x}$$

$$\frac{\partial^2 \epsilon_{xx}}{\partial y \partial z} = - \frac{\partial^2 \epsilon_{yz}}{\partial x^2} + \frac{\partial^2 \epsilon_{xz}}{\partial x \partial y} + \frac{\partial^2 \epsilon_{xy}}{\partial x \partial z}$$

$$\frac{\partial^2 \epsilon_{yy}}{\partial z \partial x} = - \frac{\partial^2 \epsilon_{zx}}{\partial y^2} + \frac{\partial^2 \epsilon_{yx}}{\partial y \partial z} + \frac{\partial^2 \epsilon_{yz}}{\partial y \partial x}$$

$$\frac{\partial^2 \epsilon_{zz}}{\partial x \partial y} = - \frac{\partial^2 \epsilon_{xy}}{\partial z^2} + \frac{\partial^2 \epsilon_{zy}}{\partial z \partial x} + \frac{\partial^2 \epsilon_{zx}}{\partial z \partial y} .$$

Elastic stress/strain relations. The stress/strain relations introduce the properties of the material into the consideration. For an isotropic elastic material the general relations can be written in compact form as:

$$\sigma_{ii} = 3K \epsilon_{ii}$$

$$\sigma'_{ij} = 2G \epsilon'_{ij} .$$

Alternatively, using E and ν and expanding for rectangular coordinates:

$$\epsilon_{xx} = \frac{1}{E} \{ \sigma_{xx} - \nu(\sigma_{yy} + \sigma_{zz}) \}$$

$$\epsilon_{yy} = \frac{1}{E} \{ \sigma_{yy} - \nu(\sigma_{xx} + \sigma_{zz}) \}$$

$$\varepsilon_{zz} = \frac{1}{E} \left\{ \sigma_{zz} - \nu(\sigma_{xx} + \sigma_{yy}) \right\}$$

$$\varepsilon_{xy} = \frac{1}{2G} \sigma_{xy} \quad , \quad \varepsilon_{xz} = \frac{1}{2G} \sigma_{xz} \quad , \quad \varepsilon_{yz} = \frac{1}{2G} \sigma_{yz} \quad .$$

Or, putting stress in terms of strain:

$$\sigma_{xx} = \frac{E}{1 + \nu} \left\{ \frac{\nu}{(1 - 2\nu)} \left(\varepsilon_{xx} + \varepsilon_{yy} + \varepsilon_{zz} \right) + \varepsilon_{xx} \right\}$$

$$\sigma_{yy} = \frac{E}{1 + \nu} \left\{ \frac{\nu}{(1 - 2\nu)} \left(\varepsilon_{xx} + \varepsilon_{yy} + \varepsilon_{zz} \right) + \varepsilon_{yy} \right\}$$

$$\sigma_{zz} = \frac{E}{1 + \nu} \left\{ \frac{\nu}{(1 - 2\nu)} \left(\varepsilon_{xx} + \varepsilon_{yy} + \varepsilon_{zz} \right) + \varepsilon_{zz} \right\}$$

$$\sigma_{xy} = 2G \, \varepsilon_{xy} \quad , \quad \sigma_{xz} = 2G \, \varepsilon_{xz} \quad , \quad \sigma_{yz} = 2G \, \varepsilon_{yz} \quad .$$

In cylindrical coordinates the relations can be written as:

$$\varepsilon_{rr} = \frac{1}{E} \left\{ \sigma_{rr} - \nu(\sigma_{\theta\theta} + \sigma_{zz}) \right\}$$

$$\varepsilon_{\theta\theta} = \frac{1}{E} \left\{ \sigma_{\theta\theta} - \nu(\sigma_{rr} + \sigma_{zz}) \right\}$$

$$\varepsilon_{zz} = \frac{1}{E} \left\{ \sigma_{zz} - \nu(\sigma_{rr} + \sigma_{\theta\theta}) \right\}$$

$$\varepsilon_{r\theta} = \frac{1}{2G} \sigma_{r\theta} \quad , \quad \varepsilon_{rz} = \frac{1}{2G} \sigma_{rz}, \quad \varepsilon_{\theta z} = \frac{1}{2G} \sigma_{\theta z} \quad .$$

The preceding sets of equations, together with the boundary conditions of the problem, provide everything needed for a solution. However, the various sets of equations can be transformed. For example, the equilibrium equations can be written for strain instead of stress by applying the stress/strain relations, and similarly the compatibility conditions can be given in terms of stress.

Linear viscosity

Linear viscosity is analogous to linear elasticity, and for any solution to an elastic problem there is, in principle, a corresponding solution to a viscous problem, provided certain conditions are met.

In developing the analogy, velocity of viscous deformation corresponds to elastic displacement, and viscous strain rate corresponds to elastic strain. The equilibrium equations remain unchanged, provided that there is slow flow with zero acceleration. The strain/displacement equations are replaced by strain-rate/velocity relations of identical form, i.e. $\dot{u}$ replacing u, and $\dot{\varepsilon}$ replacing ε. Again, there is a requirement for slow, non-accelerating flow. The elastic stress/strain equations are replaced by viscous stress/strain-rate equations. If the material is homogeneous and

28

isotropic, the viscous properties can be described by two constants, and it is convenient to choose these as a "bulk viscosity" η and a shear viscosity μ. Thus

$$\sigma_{ii} = 3 \eta \dot{\epsilon}_{ii}$$

$$\sigma'_{ij} = 2 \mu \dot{\epsilon}_{ij} .$$

For ice of low porosity, it may be permissible to assume incompressibility in a flow problem, i.e. η is infinite, and the viscous analogue of Poisson's ratio is 1/2.

Plane stress and plane strain

In this summary, the general relations have been given for three-dimensional stress and strain, but many problems can be simplified as two-dimensional problems. There are two ways of reducing to two dimensions. In plane stress, stresses in the z-direction are assumed to be zero, usually because the x-y planes at the z boundaries are free from normal stress. In plane strain, displacement gradients, or strains, in the z-direction are assumed to be zero, usually because the material is perfectly confined at the limits of z, or because the width of the body in the z-direction is effectively infinite.

FAILURE CRITERIA

As regards the behavior of a material, the meaning of the term "failure" is arbitrary. In other words, a material may be said to have "failed" when it ceases to meet certain arbitrary requirements. For example, when a typical engineering material fractures it clearly has failed. However, a material can fail without fracturing, and the definition of failure might be based on a transition from elastic deformation to plastic yielding, or on irreversible acceleration of strain rate, or on development of permanent strain, or yet again on the development of internal cracking. Whatever definition of failure is accepted, formal analysis requires specification of the stress or strain conditions which control the failure.

Plastic yielding of an isotropic, incompressible solid gives a fairly simple introduction to failure criteria.

Maximum shear stress criteria (Tresca/von Mises)

When typical metals are deformed at moderate rates, it is found that the bulk stress σ does not influence the onset of plastic yield to any significant extent. One reasonable assumption is that yielding occurs when the maximum shear stress, $(\sigma_1 - \sigma_3)/2$, reaches a critical value. This assumption, or postulate, is usually called the Tresca criterion, although it was put forward by Coulomb almost a hundred years before Tresca thought of it.

$$\sigma_1 - \sigma_3 = \text{constant}$$

29

Another reasonable postulate is that yielding will occur when the second invariant of the deviator stress, J_2, reaches a critical value. This criterion, attributed to <u>von Mises</u>, can be written

$$J_2 = \frac{1}{2}\left(\sigma_1'^2 + \sigma_2'^2 + \sigma_3'^2\right)$$

$$= \frac{1}{6}\left[\left(\sigma_1 - \sigma_2\right)^2 + \left(\sigma_2 - \sigma_1\right)^2 + \left(\sigma_3 - \sigma_1\right)^2\right]$$

$$= \text{constant} .$$

Another interpretation of the von Mises criterion, credited to Hencky or Huber, is that yielding occurs when the elastic strain energy of distortion reaches a critical value. Since J_2 and the octahedral shear stress $\sigma_{s\ oct}$ have a simple relationship to each other, the von Mises criterion can be written in terms of octahedral shear stress:

$$J_2 = \left(\frac{3}{2}\right) \sigma_{s\ oct}^2 = \text{constant}$$

i.e. yielding occurs at a critical value of $\sigma_{s\ oct}$. In uniaxial tension or compression, where $\sigma_2 = \sigma_3 = 0$, both the Tresca and Mises criteria require that plastic yielding sets in when the uniaxial stress σ_1 reaches a critical value Y, in either tension or compression. The corresponding value of the octahedral shear stress is $\sqrt{2}\ Y/3$. The Tresca and von Mises criteria differ somewhat when they are compared in detail. For example: 1) the intermediate principal stress σ_2 influences failure according to von Mises, but not Tresca, 2) the yield stress in pure shear is Y/2 according to Tresca, but $Y/\sqrt{3}$ according to von Mises, 3) the yield surface in principal stress space is a circular cylinder according to von Mises but a hexagonal prism according to Tresca, the longitudinal axis being the hydrostat line $\sigma_1 = \sigma_2 = \sigma_3$ in both cases (Fig. 11).
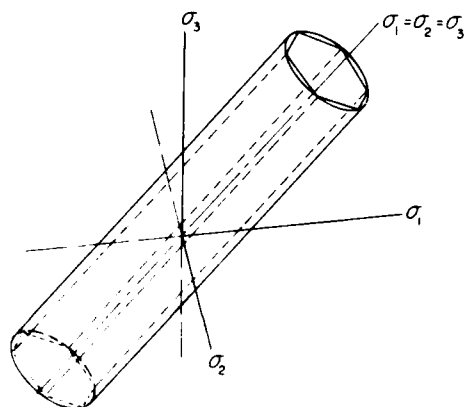
Figure 11. Failure surfaces in three-dimensional principal stress space for the Tresca and von Mises criteria.

30

Coulomb/Navier/Mohr criteria

The Tresca and von Mises criteria assume that hydrostatic pressure has no effect on the resistance to shear deformation. While this may be a good approximation for metals at moderate rates of loading, it is not true for materials generally. For many materials, especially brittle non-metallic solids, the resistance to shear deformation increases as the hydrostatic pressure increases. A yield criterion representing this type of behavior evolved from the work of Coulomb, with subsequent modifications that are associated with the names Rankine, Navier and Mohr. The Coulomb-Navier, or Coulomb-Mohr, criterion assumes that failure in an isotropic material is determined by the extreme principal stresses σ_1 and σ_3, with the intermediate principal stress σ_2 exerting no influence. It is usually developed for the two-dimensional case, making the physical assumption that shear resistance on a plane is proportional to the "friction" developed on that plane by normal stress. If the constant "friction coefficient" is denoted by μ or by $\tan \phi$, the criterion becomes

$$\sigma_1[(\mu^2 + 1)^{1/2} - \mu] - \sigma_3[(\mu^2 + 1)^{1/2} + \mu] = 2c$$

or,

$$\left(\frac{\sigma_1 - \sigma_3}{2}\right) - \left(\frac{\sigma_1 + \sigma_3}{2}\right) \sin\phi = c \cos\phi$$

where c is a constant identified as the inherent shear strength of the material under zero normal stress. Since $(\sigma_1 - \sigma_3)/2$ is the maximum shear stress and $(\sigma_1 + \sigma_3)/2$ is the mean stress, the criterion says that the maximum shear stress at yielding is equal to a constant plus a multiple of the mean stress (Fig. 12). It also appears to imply that the uniaxial compressive strength σ_c will differ from the uniaxial tensile strength σ_T by the factor:

$$\frac{\sigma_c}{\sigma_T} = \frac{(\mu^2 + 1)^{1/2} + \mu}{(\mu^2 + 1)^{1/2} - \mu}$$

but the implicit physical assumption that confining stress should be compressive limits the applicability of the criterion in the tension-compression quadrants, as shown in Figure 12b, where there is a cutoff at $\sigma_c/2$.

It might be noted that the Tresca criterion can now be regarded as a special case of the Coulomb-Navier, or Coulomb-Mohr, criterion with $\phi = 0$. Taking $\phi = 0$,

$$\left(\sigma_1 - \sigma_3\right) = 2c = \sigma_T = \sigma_C = Y .$$

The assumption that the increase of shear resistance is directly proportional to compressive bulk stress is, of course, an approximation. Experimental results show that the usual trend is for increases of confining stress to become less significant as the magnitude of the confining stress increases. In other words, the effective value of ϕ decreases as σ increases. A simple way to accommodate this effect is to assume that the

31
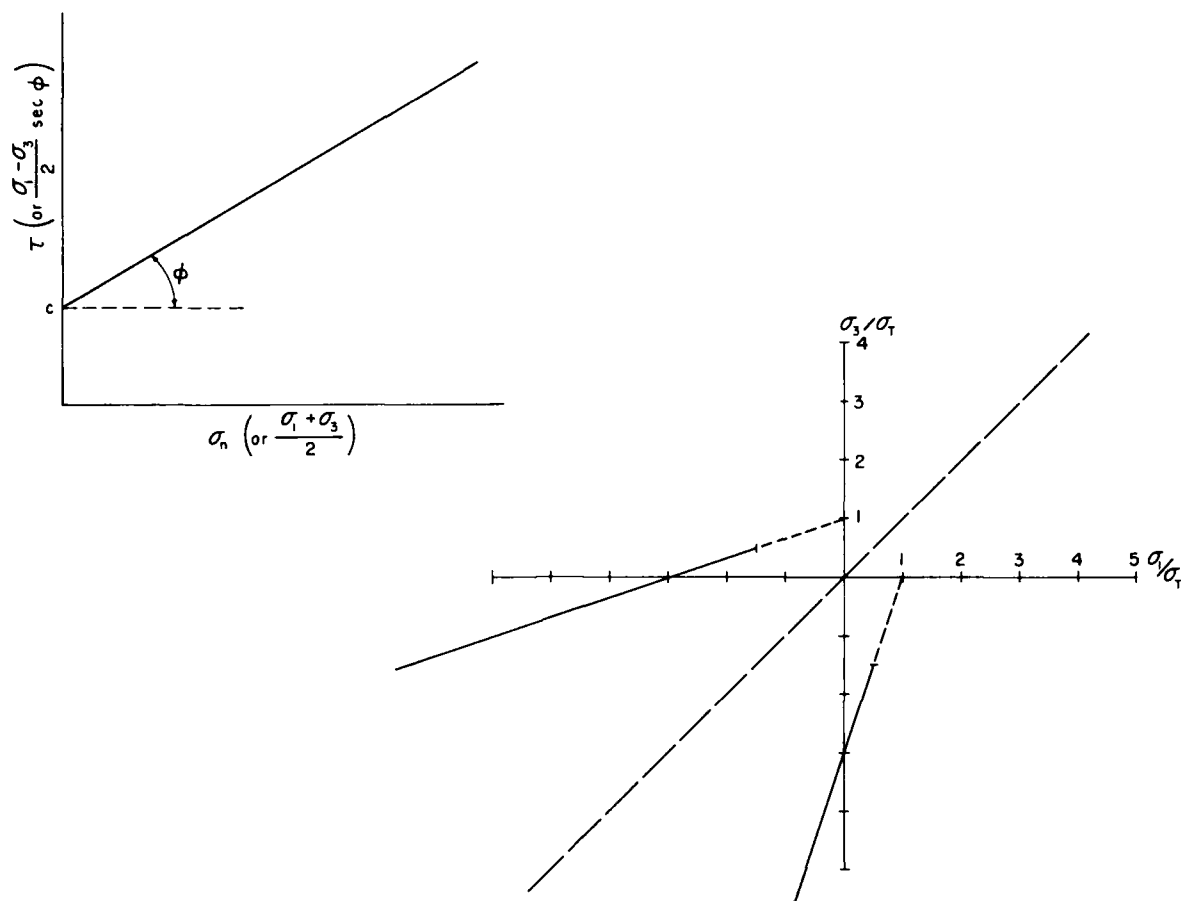
Figure 12. Linear Coulomb-Navier-Mohr criterion for $\phi = 30°$.

relation between shear resistance and bulk stress is parabolic or, in other
words, to assume a parabolic Mohr envelope. Assuming that failure is not
influenced by the intermediate principal stress, the form of the relation
is thus

$$(\sigma_1 - \sigma_3)^2 = A(\sigma_1 + \sigma_3) + B$$

where A and B are constants.

In terms of geometric representation, the two-dimensional linear
Coulomb-Navier criterion can probably be generalized to define a failure
surface in three-dimensional principal stress space. This surface would
take the form of a pyramid or cone, depending on whether the intermediate
principal stress is assumed to have an effect. The pyramid or cone has to
be truncated in the absence of knowledge (or speculation) about behavior in
the tension-tension quadrants of the principal stress planes. For a para-
bolic Coulomb-Navier criterion, the simplest generalization of the failure
surface is a paraboloid, with the hydrostat line $\sigma_1 = \sigma_2 = \sigma_3$ as the axis
of revolution and truncation at limits of the tension-tension quadrants
where $\sigma_1 = \sigma_T$, $\sigma_2 = \sigma_T$, $\sigma_3 = \sigma_T$. Within the domain where all stresses
are tensile, the simplest assumption is that the failure surface is a
pyramid with its apex at $\sigma_1 = \sigma_2 = \sigma_3 = \sigma_T$.

32

The Griffith criterion and its derivatives

The Tresca and von Mises criteria are empirical relations, while the Coulomb-Navier-Mohr criterion is based partly on physical reasoning. There are other criteria which derive more directly from physical reasoning and associated mathematical models, the most notable being the Griffith criterion.

Starting from the observation that the bulk strength of brittle solids is, in general, orders of magnitude lower than the theoretical strength deduced from consideration of interatomic forces, Griffith postulated the existence of minute cracks and associated stress concentrations. Drawing upon the stress analysis given by Inglis for a two-dimensional elliptic crack in an elastic plate, Griffith equated the change of potential energy in the plate to the change of surface energy in the crack as the crack grew in length. For a thin elliptic crack of length 2c:

$$\frac{\partial}{\partial c} \left(\frac{\pi \sigma^2 c^2}{E}\right) = \frac{\partial}{\partial c} (4c\gamma)$$

where E is Young's modulus for the plate, γ is the specific surface energy of the material and σ is the applied stress (tensile and perpendicular to the long axis of the crack) at which crack growth occurs. Thus

$$\sigma = \left(\frac{2}{\pi}\right)^{1/2} \left(\frac{E\gamma}{c}\right)^{1/2}$$

for plane stress. For plane strain the corresponding relation is

$$\sigma = \left(\frac{2}{\pi(1 - \nu^2)}\right)^{1/2} \left(\frac{E\gamma}{c}\right)^{1/2}$$

where ν is Poisson's ratio. Numerically, the two versions are not much different.* Much the same result is obtained by direct consideration of theoretical material strength and stress concentration at the end of an elliptic crack. From consideration of interatomic forces as a function of separation, the theoretical tensile strength of the material σ_* is

$$\sigma_* = \left(\frac{E\gamma}{a}\right)^{1/2}$$

where a is the atomic spacing in the unstrained state. From the Inglis stress analysis for an elliptic crack with tip radius ρ, the stress at the crack tip σ_{ct} is

$$\sigma_{ct} = 2\sigma \left(\frac{c}{\rho}\right)^{1/2}$$

where σ is the applied stress in the plate. Equating σ_{ct} to σ_* for crack growth:

* For a "penny-shaped" crack, $\sigma = [\pi/4(1-\nu^2)]^{1/2}(E\gamma/c)^{1/2}$, which is also not much different numerically.

$$\sigma = \left(\frac{\rho}{4a}\right)^{1/2} \left(\frac{E\gamma}{c}\right)^{1/2}$$

in which ρ is considered to be of the same order of magnitude as $\underline{a}$ for a sharp crack. This version is identical to Griffith's plane stress relation if

$$\rho = (8/\pi)\, a = 2.55\, a.$$

It might be mentioned in passing that γ can be reduced by adsorption of certain surface active chemicals; this is known as the Rehbinder Effect or the Joffe Effect.

Having derived a condition for crack growth under simple tension normal to the crack axis, Griffith considered a biaxial stress field and variable orientation of the crack relative to the principal directions of stress, thus determining the critical crack orientation for initiation of crack growth. This gave a failure criterion for material which contains numerous cracks with random orientation:

$$\left(\frac{\sigma_1 - \sigma_3}{2}\right)^2 + 4\,\sigma_T\left(\frac{\sigma_1 + \sigma_3}{2}\right) = 0$$

if $3\sigma_1 + \sigma_3 < 0$

and

$$\sigma_1 = \sigma_T$$

if $3\sigma_1 + \sigma_3 > 0$

where σ_T is the uniaxial tensile strength, and $\sigma_1 > \sigma_3$ (tension positive). One of the implications of this criterion is that

$$\left|\frac{\sigma_c}{\sigma_T}\right| = 8.$$

Another point worth noting is that the Griffith criterion for $3\sigma_1 + \sigma_3 < 0$ is identical in mathematical form to the parabolic variant of the Coulomb-Navier-Mohr criterion. It can be generalized in three dimensions as a paraboloid, as already described for the parabolic Coulomb-Navier criterion.

Analysis of the three-dimensional Griffith criterion (Murrell 1963, Jaeger and Cook 1976) gives the relation for $3\sigma_1 + \sigma_3 < 0$ as:

$$\left(\frac{\sigma_1 - \sigma_2}{2}\right)^2 + \left(\frac{\sigma_2 - \sigma_3}{2}\right)^2 + \left(\frac{\sigma_3 - \sigma_1}{2}\right)^2 + 18\sigma_T\left(\frac{\sigma_1 + \sigma_2 + \sigma_3}{3}\right) = 0.$$

This gives a ratio of uniaxial compressive strength σ_c to uniaxial tensile strength σ_T that is different from the ratio for the two-dimensional criterion:

$$\left|\frac{\sigma_c}{\sigma_T}\right| = 12 \ .$$

It also allows some different predictions to be made for multiaxial stress states, i.e. for the biaxial stress state when $\sigma_2 = 0$, for the conventional triaxial test condition when $\sigma_2 = \sigma_3$, and for the triaxial state where $\sigma_1 \neq \sigma_2 \neq \sigma_3$.

In recent times investigators have proposed various modifications to the older failure criteria in order to meet special requirements for rocks, polymers, and other materials. For example, the McClintock-Walsh criterion in rock mechanics comes from a modification of the Griffith analysis. It is assumed that when flat cracks are closed by pressure, friction develops between their faces. The resulting limit equation is identical to the Coulomb-Navier criterion if $2\sigma_T$ is substituted for the cohesion c.

A more interesting criterion for present purposes is a generalization of the two-dimensional Griffith criterion made by Babel and Sines (1968), who allowed the ellipticity of the idealized Inglis crack to vary so as to represent straight cracks, circular holes, and all elliptic shapes in between these limits. If σ_* is the theoretical strength of the material, a and b are the major and minor semiaxes of the elliptic crack respectively, and a/b = r, then consideration of stresses and critical ellipse orientations gives the following relations:

$$(1 + 2r)\ \sigma_1 - \sigma_3 = \sigma_*$$

when the major axis of the ellipse is normal to the direction of σ_1, and

$$\left(\frac{\sigma_1 - \sigma_3}{2}\right)^2 + \frac{2r}{(r+1)^2}\ \sigma_* \left(\frac{\sigma_1 + \sigma_3}{2}\right) = 0$$

for other orientations. The latter is obviously a parabolic relation of the same mathematical form as the Griffith criterion and the parabolic Coulomb-Navier-Mohr criterion. The transition between the regions of applicability for the first and second equations is given by

$$\sigma_1 + \left(\frac{r-1}{3r+1}\right)\ \sigma_3 = 0 \ .$$

Application of the first equation to the uniaxial tensile test ($\sigma_1 = \sigma_T$, $\sigma_3 = 0$) gives

$$\frac{\sigma_*}{1 + 2r} = \sigma_T$$

and application of the second equation to the uniaxial compression test gives

$$\frac{2r}{(r+1)^2}\ \sigma_* = \frac{\sigma_c}{2}$$

35

and the ratio of σ_c to σ_T is thus

$$\left|\frac{\sigma_c}{\sigma_T}\right| = \frac{4r(1 + 2r)}{(r + 1)^2} .$$

A case that is of special interest is the one where the elliptic crack becomes a circular (or cylindrical) hole, with $r = 1$. The ratio σ_c/σ_T then becomes 3, as can be shown more directly by analysis of a circular hole in an elastic plate.

An important, and often overlooked, point about Griffith theory and its derivatives is that these theories treat the <u>onset</u> of crack growth, implicitly defining the start of crack growth as failure. In reality, while the beginning of internal crack growth may represent the <u>start</u> of the failure process, the applied stress needed to reach this stage may be far below the short-term structural strength of a test specimen.

Orowan/Irwin modifications of Griffith theory

Griffith developed his theory primarily to explain the properties of glass, and it was believed to be generally applicable to brittle solids. However, if the strength equations which contain the surface energy γ are applied to metals or polymers the predicted strength is very much lower than the actual strength of the real material. This can be explained by plastic yielding at critical stress concentrations, which has the effect of blunting the cracks.

In the late forties, Orowan and Irwin independently modified the Griffith equation for strength by taking into account the energy dissipated in localized plastic yielding, while at the same time retaining the elastic analysis for the overall effect of a crack because the plastic yield zones were considered small relative to the crack length. Orowan substituted for the surface energy γ a term which included a specific energy for plastic working γ_p:

$$\sigma = \left(\frac{2}{\pi}\right)^{1/2} \left(\frac{E(\gamma + \gamma_p)}{c}\right)^{1/2} \approx \left(\frac{2}{\pi}\right)^{1/2} \left(\frac{E\gamma_p}{c}\right)^{1/2}$$

for plane stress. The approximation follows from the fact that $\gamma_p \gg \gamma$. Irwin expressed the same idea by denoting the critical rate of change of energy with crack length by a parameter G_c. Being an energy per unit area, G_c has the dimensions of force per unit length, and it is referred to as a crack extension force. In the Irwin formulation

$$\sigma = \left(\frac{1}{\pi}\right)^{1/2} \left(\frac{EG_c}{c}\right)^{1/2}$$

for plane stress. Thus the Orowan and Irwin expressions are identical with

$$G_c = 2(\gamma + \gamma_p) .$$

36

At this stage in the development of theoretical ideas it may seem that the elegant simplicity of Griffith's original ideas has been clouded by black magic, but as far as the failure criteria are concerned, the general approach probably remains valid for fracture which is not perfectly brittle.

FRACTURE MECHANICS AND FRACTURE TOUGHNESS

The name "fracture mechanics" has come to be used, somewhat restrictively, for study of the effect of cracks on the bulk strength of solid materials. It derives from the theory of Griffith, and from the later modifications of that theory by Irwin and Orowan. These theoretical ideas have already been introduced as part of the discussion of failure criteria.

Analysis of crack extension

Griffith's original idea was that fracture occurred when a crack extended without limit because an increment of crack extension involved a gain of surface energy U_s less than the drop of potential energy of the surrounding elastic material U_p:

$$\left| \delta U_p \right| > \left| \delta U_s \right| .$$

Irwin and Orowan introduced the idea of energy dissipation by plastic yielding at a crack tip (δW_p) and the possibility of external work input to the system (δW_e), making the critical energy balance

$$\delta U_p + \delta W_e \geq \delta U_s + \delta W_p .$$

Since $\delta W_p \gg \delta U_s$ and δW_e is, for all practical purposes, zero, the condition simplifies to

$$\delta U_p \geq \delta W_p .$$

The change of potential energy δU_p as the crack extends by an increment of length δx can be equated to a unit force G multiplied by δx:

$$\delta U_p = G \, \delta x$$

or

$$G = \frac{\delta U_p}{\delta x} .$$

This is Irwin's crack extension force, which was mentioned earlier. From elastic analysis, the critical value G_c for unstable crack extension is

$$G_c = \frac{\pi c}{E} \sigma^2$$

37

for plane stress, and

$$G_c = \frac{\pi(1 - \nu^2)c}{E}\, \sigma^2$$

for plane strain, where σ is the applied stress at failure.

Analysis of the stress distribution around an idealized crack in an elastic plate gives stress fields that are geometrically similar for geometrically similar "cracks." The absolute magnitude of a given stress component is proportional to the stress applied to the plate, σ, and it is also proportional to the square root of a characteristic linear dimension of the crack, such as the half-length of the major axis c. Thus the effects of geometric scale and stress level can be expressed by a stress intensity factor K which contains the product $\sigma \times \sqrt{c}$. For convenience, K is defined as

$$K = \sigma(\pi c)^{1/2} .$$

This is obviously another way of expressing the crack extension force G. In terms of the critical values for failure, K_c and G_c:

$$G_c = \frac{K_c^2}{E}$$

for plane stress, and

$$G_c = \frac{K_c^2 (1 - \nu^2)}{E}$$

for plane strain.

Modes of displacement and crack propagation

In this summary of crack analyses the basic ideas have been developed with reference to the opening or closing of a two-dimensional crack in a plate that is under uniaxial tension or compression. However, in fracture mechanics three distinct types of crack motion are recognized (Fig. 13).
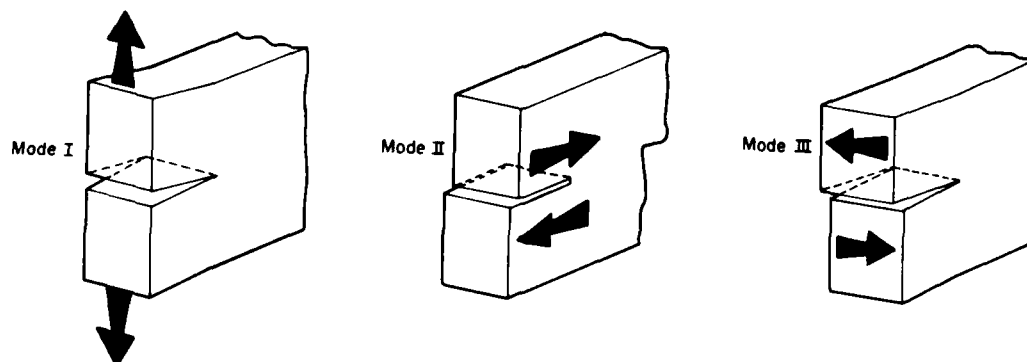
Figure 13. Displacement and crack propagation modes.

Mode I is the simple separation considered for the foregoing discussion. Mode II is in-plane shearing displacement, with opposite faces of a flat crack sliding across each other in the direction of the crack's major axis. Mode III involves twisting, and sliding of opposing crack faces in a direction normal to both axes of the two-dimensional crack. As far as materials testing is concerned, interest centers on Mode I, and virtually all test methods are designed to extend cracks according to Mode I. The critical value of the stress intensity factor for Mode I is denoted by K_{Ic}.

Toughness

Toughness is a poorly defined concept in engineering, but traditionally it has been associated with the capacity of a material to absorb energy before fracturing. Clearly energy alone, as represented by the area under a stress/strain curve, is not an adequate measure of toughness, since high strength and small failure strain could indicate a large energy for a very brittle material. Perhaps the best way to define and measure toughness is in terms of the ability to dissipate energy before fracturing. In other words, toughness can be associated with the integral of stress multiplied by inelastic strain, or with total strain energy minus the recoverable strain energy.

In fracture mechanics toughness, or fracture toughness, is defined as the critical value of the Irwin parameter G, which is also known as a "crack extension force." G, or G_c, has the dimensions of energy per unit area and it is, in fact, equal to the effective specific surface energy for fracture, γ, as pointed out earlier. However, with fine disregard for language and logic, many practitioners of fracture mechanics refer to the critical stress intensity factor K_c as the fracture toughness of a material, even though K_c has dimensions which have no direct relation to any reasonable definition of toughness.
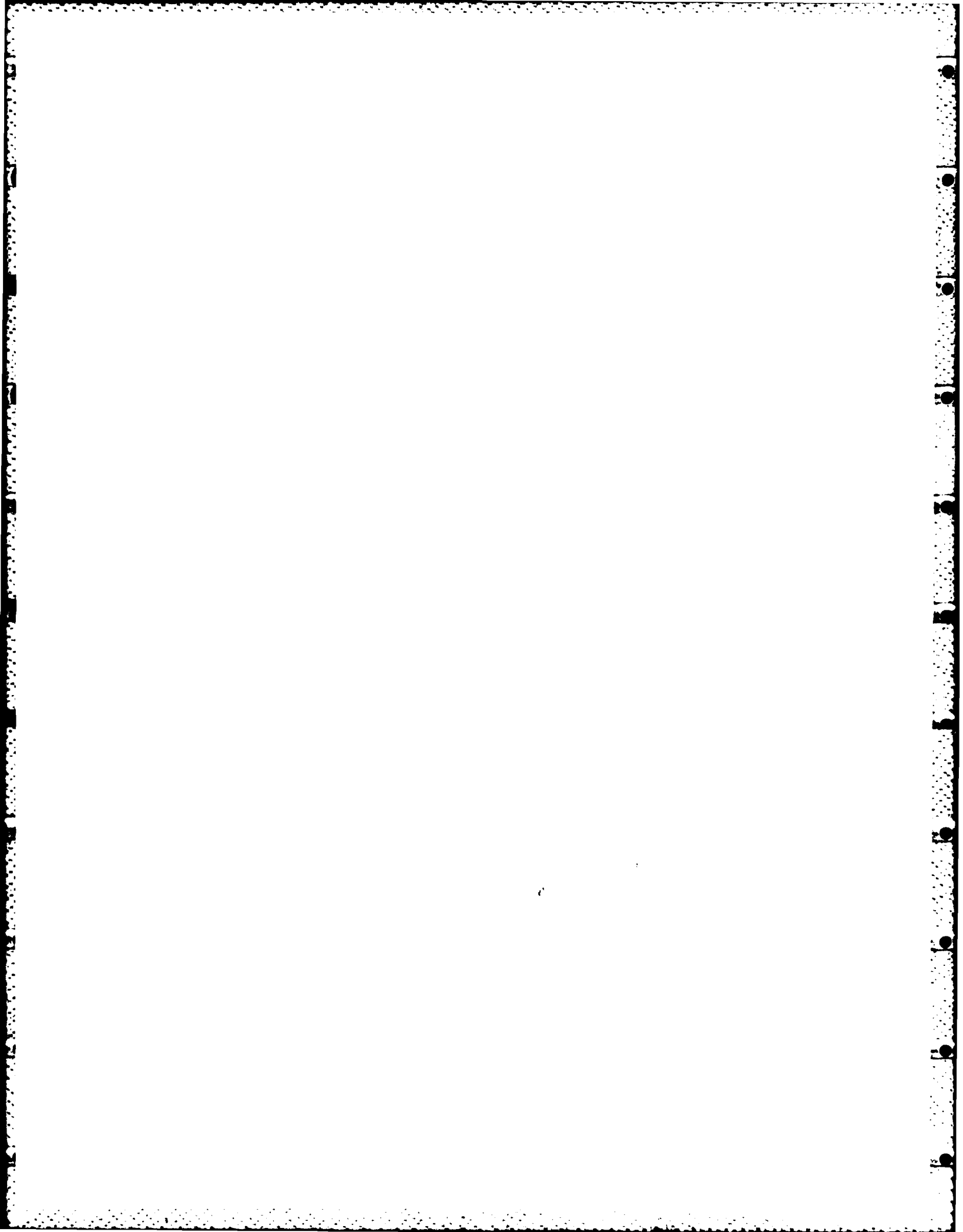
PART II. THE MECHANICAL PROPERTIES OF ICE

Ice tends to display rather complicated mechanical properties, largely because it exists in nature at high homologous temperatures, commonly above 0.95, and almost always above 0.9. It behaves elastically when deformed at high strain rates, or when loaded for very brief periods but, under sustained loadings which induce deviatoric stresses and strains, ice behaves inelastically, experiencing large irreversible strains. Under constant stress ice creeps, the strain rate varying with time and strain. At any given stage of the creep process, the relationship between strain-rate and stress is strongly nonlinear, which means that the ice is viscoplastic rather than linearly viscous.

Because ice properties are so sensitive to strain rate and temperature, strength varies greatly, depending on the prevailing conditions. The general effects of multiaxial stress states, as represented by failure criteria, also change drastically as strain-rate and temperature vary.

For non-saline ice, mechanical properties have to be specified as functions of temperature, strain rate (or stress rate), porosity, grain size, and grain structure. All of these variables remain important for sea ice, and in addition there are the complications of salinity, variations of brine volume with temperature, and geometry of the pore structure.

It is not yet possible to give a clear and complete description of the mechanical properties of non-saline ice, since more and better experimental data are needed. For sea ice the situation is worse, because the material is inherently more complicated than freshwater ice, and because experimental investigations still have a long way to go. In the following notes an attempt is made to piece together a coherent story, not only by summarizing experimental data, but also by deliberately ignoring some experimental results which seem to be incorrect or misleading.

DEFORMATION AND FAILURE UNDER CONSTANT STRESS OR CONSTANT STRAIN-RATE

Much of what is known about the rheology and strength of ice has been derived from laboratory experiments. The two most common tests involve uniaxial compression of a right circular cylinder, with either load or displacement rate held constant. With constant load, which for small strains approximates constant stress, the test is the classic creep test, which has been favored by glaciologists interested in long-term flow under low deviatoric stress. With constant displacement rate, which approximates constant strain rate, the test is the traditional strength test, which is important in ice engineering problems involving rapid loading to failure. For comparable ranges of stress and strain-rate, the two tests ought to provide essentially the same information, as discussed later.

41

Constant stress tests

At high temperatures and relatively low stress (< 1 MPa) the creep of non-saline fine-grained ice appears to be purely ductile, with no apparent formation of internal microcracks. The general form of the creep curve, plotted according to long-established conventions, is as shown in Figure 14. If good test data are available, more informative curves can be obtained by plotting strain <u>rate</u> $\dot{\varepsilon}$ against either time t or strain ε, as indicated in Figure 15 for strains greater than 0.1%. A very interesting fact then emerges: the failure strain for ductile yield, as indicated by the point of minimum strain rate, is more or less constant at approximately 1% axial strain.

If the applied stress is relatively high, say greater than 1 MPa, deformation occurs both by plastic straining of the ice and by internal cracking. In fine-grained ice, cracks begin to form at small strains, and the highest rate of crack formation occurs before the yield point near 1% is reached. Although creep data for small strains are sparse, it appears that there may be another strain rate minimum in the creep curve at very small strains.
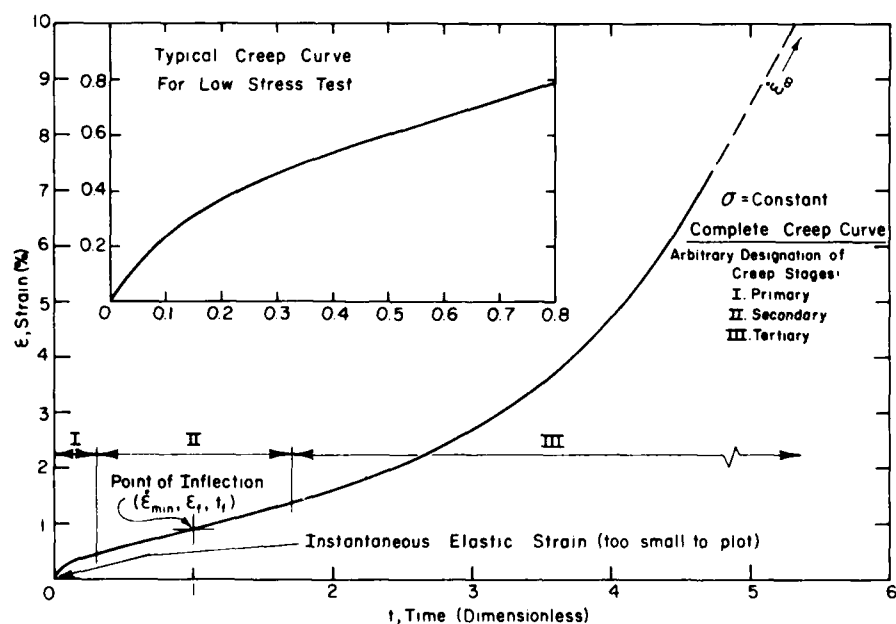
Figure 14. Idealized creep curve for constant stress test on polycrystalline ice.
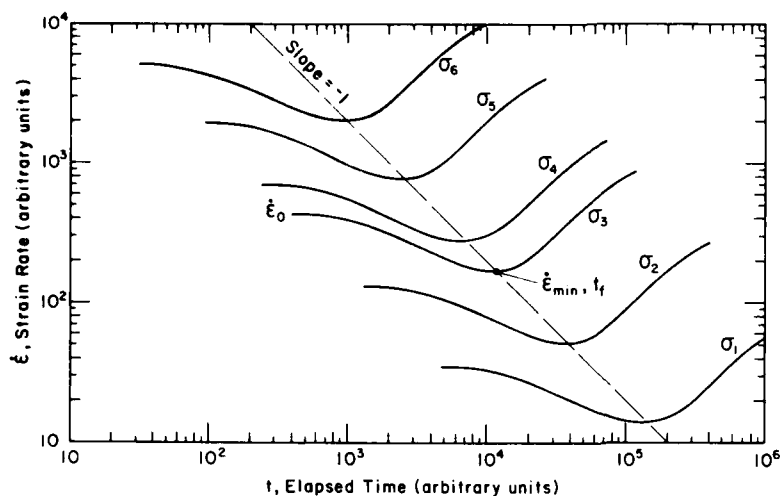
a. Log strain rate is plotted against log time.
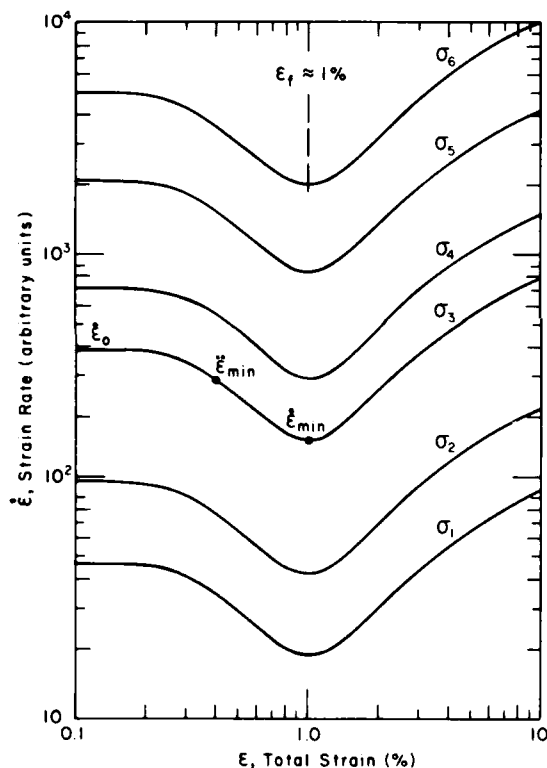
b. Log strain rate is plotted against log strain, for strains greater than 0.1%.

Figure 15. Idealized creep curves for polycrystalline ice that is initially isotropic.

Constant strain-rate tests

Constant rate tests are usually limited to fairly high applied strain rates ($> 10^{-7}$ s^{-1}) for practical reasons. The resulting stress/strain curves for non-saline fine-grained ice often show two yield points (Fig. 16): an initial yield point associated with the onset of internal cracking, and a secondary yield point associated with final ductile failure. The relative magnitudes of stress at the two yield points vary a good deal, and at very high strain rates the initial yield becomes dominant. As long

43
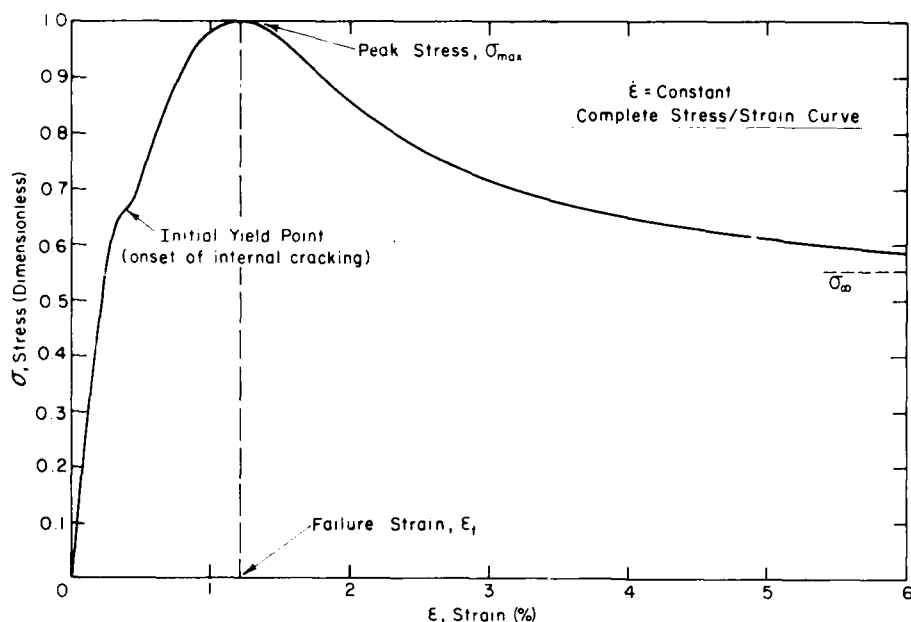
Figure 16. Idealized stress/strain curve for constant
strain-rate test on fine-grained ice.

as there is a secondary yield, it occurs at axial strains close to 1%. By
contrast, the strain at the initial yield point increases with increasing
strain rate.

Columnar-grained ice with relatively large grains seems to behave
differently than fine-grained isotropic ice. Yielding usually occurs at
small strains, and no secondary yield point appears on the stress/strain
curves. In metals, a stress/strain curve with two yield points is con-
sidered to represent ductile failure, and for given conditions it is
regarded as characteristic of fine-grained material. The same polycrystal-
line metal with larger grain size may, under the same conditions, suffer
brittle fracture, giving a stress/strain curve which terminates at the
first yield point.

Comparison of data from constant stress tests
and constant strain-rate tests

The correspondence between creep curves and stress/strain curves has
been discussed in detail elsewhere (Mellor and Cole 1982, 1983). For
present purposes it is sufficient to note that a strain-rate minimum on a
creep curve corresponds to a peak on a stress/strain curve. To a first
approximation, the stress/strain-rate relations given by strain-rate minima
in creep are the same as stress/strain-rate relations given by peaks on
stress/strain curves. The significance of this for sea ice studies is that
the very sparse data from creep tests can be supplemented by "creep data"
derived from "strength tests."

44

MEASUREMENT OF THE MECHANICAL PROPERTIES OF ICE

Mechanical tests on ice are intended to provide information on the strength of the material (failure criteria), and on the stress/strain/time relations (constitutive relations). In principle and in practice, it is very difficult to design and execute truly valid tests. The full ranges of ideal tests required by a theoretical mechanician are not practically feasible, especially for anisotropic material, but simple tests which suffice for some other engineering materials are not always adequate for ice. Thus the real aim is to devise tests which are both valid and manageable, and this demands a thorough understanding of both the behavior of ice, and the detailed mechanics of the test. The following notes do not describe tests in detail, nor do they give recommendations on test procedures. The intention is to indicate where caution may be called for, and where detailed information can be found. Some test guidelines have been drawn up and published by an international group (Schwarz et al. 1981), but these may change as techniques and equipment improve.

Uniaxial compression

Uniaxial compression is a much-maligned test which remains the most useful one for engineering purposes. Although apparently very simple, it is difficult to do well at high strain rates because of stress concentrations and stress field perturbations at and near the end planes, where load is applied. When a specimen in the form of a right circular cylinder is used , direct contact between the ice and steel platens is usually unsatisfactory for strain rates approaching and exceeding 10^{-3} s^{-1}, even when the specimen end planes are machined flat and square to close tolerances. Interface cushions of thin "crushable" material (such as paper or thin cardboard) may help, but cushions of "extrudable" material (such as rubber or soft plastic) are undesirable because they can introduce tensile radial stresses.

For simple field tests, special end caps filled with radially confined compliant material are useful (Haynes and Mellor 1977). For high-quality laboratory tests, bonded end caps are satisfactory (Mellor and Cole 1982), and if tests are to be run to large strains (several percent axial) a carefully designed dumbbell specimen with bonded end caps gives good results (details to be published later).

Measurements of axial strain are best made within the central section of the specimen itself for small strains (< 1%), but for large strains demountable displacement transducers have to be attached to the end caps to avoid undue disturbance of the transducers' attachments. So far, bonded strain gages have not been used successfully, but with some development effort this situation could change, especially on large specimens where some surface disturbance can be tolerated.

Radial or circumferential strain should be measured at the mid-section of the specimen, noting that the mid-section moves relative to the loading platens and the end caps as the specimen strains axially. If the radial strain transducer is in contact with the ice, its contact points must be free to travel axially with the ice. If non-contact proximity gauges are used, some axial displacement between the pickup and the targets can be tolerated.

45

Uniaxial tension

The only reliable way to measure the uniaxial tensile strength of ice is by direct application of uniaxial stress in the classic test. Tests depending on flexure, or on diametral compression of discs, cylinders or annuli, are indirect, in that the stress field has to be calculated from elastic theory, and a failure criterion has to be assumed. In other words, in an indirect test it is necessary to assume mechanical properties in order to measure mechanical properties.

In making a uniaxial tensile test on ice, the main difficulty is gripping the specimen and straining it while maintaining true uniaxial stress in the test section. The specimen is attached to end caps by mechanical grips or by adfreeze bonding. Whatever method is used, it will certainly create a triaxial stress field near the end caps, and if the specimen is a simple right circular cylinder it is likely to fracture near the end caps, in a stress field which is not uniaxial. Thus it is necessry to use dumbbell specimens for high quality laboratory tests. The fillet radius of a dumbbell specimen controls the stress concentration in the transition zone. If D is the diameter of the specimen "neck," a fillet radius of 8D gives a stress concentration factor of 1.02, and a fillet radius of 1.4D gives a factor of 1.05. Photoelastic model tests and practical experience indicates that a fillet radius of 2D is satisfactory for ice (Hawkes and Mellor 1972). Precise dimensional tolerances for the specimen and the pulling device are important, and avoidance of eccentricity or twist in the pulling systems is essential.

The considerations relating to measurement of axial and radial strain are essentially the same as those for uniaxial compression.

Shear tests

Shearing deformation is obviously very important. However, direct shear tests tend to be poorly understood, and in many cases simplistic and ill-conceived.

In plane stress or plane strain, pure shear exists when the in-plane principal stresses are equal in magnitude and opposite in sign. It is not easy to make a test which gives these conditions.

The usual experimental approach is to impose so-called "simple shear," using a prismatic specimen. A slab or block of the test material is deformed in such a way that its longitudinal cross section is changed from a square to a rhombus, or from a rectangle to a parallelogram, with zero normal stress on the surfaces which are subject to traction. This can be done with a suitably designed parallelogram frame, but there will be some perturbation of the stress field near the surfaces of the shearing plates. One research group has sheared ice by means of parallel plates which are maintained at constant separation by steel balls running in vee-grooves. This is suitable for shearing a deck of cards, but not an isotropic deformable solid.

Direct shear tests are often intended to measure the effect of normal stress on shear resistance. The general idea is to distort a specimen as

for "simple shear," while applying normal stress to the traction surfaces. The traditional shear box used in soil mechanics is intended for this purpose, but it perturbs the stress field and forces failure along a particular plane. Similarly, tests which use a segmented steel cylinder to fail a cylindrical specimen in double shear are unacceptable.

A more appealing method for applying shear deformation directly is torsion of a hollow cylinder, with or without axial forces or surface pressures. In practice, torsion tests on ice are very difficult.

It is not necessary to apply surface tractions or to induce direct shear in order to define deviatoric stress/strain relations and failure criteria. Tests which induce deviatoric strains by controlling principal stresses can provide the required information.

Beam flexure tests

Beam flexure is used to measure the strength of ice, and the elastic modulus. Tests are made in the laboratory on small beams, and field tests are made on large beams (often in situ), using either simple beams (in 3-point or 4-point bending) or cantilevers. Since it is usually assumed that the ice is linearly elastic, with equal moduli in tension and compression, the tests should be of very short duration (of the order of 1 s or less). For beams tested in situ, there are often steep temperature gradients within the beam, and buoyancy effects may be important. The ends of in situ beams sawn in an ice sheet are not rigidly encastré; flexure of the beam can flex the adjacent ice to some extent. Thus the proportions of the beam are important, and stress-concentrating corners at the beam root have to be considered. The IAHR recommendations suggest that beam length should be 7 to 10 times the ice thickness, and beam width should be 1 to 2 times the ice thickness (Schwarz et al. 1981).

A beam breaks when the ice fails in tension at the convex surface, and the resulting crack propagates through the thickness of the beam. The critical tensile stress is first reached at the surface, and the crack propagates through ice which has a stress gradient. The calculated value of this tensile stress is usually significantly different from the uniaxial tensile strength of bulk material, not only for ice but for most non-metallic materials. Thus it is termed the "flexural strength" or "modulus of rupture" to avoid confusion.

The elastic assumption is justifiable for high strain rates and low temperatures, but it is completely unrealistic for low strain rates and high temperatures. Thus beam flexure tests cannot really be used to determine variations of tensile strength with strain rate or temperature.

Diametral compression tests

When a solid cylinder or a disc of elastic material is squeezed from opposite ends of a diameter, the center section of the diametral plane experiences a tensile principal stress at right angles to the loading direction, and a compressive principal stress parallel to the loading direction. The magnitude of the compressive stress is three times that of

47

the tensile stress. If contact stresses at the loading platens are proper-
ly controlled, a disc or cylinder of brittle material will fail by
splitting, with the crack initiating at the center of the specimen.

For a "Griffith type" material, in which the ratio of uniaxial com-
pressive strength σ_c to uniaxial tensile strength σ_T is 8 or greater,
the tensile stress is equal to the uniaxial tensile strength, even though
failure occurs in a biaxial stress field (see section on Griffith theory).
However, in ice $\sigma_c/\sigma_T < 8$, and the critical stress induced by elastic
compression of a disc or cylinder is not equal to the uniaxial tensile
strength. The calculated tensile failure stress is $2P/\pi dt$, where P is
applied force at failure, d is disc diameter, and t is disc thickness.
This stress is much smaller than σ_T, and the test result probably has to
be interpreted in terms of the failure envelope for a biaxial stress field,
with $\sigma_1 = -\sigma_3/3$, and $\sigma_2 = 0$.

The other diametral compression test which has been applied to ice
involves diametral compression of an annulus. This is a rather complicated
test, and as far as is now known it does not give a useful measure of
tensile strength for ice or any other material (Mellor and Hawkes 1971).

Conventional triaxial tests

The test which is usually known as a triaxial test is similar to a
uniaxial compression test, but with radial pressure applied to the specimen
by means of gas or liquid in a confining cylinder. The stress state is
triaxial, but $\sigma_2 = \sigma_3$. The test is usually performed as a "strength test,"
with σ_1 increasing at approximately constant rate, and frequently with some
confusion about the time relations for σ_2 and σ_3. The test can also be
carried out as a constant stress creep test.

The triaxial test has not been used to any great extent in ice test-
ing, but it is potentially an important test. New equipment and techniques
are being developed at CRREL.

Mixed tension/compression triaxial tests

An interesting variant of the conventional triaxial test is a test in
which cell pressure alone is used, but the test specimen has a dumbbell
shape. Pressure acting axially on the flared ends of the specimen induces
axial tension, while at the same time the pressure exerts a radial
compressive stress. Thus the specimen fails with σ_1 tensile and σ_2, σ_3
compressive, giving a point on the failure envelope for the
tension-compression quadrants of principal stress space. The ratio of σ_1
to σ_2, σ_3 can be varied by changing either the neck diameter of the
specimen, or the diameter of the end caps. A pressure cell for making
tests of this kind was developed by I. Hawkes and D. Garfield at CRREL, and
tests were made by F.D. Haynes (1973).

Polyaxial compression tests

In a true triaxial, or polyaxial, test $\sigma_1 \neq \sigma_2 \neq \sigma_3 \neq 0$. The test
specimen has to be a cube, and all faces have to be free of surface
tractions. For tests on a "creepy" material such as ice, the loading

actuators which apply σ_1, σ_2 and σ_3 all have to be programmable with respect to time.

The only known polyaxial tests on ice are those done by Häusler (1981). Load is applied to each face of the specimen by a "brush" platen, which consists of a cluster of slender metal columns, each free to deflect sideways independently of its neighbors. As there is no access to any of the surfaces, strains are obtained directly from platen displacements.

Fracture toughness tests

Although there are three distinct modes of displacement for crack propagation (see section on Fracture Mechanics), only the tensile Mode I is used in testing. The general procedure is to propagate a crack in a tensile stress field, and sometimes to arrest the crack.

A form of test that has been used widely for ice involves four-point bending of a beam into which a "crack" has been cut on the tension side. Another popular test is one based on the so-called Compact Tension Specimen. This is a block with a sawcut, and it is pulled, or torn, apart. For crack-arrest measurements a slender wedge is forced into a sawcut, propagating a crack which eventually stops as the stress drops back, to a low level. All of these tests assume linear elastic response in the test material, and it seems likely that they could give misleading results for low strain rates and high temperatures.

THE ELASTIC MODULI OF ICE

Since ice is markedly viscoelastic at the temperatures and strain rates which have often been used in conventional strength tests (say $-5°$ to $-10°C$ and 10^{-4} to 10^{-3} s^{-1}), a conventional stress/strain curve does not give an accurate measure of the elastic modulus. For example, a uni-axial test under constant strain rate, either in compression or tension, is likely to yield a stress/strain curve which is "convex up," i.e. $d\sigma/d\varepsilon$ decreases as σ and ε increase (Fig. 17). Thus the "tangent modulus," given by $d\sigma/d\varepsilon$ at some arbitrary point on the curve, may have little relation to the true Young's modulus. Similarly the overall secant modulus, represent-ing the average slope of the stress/strain curve from the origin to the peak stress, may be very different from the true Young's modulus. In principle, the initial tangent modulus, $(d\sigma/d\varepsilon)_{\varepsilon=0}$, should be equal to Young's modulus, but with typical test data the initial tangent modulus cannot be read accurately from a stress/strain curve. In fact, unless strain measurements are made on the test specimen itself (instead of across the platens of the testing machine), the initial tangent modulus cannot be measured at all. However, with good test data, $d\sigma/d\varepsilon$ can be calculated as a function of σ or ε, and when $d\sigma/d\varepsilon$ is plotted against σ or ε the zero intercept gives a value which ought to approximate Young's modulus.

A much simpler way to study Young's modulus and its variation with temperature, salinity, air content and so forth is to use high frequency vibrational methods. These may involve the propagation of small-amplitude waves or pulses in laboratory specimens or large natural ice masses, or they may involve flexural or torsional oscillations of beams or cylinders.
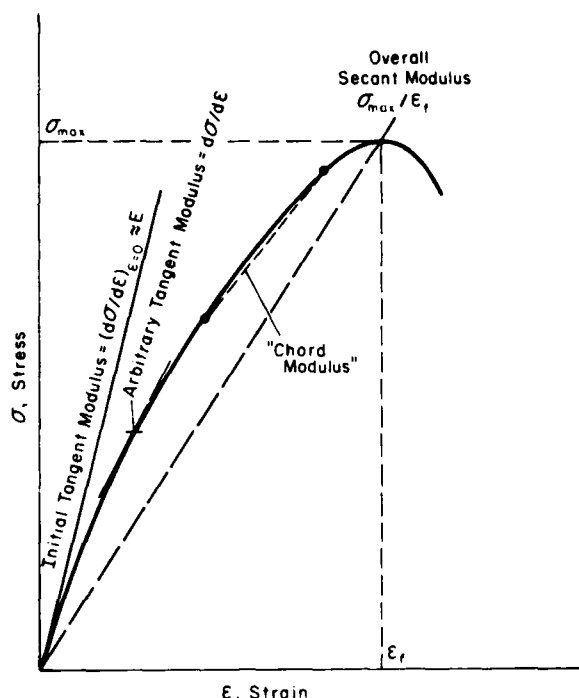
49

Figure 17. Modulus definitions for nonlinear stress/strain characteristic

For polycrystalline ice of low porosity (density $\rho \to 0.917$ Mg/m^3), high frequency dynamic measurements of Young's modulus E give values of approximately 9.0 to 9.5 GPa in the temperature range $-5°$ to $-10°$C. Careful measurements of the initial tangent modulus for uniaxial compression tests have given values very close to the dynamic values of E (9-10 GPa) for ice of similar type (e.g. Gold 1958, Hawkes and Mellor 1972, Sinha 1978 a,b). Much higher values of initial tangent modulus (up to 25 GPa) have been reported by Haynes (1978), but so far there is no independent confirmation (the highest values exceed theoretical values for a perfect monocrystal).

Temperature does not have a strong effect on the true Young's modulus of non-saline ice. As temperature decreases, E increases nonlinearly, as indicated in Figure 18.

The value of E does vary significantly with porosity in non-saline ice, and we would expect a similar effect in sea ice. The porosity of sea ice derives from two sources: 1) the air bubbles, which do not vary much in volume as temperature changes, and 2) the brine cells, which adjust their volume so as to preserve phase equilibrium as temperature changes. In most studies on sea ice, mechanical properties have been related to brine volume (as calculated from the salinity and the temperature), but air volume has not been measured in many cases. Thus we have to use "brine porosity" instead of total porosity in examining most data sets.

Figure 19 is a plot of Young's modulus E against porosity n. A data band is given for cold, non-saline ice, in which the voids contain only air. Over this band are located data envelopes for tests on small saline specimens. The results of Langleben and Pounder (1963), and also of Abele and Frankenstein (1967), were obtained by propagation of high frequency

50
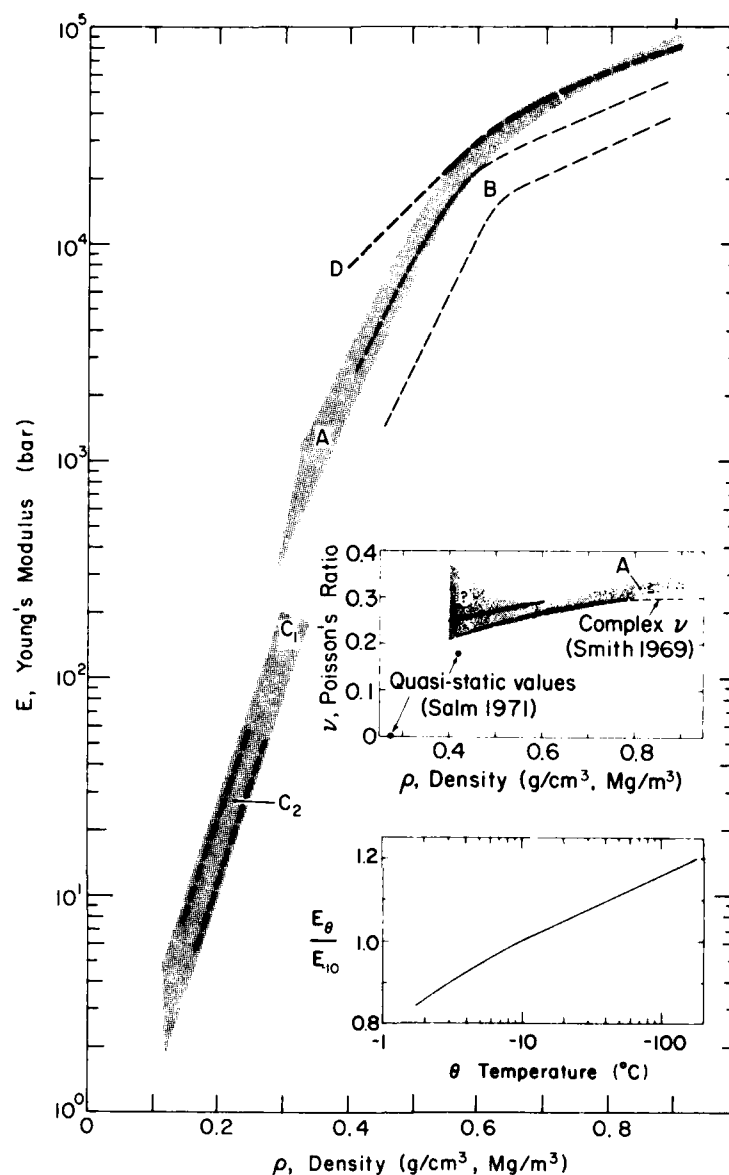
Figure 18. Summary of Young's modulus data for non-saline ice and snow (for source details, see Mellor 1975).

pulses; those of Tabata (1958) were obtained by flexural vibration of small beams. These results for sea ice agree quite closely with the results for non-saline ice, in spite of the fact that some of the pore volume is occupied by water. The tendency for the sea ice values to decrease more rapidly than the fresh ice ones can probably be explained by the fact that temperature is an implicit variable for the sea ice. The range of n could represent a temperature change of 20°C, and this could change E for the ice matrix by 10% or so.

The results of Kohnen (1972) were obtained from seismic wave data for broad expanses of sea ice. Those of Brown (1963), and of Anderson (1958),

51
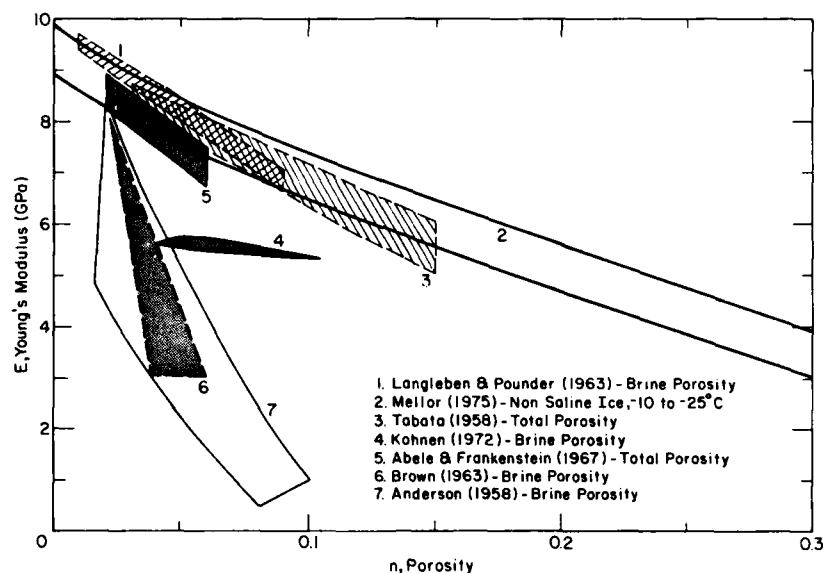
Figure 19. Young's modulus as a function of porosity.
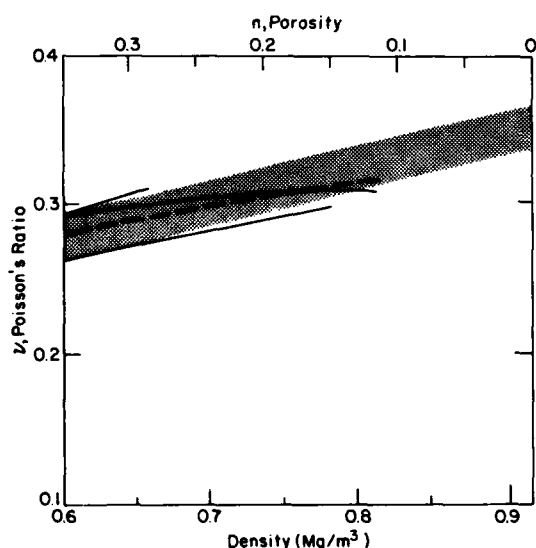
Figure 20. Summary of data for Poisson's ratio of non-saline ice as a function of porosity (see Mellor 1975 for details of data sources).

were also obtained from field measurements, but they involved flexural waves in the ice sheet. The data of Brown and Anderson, and perhaps those of Kohnen, appear to represent something other than the true Young's modulus of sea ice, and where flexure has been involved in the testing it is not difficult to find an explanation.

A sheet of sea ice is not a homogeneous elastic slab. It is often subject to steep temperature gradients, with the top cold and of low porosity, and the bottom warm and of high porosity. If flexure of such a slab is treated by simple elastic beam theory, the deduced value for the elastic modulus will _not_ be Young's modulus, but some kind of "effective" flexural

52

modulus. For very low values of ice porosity, which prevail at low temperatures and/or low salinities, the flexural modulus may be a good approximation to Young's modulus. However, at high porosities, which are produced by high salinity and high temperature, the flexure will not be a purely elastic process, and the flexural modulus will be far lower than Young's modulus.

Values of Poisson's ratio ν have not been studied systematically for sea ice. Weeks and Assur (1967) speculate that ν will decrease as temperature and brine volume decrease, adducing Russian seismic data in support. This speculation is a bit surprising at first sight, since one would expect the opposite trend if the pores were air-filled (see Fig. 20, which shows that ν for non-saline ice decreases as density decreases and porosity increases). However, with water-filled pores it seems quite possible for ν to increase with porosity, as can be seen from the following argument. Poisson's ratio ν can be expressed in terms of Young's modulus E and the bulk modulus K as

$$\nu = \frac{3K - E}{6K} = \frac{1}{6}\left(3 - E/K\right).$$

Since the bulk modulus of water is not greatly lower than that of ice, a small increase in the volume of water-filled pores will not have much effect on the overall value of K. Thus the variation of ν with porosity n will be controlled largely by the corresponding variation of E. Since E decreases as n increases, ν would thus increase as n increases. However, one would not expect much variation of ν. The value of ν for non-saline ice of very low porosity is about 0.33 ± 0.03, and variation with porosity in sea ice is likely to be within the limits of uncertainty for the pure ice value.

The bulk modulus K and the shear modulus G have not received much explicit attention in sea ice studies, but if it is accepted that ν will not vary much, then these constants can be given as simple multiples of E. Taking $\nu = 1/3$:

$$K = \frac{E}{3(1-2\nu)} = 1.0 \; E$$

$$G = \frac{E}{2(1+\nu)} = 0.375 \; E \;.$$

"EFFECTIVE" MODULI FOR LOW STRAIN RATES

In ice mechanics, elastic analysis is often applied in problems that do not involve purely elastic processes. Pseudo-elastic constants are determined from quasi-static tests, and from field observations of low-rate deformations. It can be very confusing when these constants are regarded as true elastic moduli, but there is no getting away from the fact that the numbers are useful for many practical purposes.

If no rate or temperature restrictions are placed on tests and processes, then "effective moduli" cease to have much relevance. However, if the

53
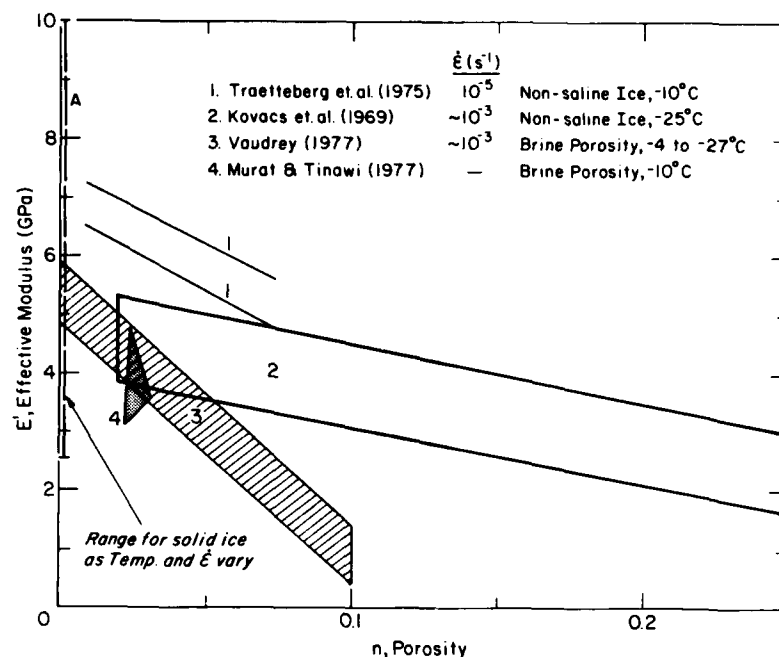
Figure 21. Summary of data for effective modulus E'
plotted against porosity.
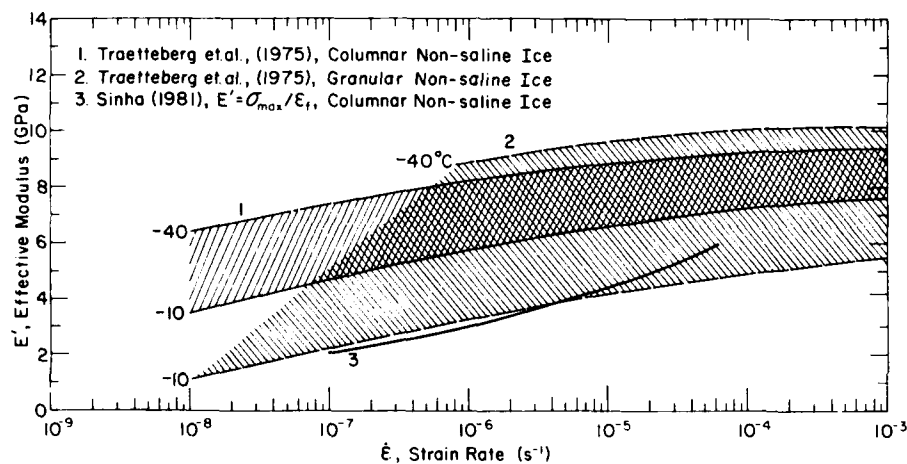
Figure 22. Summary of data for effective modulus E' plotted
against strain rate.

consideration is limited to relatively high strain rates, say of the order
of 10^{-4} s^{-1} or greater at temperatures below $-10°C$, then elastic analysis
is perfectly reasonable and appropriate effective moduli can be used.

Figure 21 gives an impression of the approximate magnitude of the
effective modulus E' as porosity n varies. The data by Vaudrey (1977) seem
to be reasonable working values, and they are of comparable magnitude to
the values obtained in a different way by Anderson and Brown (see Fig. 19).

54

Effective moduli should always be used with great caution, recognizing that E' for any given specimen can vary considerably as temperature and/or strain rate vary, and even the way it is defined can vary at the discretion of the investigator. Figure 22 shows how E' varies with strain rate at various temperatures, using data for freshwater ice in the absence of information for saline ice. At low temperatures and high strain rates, E' is approximately equal to the true Young's modulus E, but at low strain rates and/or relatively high temperatures, E' may be only 25% to 30% of E. Lainey and Tinawi (1981) showed similar behavior in ice of 5‰ salinity, presenting their values of E' for beam flexure as functions of stress rate (Fig. 23).

Figure 23. Variation of E' with stress rate and temperature (Lainey and Tinawi 1981).

Figure 24. Variation of E' with frequency, as deduced from strain rate data (after Sinha 1978a).

Sinha (1981c) has shown that the apparent value of the effective modulus can vary with the characteristics of the loading and measuring system. Of particular concern is the discrepancy between the apparent strain rate, as sensed across the specimen and its end contacts, and the true strain rate within the specimen. For rapid tests, the average <u>stress rate</u> may give a more reliable estimate of true strain rate, assuming linear elastic response.

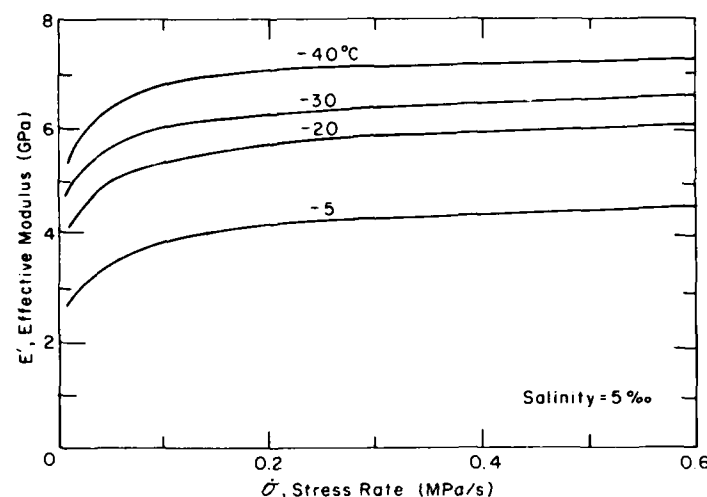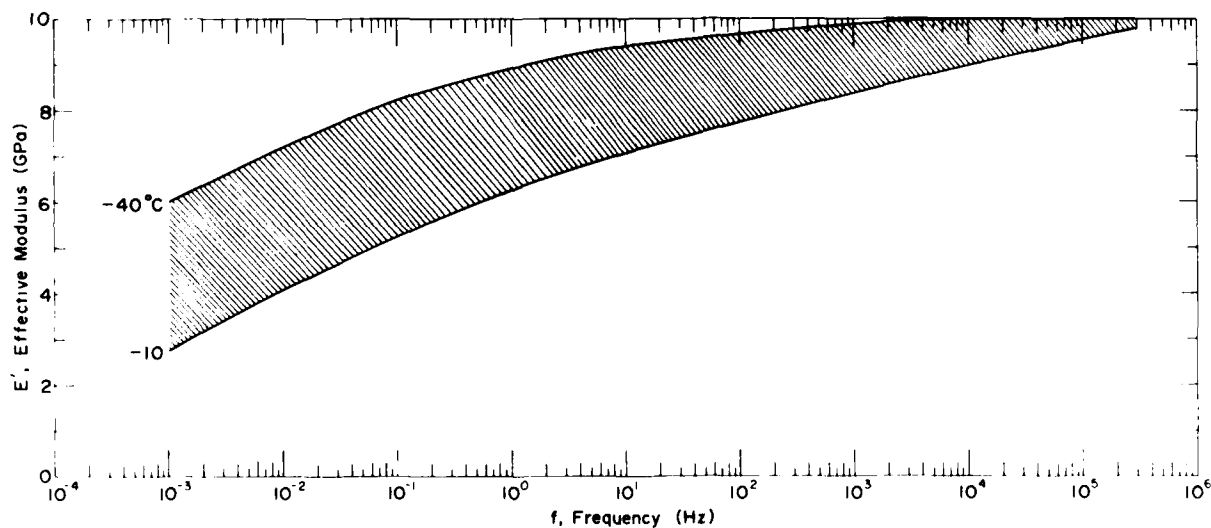The variation of E' with strain rate $\dot{\varepsilon}$ means that there will also be variation of E' with frequency f in the case of oscillation or vibration. Figure 24 indicates the rate of variation deduced by Sinha (1978a) from the strain-rate data for freshwater ice summarized in Figure 22.

It was mentioned earlier that the true Young's modulus E for freshwater ice is not very sensitive to temperature, but the same general statement cannot be made for the effective modulus E', even in freshwater ice. Figure 25, from Sinha (1978a), shows how E' for columnar-grained ice varies with temperature for various load durations and two stress levels. The values of E' in this figure are normalized with respect to the modulus E for very rapid loading. Absolute values of E', obtained from beam tests on ice of $5^0/_{00}$ salinity, are indicated in Figure 26, which is based on data by Lainey and Tinawi (1981). In the case of saline ice, it has to be kept in mind that a change of temperature implies a change of porosity if the ice is of fixed salinity.

When "effective" values of Young's modulus are employed, we need also "effective" values of Poisson's ratio, ν'. Effective values of ν' are only just beginning to enter the literature, but some deductions can be made. As material response becomes more ductile, the usual trend is for ν' to increase up to a limit of 1/2, which represents incompressible flow, with E'/K tending to zero. When all the pores of the ice are filled with water, there is no reason for the bulk modulus K to vary much with porosity, temperature, or strain rate, and for a first approximation it can be
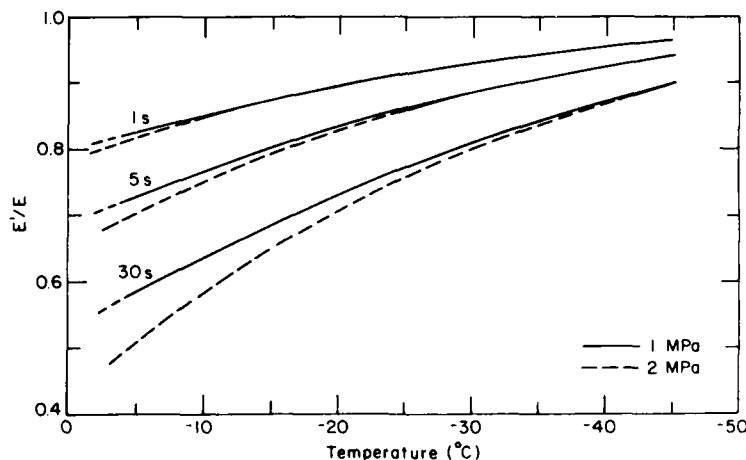
Figure 25. Variation of E' with temperature for different stress levels and load durations (Sinha 1978a).
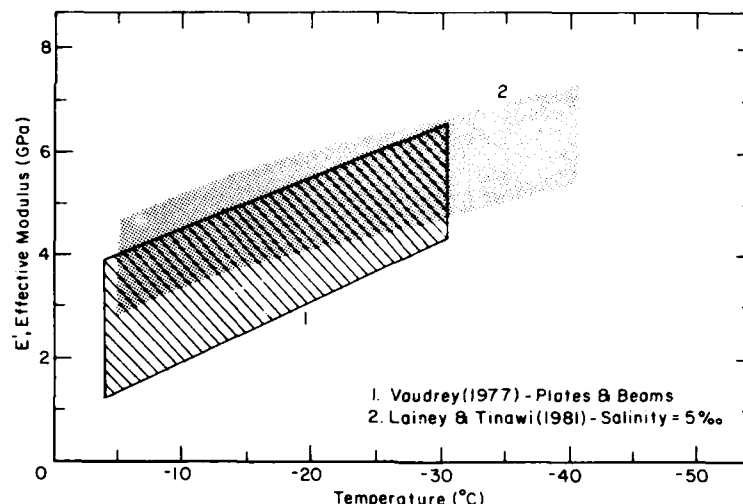
Figure 26. Summary of absolute values for E'
plotted against temperature.

assumed equal to the true Young's modulus for zero porosity, E_o. Thus
the effective Poisson's ratio for isotropic material can be expressed as:

$$\nu' = \frac{1}{2} - \frac{1}{6}\frac{E'}{E_o}$$

which gives a systematic variation between the limits 1/3 and 1/2. If the
ice is anisotropic, more extreme values of ν' for particular directions are
possible.

The expected general trend is confirmed by data from beam flexure
tests made on saline ice by Murat and Lainey (1982). Values of ν' de-
creased from a value of approximately 0.5 as strain rate and stress rate
increased. At the highest test rates (0.6 MPa/s, and up to 1.6×10^{-4}
s^{-1}), ν' was between 0.35 and 0.4. Mean values for high rate testing de-
creased with decreasing temperature, from about 0.4 at -5°C to 0.37 at -30°
and -40°C. This agrees with the prediction of Weeks and Assur (1967) that
was discussed earlier in the context of "true" Poisson's ratio.

UNIAXIAL COMPRESSIVE STRENGTH

Uniaxial compressive strength σ_c is a very important parameter which
appears easy to measure. In fact, accurate measurement of σ_c is very
difficult for highly brittle materials. When a simple right circular
cylinder is pressed between platens, the stress field is triaxial rather
than uniaxial near the end planes, and stress concentrations develop at the
platen/specimen interface. This means that many of the reported values of
σ_c for high loading rates and/or low temperatures are probably wrong.

In assessing the uniaxial compressive strength of ice, the main vari-
ables are:

57

(1) Ice type (grain structure and texture, porosity, salinity, solid inclusions)

(2) Strain rate (or, with reservations, stress rate)

(3) Temperature (which automatically varies with porosity in saline ice).

For a start, we consider the strength of non-saline ice.

In the present context, uniaxial compressive strength will be regarded as the maximum stress that can be developed at a specified strain rate. Studies on fine-grained isotropic freshwater ice (Mellor and Cole 1982, 1983) have shown that the minimum strain rate developed in a constant stress creep test gives essentially the same limiting relationship between stress and strain rate as the constant strain rate test. We can therefore combine data from creep tests and strength tests to define the relationship between strength and strain-rate over a wide range. Figure 27 shows that at low strain rates, say 10^{-7} to 10^{-5} s^{-1}, strength increases with about the one-third power of strain rate, while at higher rates, say 10^{-5} to 10^{-3} s^{-1}, strength appears to increase with a one-fourth, or smaller, power of strain rate. This relation is the inverse of the glaciologists' "flow law," which requires minimum creep rate to be proportional to the stress raised to a power of approximately 3.

Figure 28 gives some data for saline ice by Wang (1979a). These results were selected from Wang's paper because they fit the pattern of an approximate fourth-power relation between strain rate and stress. More detailed results by Wang (1979b) provide ample confirmation of the general trend, although the author fits rather complicated trend lines to the data (Fig. 29, 30, 31). Some data by Schwarz (1971) are shown in Figure 32. Data for multi-year sea ice of low salinity are just beginning to appear in the open literature (Cox et al., in press). Values of σ_c scatter widely because of great variability in the ice structure, but variations of σ_c with strain rate are not inconsistent with the power relation just mentioned (Fig. 33).
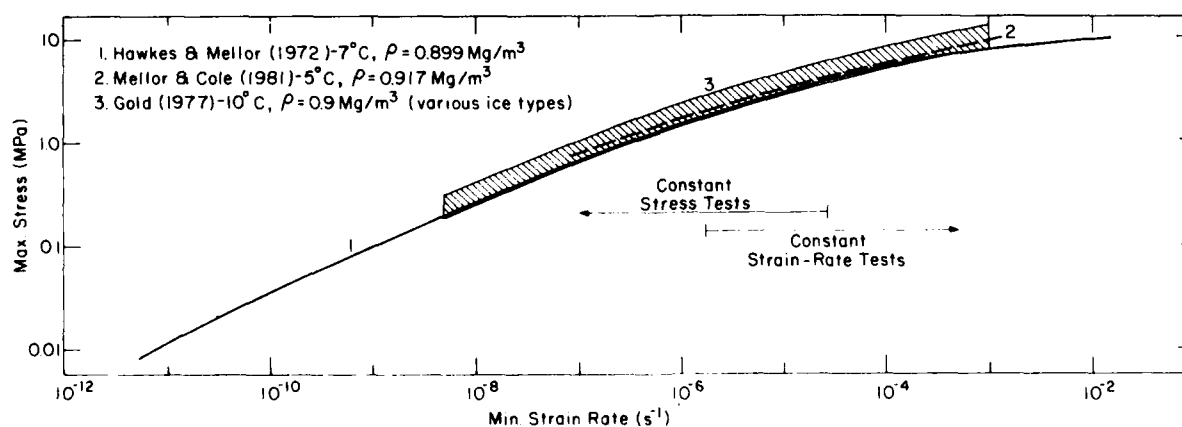
Figure 27. Maximum yield stress as a function of strain rate for nonsaline ice.
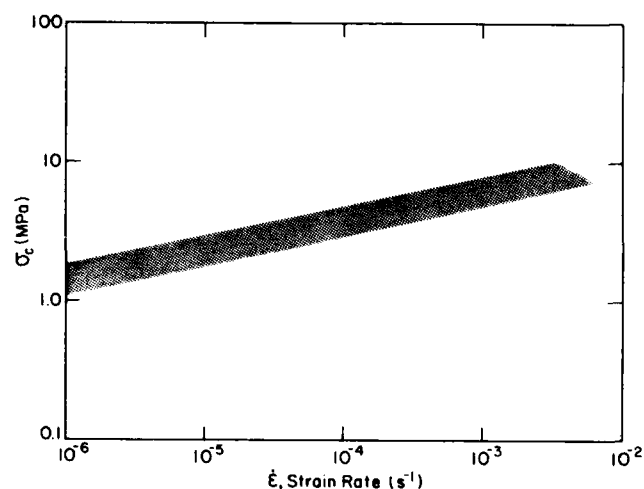
Figure 28. Uniaxial compressive strength of sea ice as a function of strain rate (after Wang 1979a).
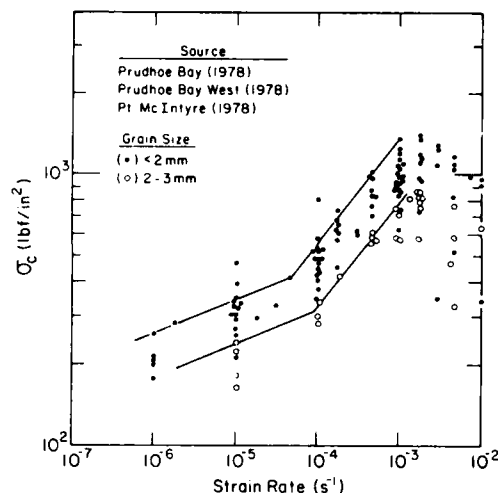
Figure 29. Variation of σ_c with strain rate in granular sea ice at $-10°C$. Data are given for two ranges of grain size (after Wang 1979b).
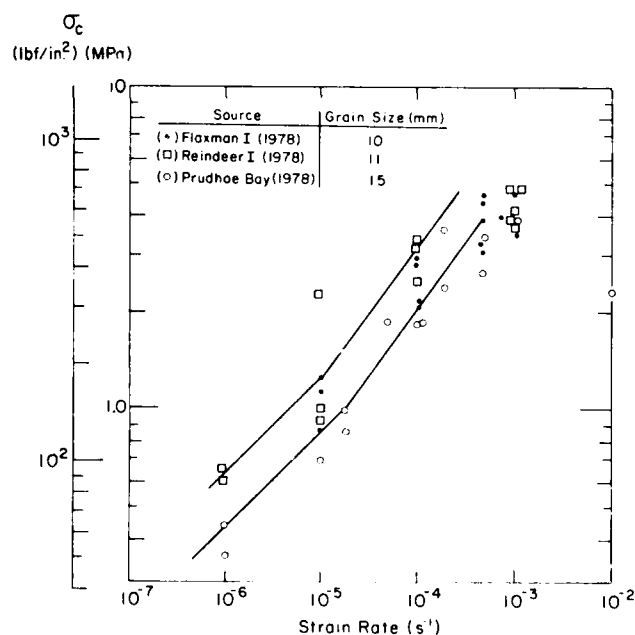
Figure 30. Variation of σ_c with strain rate in unoriented columnar sea ice at $-10°C$. Samples were taken from the upper part of the ice sheet (after Wang 1979b).
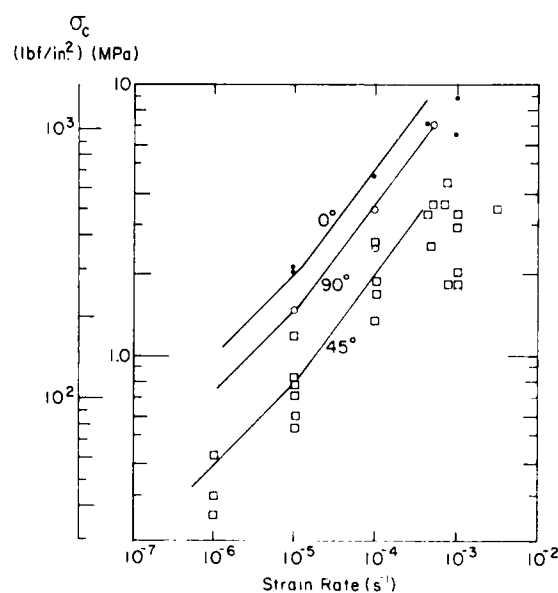
Figure 31. Variation of σ_c with strain rate in columnar sea ice at $-10°C$. The three data sets show the effect of crystal orientation. The lowest values of σ_c are measured when the c-axes are at 45° to the direction of the major principal stress. Grain size for these specimens was 11 mm (after Wang 1979b).

59
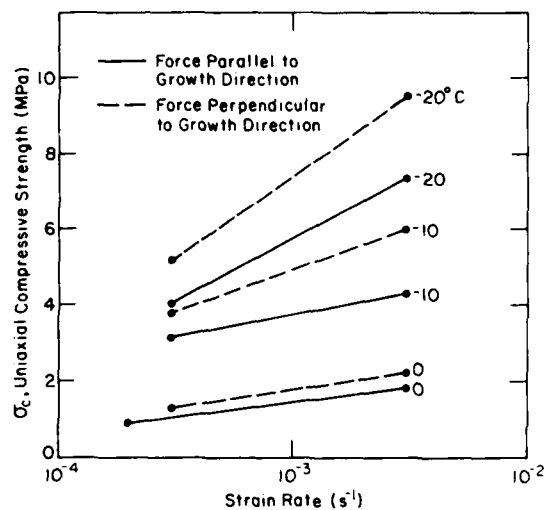
Figure 32. Variation of σ_c with strain rate, temperature and grain orientation (data selected from Schwarz 1971).
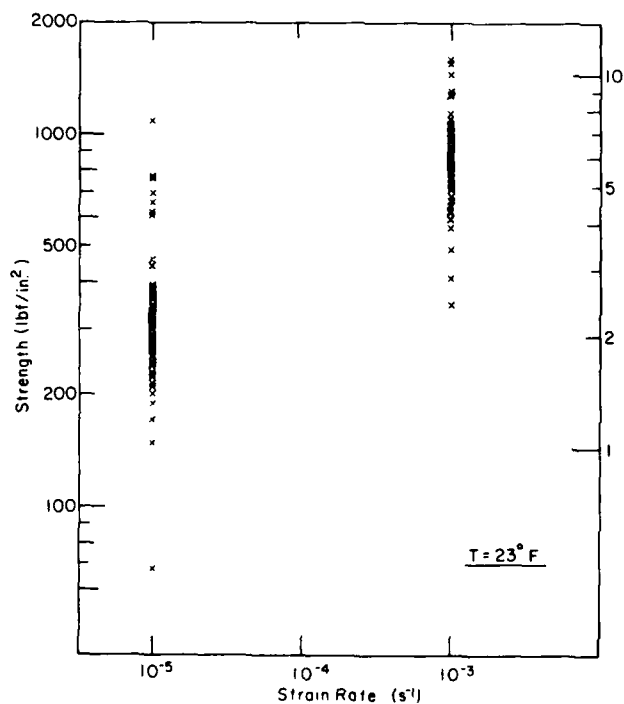
a.
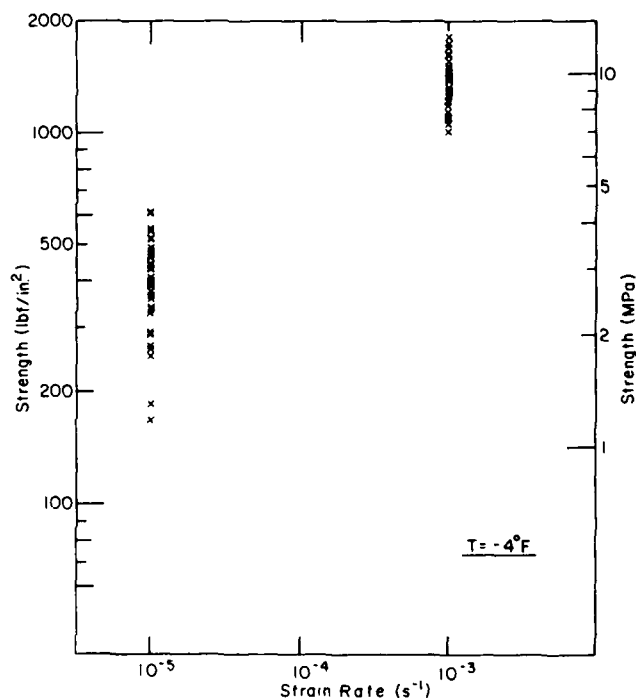
b.

Figure 33. Values of σ_c for multi-year sea ice at strain rates of 10^{-5} and 10^{-3} s^{-1}, and at temperatures of $-5°C$ and $-20°C$. The wide scatter is produced by great variability in grain and pore structures (Cox et al., in press).

60

For strain rates greater than 10^{-3} s^{-1}, many investigators have found that strength <u>decreases</u> as strain rate increases, and this is widely regarded as characteristic of brittle fracture. Such a trend would be in keeping with the ideas of fracture mechanics, but in some cases the effect may be caused by inadequacies in specimen preparation and imperfections in test technique. Present indications are that it will be necessary to use carefully designed, and precisely machined, dumbbell specimens in order to get valid test results at very high strain rates. For these reasons, the high rate data recorded in the literature will be deliberately disregarded in this survey.

The next variable for consideration is <u>temperature</u>, and we can first consider how non-saline ice responds.

At very low strain rates, where ice fails by creep rupture, it has long been the practice among glaciologists to characterize the effect of temperature on stress/strain-rate relations by an Arrhenius equation, with an activation energy of approximately 70 kJ/mole. Such a relation is definitely not valid above -10°C, and the complete empirical relation derived from experiments (e.g. Fig. 34) should be used to deduce how rupture stress varies with temperature. If creep tests give a relationship between applied stress and minimum strain rate in the form

$$\dot{\varepsilon}_{min} = A \, \sigma^n \, f(\theta)$$
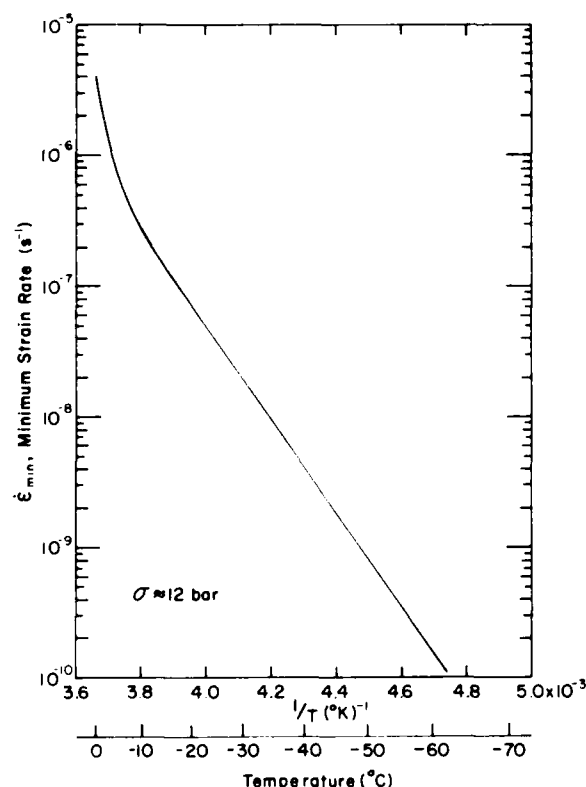
Figure 34. Empirical relation between minimum strain rate and temperature for high-stress creep (after Mellor and Testa 1969).

61

where θ is temperature, then the yield stress ought to vary with temperature according to a relation of the form

$$\sigma_{max} = \{\dot{\epsilon}/A \ f(\theta)\}^{1/n} \ .$$

In Figure 35, creep data have been used in this way to show how strength varies with temperature at low strain rates.

At very high strain rates, we would not expect much variation of strength with temperature, since the loading process is almost purely elastic. In the limit, strength might vary with temperature in much the same way as the true Young's modulus (Fig. 35).

In Figure 35 the variation of strength is examined by normalizing all strength values with respect to the value for -10°C. Taking curves 1 and 4 as the limits for high and low strain rates separately, the curves for typical testing rates might be expected to fall in between, which does seem to be the case.
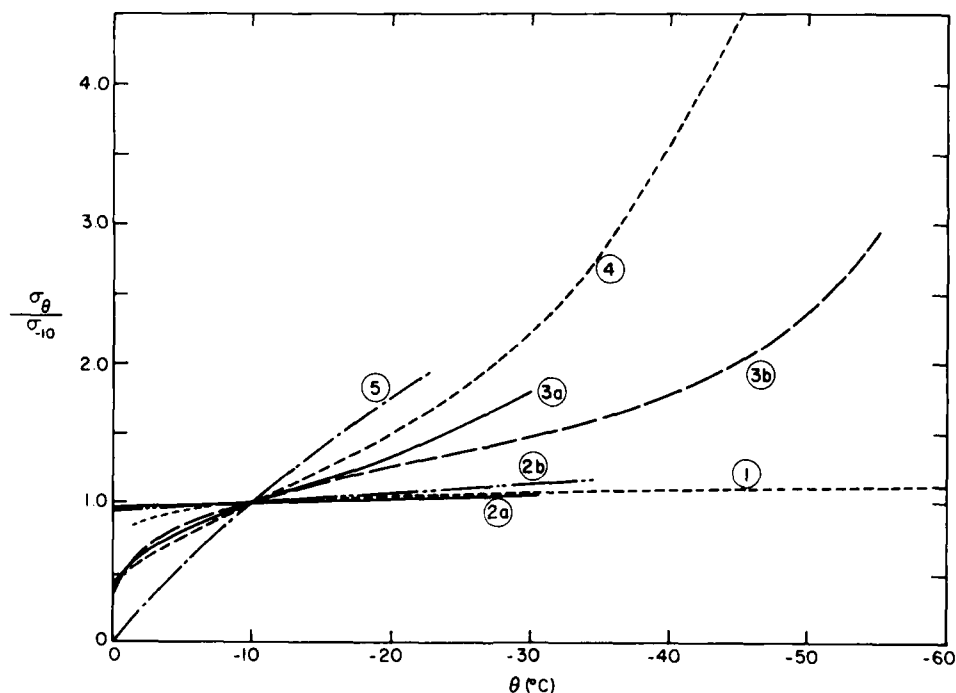
Figure 35. Compilation of temperature relationships. All the stress values are normalized with respect to the value for -10°C. 1) Variation of Young's modulus with temperature. 2a) Uniaxial tensile strength according to data by D. Carter (1970). 2b) Uniaxial tensile strength according to data by F.D. Haynes (1978). 3a) Uniaxial compressive strength according to data by D. Carter (1970). 3b) Uniaxial compressive strength according to data by F.D. Haynes (1978). 4) Ductile yield stress deduced from creep data by M. Mellor and R. Testa (1969). 5) Pressure for phase transition from Ice Ih to water under isothermal hydrostatic compression.

62

Before leaving the subject of freshwater ice, it might be mentioned that the temperature study by Haynes (1978) shows extremely high compressive strength values for high strain rates ($>10^{-3}$ s^{-1}) and low temperatures (-10° to -55°C). Virtually all values for this low temperature range exceeded 10 MPa, and some approached 60 MPa.

Temperature effects for saline ice include the effect of temperature on the solid ice component, as just discussed, but they also include the effect of porosity variations. All other things being equal, one might expect the strength of saline ice to increase more rapidly with decreasing temperature for the range where porosity is decreasing with temperature. Some data by Schwarz and Weeks (1971, 1977) seem to support this idea (Fig. 36).

Actually, temperature has not received a great deal of attention as a primary variable for saline ice. The major emphasis has been on brine volume, which will be discussed next.

The effect of porosity on the compressive strength of non-saline ice can be seen by examining the upper limits of the appropriate data band in Figure 37. As density decreases from 0.9 to 0.8 Mg/m^3, i.e. as porosity increases from 1.9% to 12.8%, the uniaxial compressive strength decreases by a factor of approximately 0.6.

In saline ice, where much of the pore volume is occupied by brine, porosity varies as temperature varies, and thus there is no easy way to separate the effects of temperature and porosity. Porosity is usually expressed as "brine volume," the volume of air rarely being known. There is a further complication in that most experimenters plot strength not against brine volume, but against the square root of brine volume. There was a rational basis for this practice in some studies, since the planar porosity of ice can be related to brine volume by assuming appropriate geometric models of pore structure. However, when the structure of the ice is uncertain, when the orientation of the pore structure to the principal stresses and the failure surfaces is variable, and when fracture mechanisms
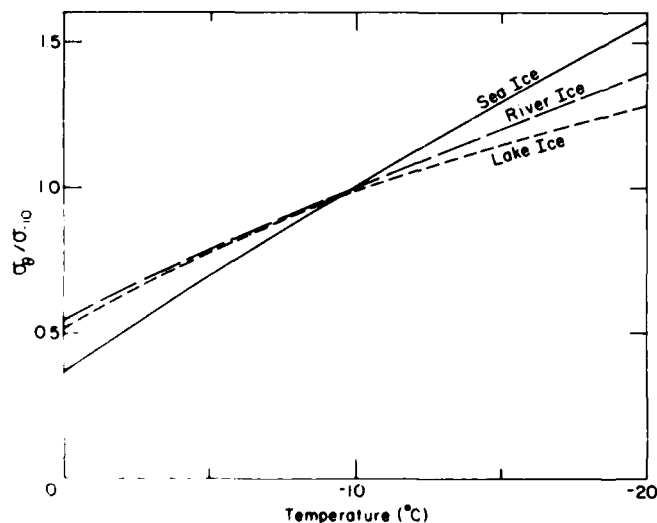
Figure 36. Variation of uniaxial compressive strength with temperature (data from Schwarz 1971).

63
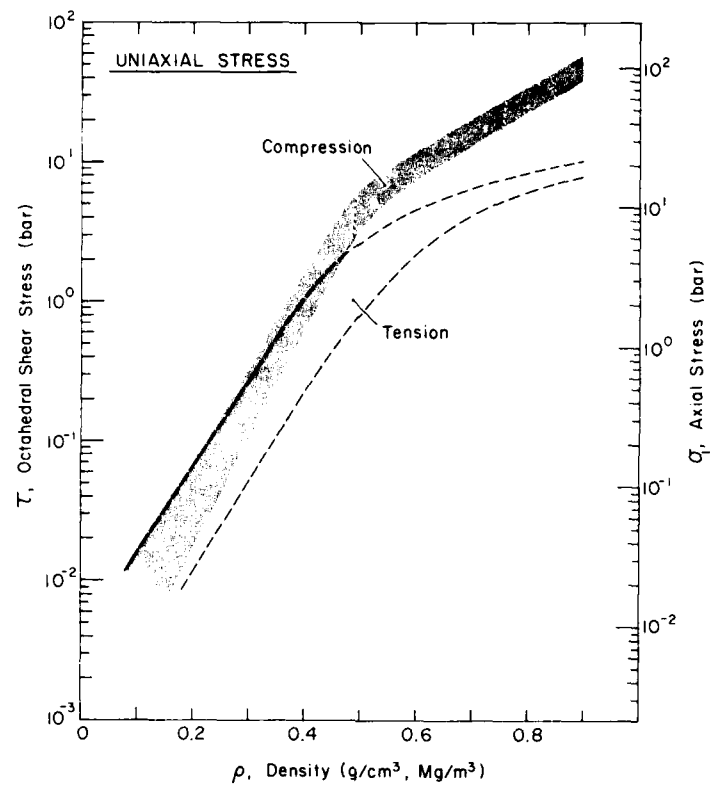
Figure 37. Summary of strength data for non-saline ice and snow (see Mellor 1975 for details of data sources).
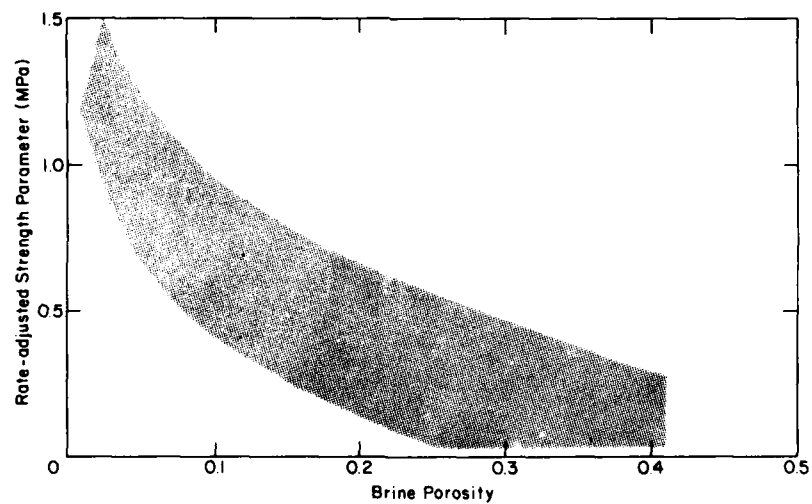
Figure 38. Strength parameter plotted against brine porosity (data from Peyton 1966).

64
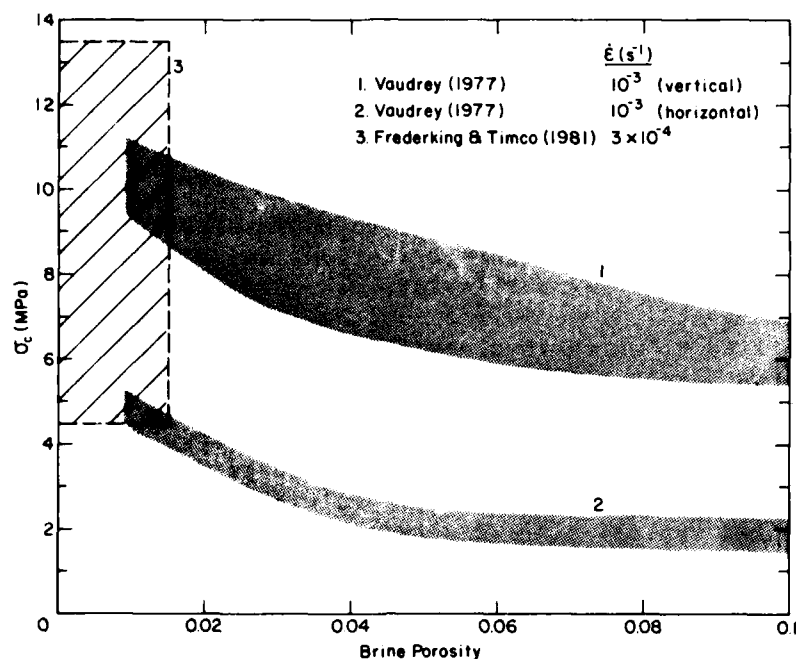
Figure 39. Summary of data for σ_c as a function of brine porosity.

are not fully understood, there is no good reason for using the square root of brine volume as a primary variable. In this respect, the present review breaks with established tradition.

Figure 38 gives a data band representing what are usually thought to be Peyton's (1966) values of rate-adjusted compressive strength as a function of brine volume (see Schwarz and Weeks 1977, Weeks and Assur 1967, Weeks and Assur 1969). Actually there is real doubt as to what these numbers mean. Peyton used the strange term "strate," giving it the units of a stress and the interpretation of a rate-adjusted strength. However, "strate" does not appear to have the dimensions of a stress according to his definition; the absolute values are extremely low, and they are inconsistent with "measured strength" values shown in another graph. The brine volume values are also surprising, reaching porosities of about 40%, which is approximately the porosity of dry sand, crushed stone, or snow of density 0.55 Mg/m^3.

Less ambiguous data for the uniaxial compressive strength of saline ice have been given by Vaudrey (1977). Figure 39 gives data bands representing his results replotted against brine porosity instead of the square root of brine volume. The general magnitude of strength values measured by Frederking and Timco (1981) is also indicated in Figure 39.

UNIAXIAL TENSILE STRENGTH

The uniaxial tensile strength of ice, σ_T, is of both practical and theoretical importance. There is only one way to measure uniaxial tensile

65

strength as a bulk property of the material, and that is by inducing failure in a fully determined uniaxial tensile stress field. The most reliable way to achieve this is to apply uniaxial tension to a dumbbell specimen which has been carefully designed, precisely machined, and mounted to close dimensional tolerances.

Indirect tension tests, which have to be interpreted by assuming a constitutive relation and a failure criterion, do not measure the uniaxial tensile strength of ice. In particular, exhaustive studies have shown that the ring tensile test is invalid for most real materials, and certainly for ice. The Brazil test, which involves diametral compression of a disc or cylinder, gives a direct measure of σ_T for "Griffith materials" when contact stresses are properly controlled, but for ice at typical loading rates it does not measure the uniaxial tensile strength (failure occurs in a biaxial stress field, with $\sigma_1 = -3\sigma_3$). Beam tests do not measure the uniaxial tensile strength of ice, but they are widely used and do constitute a rough analogue for typical plate fracture situations.

We can begin by looking at the behavior of non-saline ice under tension.

At very low strain rates, where deformation occurs mainly by flow and recrystallization, there is no reason to expect a significant difference between the compressive strength σ_c and the tensile strength σ_T. However, at high rates of loading, where brittle fracture occurs, σ_T is expected to be much lower than σ_c. Clearly there has to be a transition somewhere, and in Figure 40 it appears that the bifurcation between the σ_c and σ_T curves occurs at $\dot{\epsilon} \approx 10^{-6} \text{ s}^{-1}$ for non-saline ice at $-7°C$. Once the conditions for brittle, or quasi-brittle, fracture have been established, there appears to be little change of σ_T as strain rate increases, although σ_c continues to increase with $\dot{\epsilon}$.

If σ_T is insensitive to strain rate in the brittle range, we would expect a corresponding lack of sensitivity to variations in temperature. This expectation is borne out by the limited data for the tensile strength of non-saline ice (see Fig. 41).

The variation of σ_T with porosity in non-saline ice is indicated in Figure 37. As density decreases from 0.9 to 0.8 Mg/m^3, i.e. as porosity increases from 1.9% to 12.8%, σ_T decreases by a factor of approximately 0.8. Thus it appears that σ_T is less sensitive to porosity than is σ_c within the range that is of interest here.
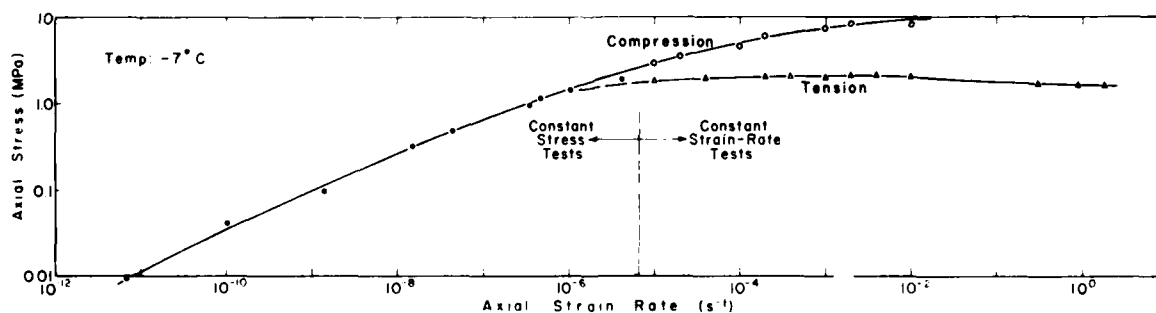
Figure 40. Effect of strain rate on σ_c and σ_T for non-saline ice (Hawkes and Mellor 1972).

66
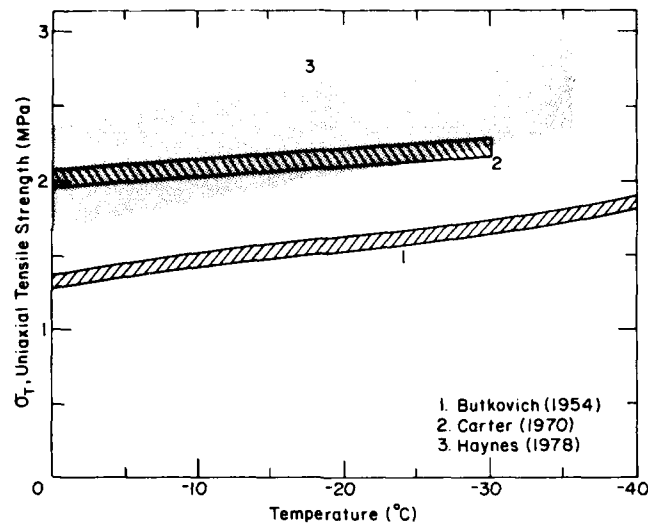
Figure 41. Variation of uniaxial tensile
strength with temperature for non-saline ice.
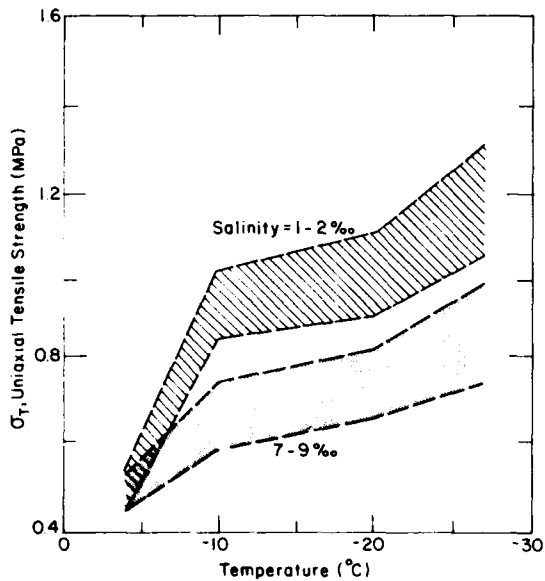
a) Vertical specimens.
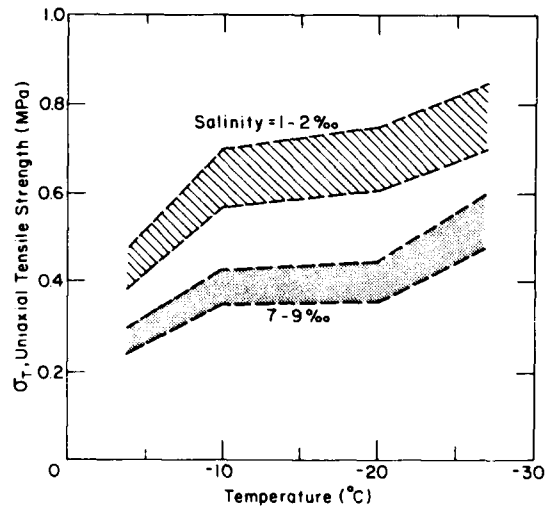
b) Horizontal specimens.

Figure 42. Variation of uniaxial tensile strength with temperature and
salinity for sea ice (from Dykins 1970).

67
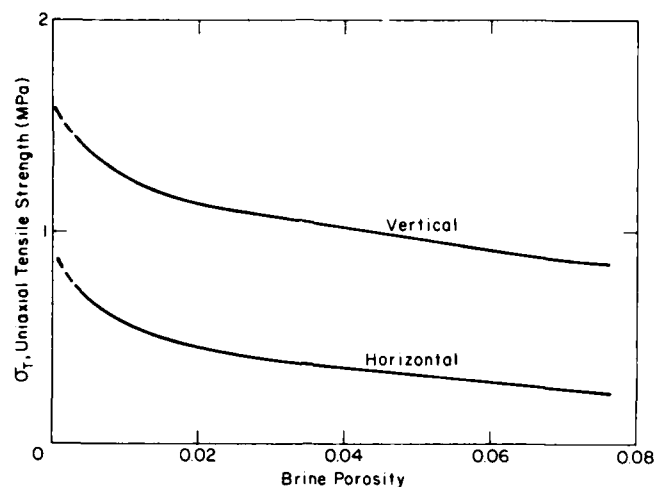
Figure 43. σ_T as a function of brine porosity for sea ice (after Dykins 1970).

It seems that there have not been many uniaxial tensile tests on saline ice. Peyton (1966) made tension tests, but the form of the report is such that the results are virtually unusable. This leaves only the work of Dykins (1970).

From consideration of the tensile strength of non-saline ice, which is relatively insensitive to strain rate, temperature, and porosity in the brittle range, we might guess that sea ice would also have relatively constant tensile strength. Just to establish perspective, if we assume that σ_T for freshwater ice varies by a factor 0.8 over the applicable range of porosity, and also by a factor of 0.8 (or 1.25) over the temperature range -30° to 0°C, then a combined effect when temperature and porosity increase together might cause σ_T to vary over the range by a factor of 0.64 (or 1.56). Figure 42 gives Dykins' (1970) data for σ_T as a function of temperature, and Figure 43 is a re-plot of his data for σ_T as a function of brine porosity. These graphs show that σ_T actually varies considerably as temperature (and therefore brine volume) varies, certainly more than might be expected from the behavior of fine-grained freshwater ice. The values of σ_T for tension applied in the vertical direction of the ice sheet are comparable to, but lower than, the values of σ_T for freshwater ice of similar temperature and porosity. The values of σ_T for tension applied in the horizontal direction of the ice sheet are much lower than values for fine-grained freshwater ice.

FLEXURAL STRENGTH

Flexure of an elastic beam induces longitudinal stresses, compressive and tensile, which increase linearly with perpendicular distance from the neutral axis. If $\sigma_T < \sigma_c$, the beam will break when the stress at the outer surface of the convex side reaches a value equal to σ_T. For a linearly elastic material which fails by brittle fracture, a measure of σ_T can be obtained by calculation from the bending moment, the moment of inertia, and the beam depth. The simple formula is based on the following

68

assumptions: 1) linearly elastic homogeneous material, 2) equal moduli in tension and compression, 3) small strains, with cross-section planes remaining plane and mutually parallel. It is important to note that fracture initiates at the surface, the zone of critical stress is very thin, and the fracture propagates in a stress gradient. For ice beams loaded at typical rates the behavior is not purely elastic, the effective moduli for tension and compression are not equal, and the material is often inhomogeneous. Recognizing that beam flexure does not measure the uniaxial tensile strength of the bulk material, the value of σ_T calculated from beam experiments probably ought to be called the modulus of rupture, or the flexural strength. The latter term will be used here with the symbol σ_{FT}.

One special feature of flexural strength measurements is that they include the results of both small-scale lab tests and large-scale field tests on in situ beams. The values of σ_{FT} for the two types of tests are very different for a variety of reasons. One is the inherent scale effect for the bulk strength of materials, which will be discussed under a separate heading. Another reason for the difference is that in situ beams sitting in water are often subject to steep and variable temperature gradients across the depth of the beam, to the extent that σ_{FT} varies with the time of day. Yet another reason is the variation of properties with ice depth, brought about by changes in the rate of ice growth.

Laboratory flexural tests may employ beams in three-point or four-point bending, while in situ tests often use cantilever beams. Cantilevers introduce additional complications, since the root of the cantilever is not anchored rigidly, especially if the beam is wide relative to its depth. There may be stress concentrations at the corners of the beam root (unless curved fillets are formed), and the effects of stress concentrations in ice are strongly sensitive to loading rate and temperature.

Measured flexural strength is sensitive to rate of loading, but the nature of the relationship is not well defined. There seem to be no systematic data for freshwater ice, and the results for saline ice are somewhat inconsistent. For small beams, Tabata (1967) showed σ_{FT} with a minimum at 0.01 MPa/s, and an increase with $\dot{\sigma}$ up to 0.2 MPa/s at a temperature of $-9°C$. In more recent work on small beams at $-10°$ and $-20°C$, Tabata et al. (1976) found no correlation between σ_{FT} and $\dot{\sigma}$ for stress rates in the range 0.01 to 1.0 MPa/s. Lainey and Tinawi (1981) showed σ_{FT} dropping from a maximum at rates just below 0.1 MPa/s, with a slow but steady decrease of σ_{FT} as $\dot{\sigma}$ increased from 0.1 to 0.6 MPa/s. These data covered the temperature range $-5°$ to $-40°C$. Saeki and Ozaki (1981) found a slight increase of σ_{FT} between 0.005 and 0.5 MPa/s, with a drop to lower values for the range 0.7 to 20 MPa/s (test temperature $-7°C$). Data given by Nippon Kokan (n.d.) for small beams at $-2°C$ show σ_{FT} decreasing very considerably (factor of 5 or more) as deflection rate increases within the range 0.1 to 100 mm/s.

For large in situ beams, Tabata et al. (1967) showed σ_{FT} increasing greatly (factor of 5 or so) as $\dot{\sigma}$ increased from about 0.05 to 5 MPa/s at $-2°C$. However, Määttänen (1976) found that $\dot{\sigma}$ had no obvious influence in the range 0.01 to 10 MPa/s, provided that inertial effects in the water and the ice were eliminated.
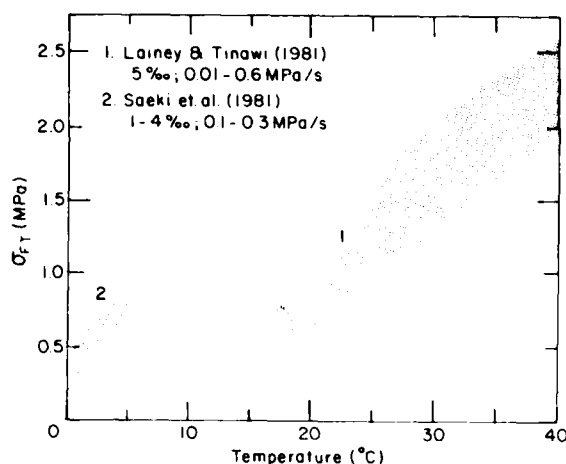
Figure 44. Variation of flexural strength with temperature.

The information on rate effects is obviously very confusing, and it is not easy to decide to what extent the various trends are influenced by real physical changes, and to what extent by imperfections of test technique.

The effects of <u>temperature</u> on σ_{FT} appear at first sight to be less controversial, even though the validity of the elastic assumptions must vary with temperature. For small beams of freshwater ice, Weeks and Assur (1969) give a summary graph which shows σ_{FT} increasing linearly as temperature decreases, but for at least one of the data sources represented in the graph, the original data are perhaps less convincing than the interpreted trend. For saline ice, Lainey and Tinawi (1981) show a small increase in σ_{FT} as temperature drops from $-5°$ to $-20°C$, and a much more rapid increase of σ_{FT} between $-20°$ and $-40°C$ (Fig. 44). This perhaps says more about the relative validity of the test interpretation as a function of temperature, but as the result of an analogue test it is interesting. Saeki and Ozaki (1981) give beam data for less saline ice at temperatures between $-0.5°$ and $-6°C$, showing, not surprisingly, a strong increase of σ_{FT} in this range. Butkovich (1959) tested small beams cut vertically and horizontally from sea ice, with temperatures in the range $-2°$ to $-26°C$. His regression lines show a small increase of σ_{FT} over the range, but the data have a great deal of scatter. In earlier work, Butkovich (1956) carried out 80 tests on small beams, but his results show no significant correlation between σ_{FT} and temperature for the range $-2°$ to $-17°C$ (σ_{FT} was mainly in the range 0.4 to 1.2 MPa).

The effect of <u>brine volume</u> on σ_{FT} was described by Weeks and Assur (1967, 1969), who compiled test data for in situ cantilever beams. The results were represented by a linear decrease of σ_{FT} as the square root of brine volume increased from zero to 0.32 (brine porosity 0 to 0.1); for greater porosities, σ_{FT} was taken as constant. An updated compilation by Schwarz and Weeks (1977) weakened the case for the latter assumption, and the argument for using the square root of brine volume as the porosity variable no longer seems greatly persuasive.

When the general body of data for small beam tests is added to the plot (Fig. 45), it is hard to perceive any orderly trend. Clearly, strength ought to decrease as porosity increases, but because increased porosity often reflects higher temperatures, the ductility of the material tends to increase with porosity.

70
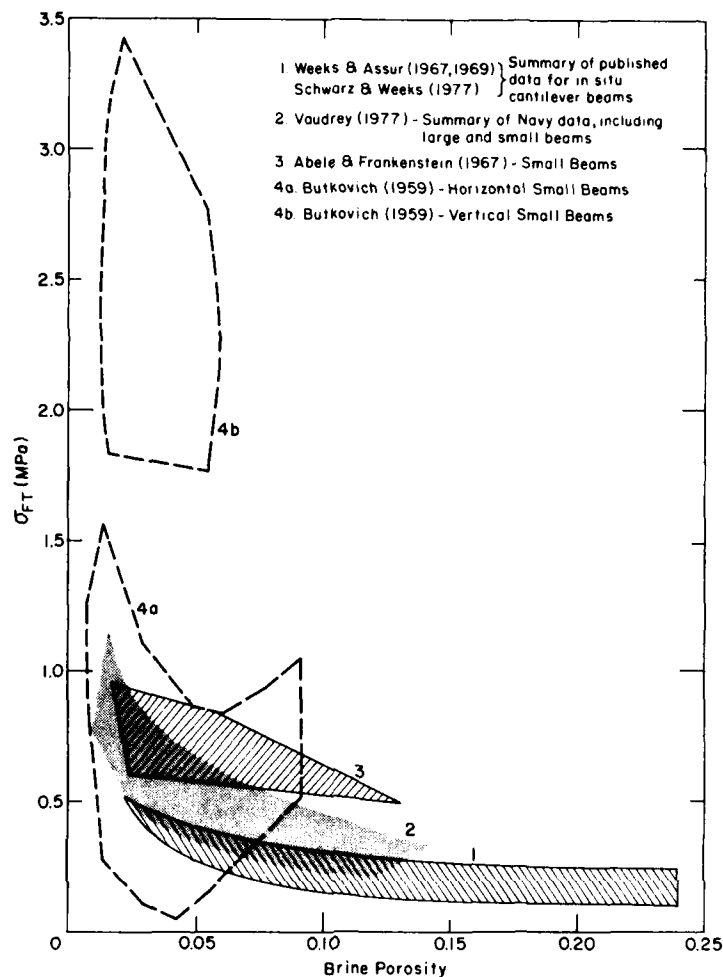
Figure 45. Summary of data for σ_{FT} as a function of brine porosity.

FRACTURE TOUGHNESS

Virtually all fracture toughness measurements on ice depend on tests which flex or pry open a crack in "Mode I." Test data are thus presented in terms of the <u>critical stress intensity factor</u>, K_{Ic}. Because the measured values for K_{Ic} vary greatly, and because we need some intuitive "feel" when considering these values, it is worth recalling what K_{Ic} means.

Toughness is measured by the specific energy dissipation at failure G_c, which is also known as the critical crack extension force. K_{Ic} is related to G_c by

$$K_{Ic} = (EG_c)^{1/2}$$

in plane stress, and

71

$$K_{Ic} = \left(\frac{EG_c}{1-\nu^2}\right)^{1/2}$$

in plane strain. Thus there is a simple direct relation between K_{Ic} and G_c if E is a constant. K_{Ic} is also related to the overall tensile failure stress of the material σ:

$$K_{Ic} = \sigma\,(\pi c)^{1/2}$$

where c is the half-length of the controlling cracks. This relation implies that, if c is constant and the stress state does not change, K_{Ic} directly proportional to the bulk strength of the material.

For ice straining at low rates, say less than 10^{-6} s^{-1}, we would not expect K_{Ic} to have any relevance, since the ice is inelastic and it flows without cracking. At extremely high rates and low temperatures, ice could conceivably become perfectly elastic and perfectly brittle, so that the original Griffith theory might apply. For such a limit, with γ_p tending to the specific surface energy γ, K_{Ic} would tend to a low value:

$$K_{Ic} \rightarrow (2E\gamma)^{1/2}$$

in plane stress. Taking E = 10 GPa and the grain boundary specific energy $\gamma = 0.1$ J/m^2 for freshwater ice, the lower limit of K_{Ic} might be about 45 kN m$^{-3/2}$ for plane stress.

Measured values of K_{Ic} for ice are typically of order 100 kN m$^{-3/2}$. This is not much higher than the "Griffith" value, and it implies that $\gamma_p \approx 5\gamma$, assuming that E is more or less constant.

When strain rate, or loading rate, is varied in a fracture toughness test for a given type of ice, we might expect K_{Ic} to decrease as $\dot{\varepsilon}$ or $\dot{\sigma}$ increases, at least for non-saline ice. While at least one set of experiments shows a trend opposite to this, the overall trend shown by compilation of published data is in the expected sense (Fig. 46, 47). Rate effects were originally expressed in terms of the speed of the testing machine, which is clearly of limited interest, but now the accepted rate variable seems to be $\dot{K_I}$, which is really the inverse of the time to failure. Strain rate has been used as a variable, but there are some problems of interpretation.

In sea ice, K_{Ic} has been found to decrease with increase of loading rate for $\dot{K_I} > 10^{-2}$ kN m$^{-3/2}$ s^{-1}, or effective $\dot{\varepsilon} > 10^{-3}$ s^{-1} (Urabe et al. 1980, Urabe and Yoshitake 1981a,b). However, for lower rates K_{Ic} appears to be insensitive to rate (Fig. 48). The lowest measured values for sea ice are lower than the expected "Griffith value" for pure ice.

In discussing rate effects, it has been assumed that K_{Ic} will decrease as the material becomes more elastic and more brittle due to higher loading rates. Extending this single line of argument to temperature effects, it might seem reasonable to expect K_{Ic} to decrease as temperature decreases, since lower temperature undoubtedly makes ice more elastic and

72
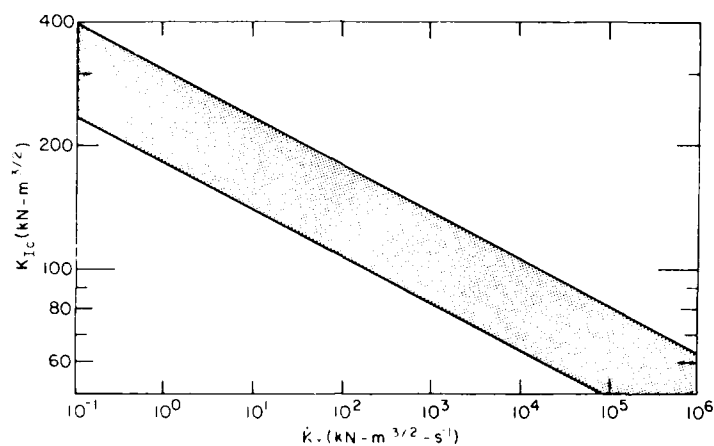
Figure 46. Effect of loading rate on K_{Ic} for non-saline ice (from data summarized by Urabe and Yoshitake 1981b).
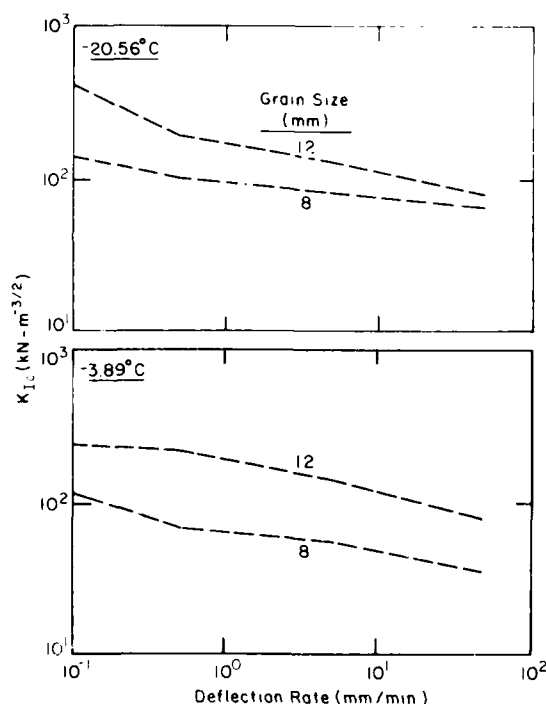
Figure 47. Variation of K_{Ic} with loading rate, grain size and temperature for columnar freshwater ice (Hamza and Muggeridge 1979).

more brittle. However, experimental data (Fig. 49) show exactly the opposite trend, with K_{Ic} increasing as temperature decreases. This observed trend is consistent with the fact that tensile strength σ_T increases as temperature decreases, since K_{Ic} is proportional to strength if the crack length $2c$ is constant. This perhaps gives a clue to the resolution of what appears at first sight to be a fundamental contradiction: K_{Ic} should be evaluated in relation to the overall strength of the material. Another potential factor is temperature-dependence of surface energy, which is mentioned later.

73
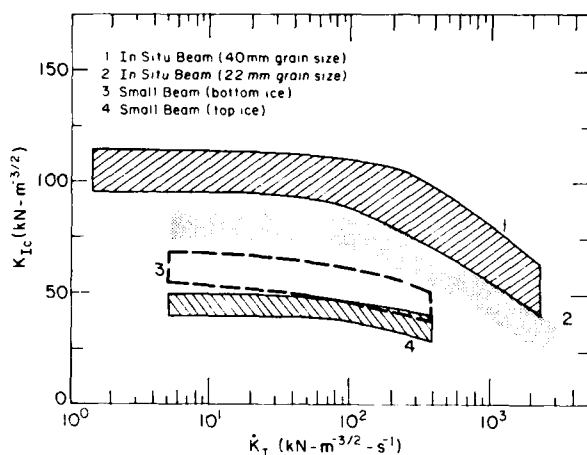
Figure 48. Effect of loading rate on K_{Ic} for sea ice (data from Urabe and Yoshitake 1981a, b).
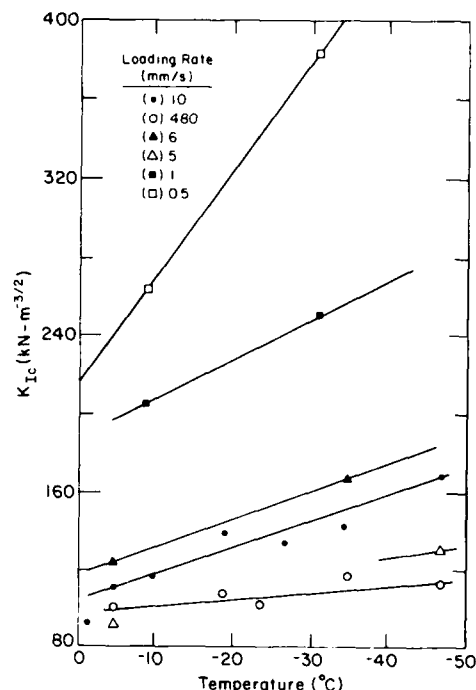
Figure 49. Variation of K_{Ic} with temperature and loading rate (from Miller 1980).

If measurements of K_{Ic} are valid, they permit a systematic treatment of flaw size. For a constant value of K_{Ic} and variation of crack length 2c between samples, the tensile strength σ_T might be expected to be inversely proportional to $\sqrt{c}$. Urabe and Yoshitake (1981b) tested both notched and un-notched beams with varying grain size in order to calculate flaw size for the ice, and they found a perfect 1:1 correlation between calculated flaw size and observed grain size. However, this experiment appears to merit further discussion, since both σ_{FT} and K_{Ic} were functions of grain size, and the effect of grain size on σ_{FT} appears to be in the wrong direction.

If we refer back to the basic Griffith equation for strength as a function of modulus, surface energy, and crack length, then theoretical values of tensile strength can be calculated by taking the flaw size 2c equal to the grain size of the ice. For ice of very low porosity, (≤ 0.01), the true Young's modulus E is 9 to 10 GPa at typical temperatures. For non-saline ice, the vapor/solid specific energy γ is approximately 0.1 J/m^2, and the liquid/solid surface energy is about 30% of the vapor/solid value (Fletcher 1970, Hobbs 1974)*. The vapor/solid value is probably the appropriate one for consideration of brittle fracture in "cold" ice, but the lower liquid/solid value might be applicable in relatively warm ice which has a "liquid-like layer" or liquid-filled

---

* Liu and Miller (1979) use values that are off by two orders of magnitude due to incorrect conversion of Fletcher's values.
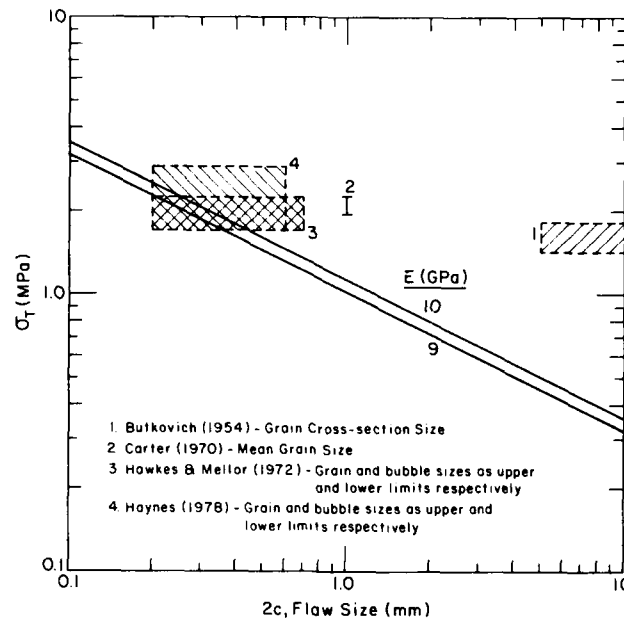
Figure 50. Comparison of theoretical
tensile strength with measured values.

flaws. The latter condition might give something equivalent to the
Rehbinder, or Joffe, effect, whereby γ is reduced by adsorption of certain
surface-active chemicals, and strength decreases in consequence.

If we substitute into the Griffith equation $E = 10$ GPa and $\gamma = 0.1$
J/m^2,

$$\sigma_T = \left(\frac{2}{\pi}\right)^{1/2} \left(\frac{10^{10} \times 10^{-1}}{c}\right)^{1/2}$$

$$= \frac{2.52 \times 10^4}{\sqrt{c}} \quad Pa$$

where the half-length of the controlling flaw, c, is in metres. In Figure
50, the resulting calculated values of σ_T are given as a function of the
flaw size 2c, which is assumed equal to grain size. The theoretical rela-
tion is compared with actual measured values of σ_T, and the agreement is
surprisingly close. Since the controlling flaws could be substantially
smaller than the grain diameter, the agreement might even be improved. The
significance of this exercise is in demonstrating that simple Griffith
theory cannot necessarily be rejected for ice.

Vaudrey (1977) measured K_{Ic} for sea ice at $-10°$ and $-20°C$, and
plotted the results against the square root of brine volume for a very
narrow range. Vaudrey drew a line on the graph to indicate linear decrease
of K_{Ic} with increase in the root of brine volume but, in fact, there was
no significant correlation between the variables (K_{Ic} values scattered by
a factor of 5). Shapiro et al. (1981) made measurements in the same range
(brine porosity 0.16 to 0.38), and showed a more convincing decrease of
K_{Ic} with increase of porosity, although there was still large scatter.

75

EFFECT OF GRAIN SIZE ON STRENGTH
AND DEFORMATION RESISTANCE

Early creep studies on non-saline ice suggested a strong increase of
strain rate with grain size, but the experiments themselves were not fully
acceptable. More recent published work by Baker (1978) showed a compli-
cated relation between creep rate and grain size, with the direction of the
trend different for different size ranges, but again the experiments seemed
questionable. Subsequent studies by Duval and LeGac (1980) showed no
significant variation of final creep rate with grain size.

For the strength of ice in the brittle range, the expectation is that
strength of isotropic material would be inversely proportional to the
square root of grain size. This is in keeping with the ideas of fracture
mechanics if grain size is identified with flaw size. Limited data for
σ_c tend to bear out this expectation (see Fig. 29, 30, 31), but systemat-
ic verification has not yet been published. Some recent values of σ_{FT}
for sea ice of varying grain size (Urabe and Yoshitake 1981b) appear to be
in direct contradiction to the expected trend, but Currier and Schulson
(1982) measured σ_T at 10^{-6} s^{-1} and found the results could be described
by the Hall-Petch relation, i.e. $\sigma_T = a + b\ d^{-1/2}$. In the ductile
range of behavior, it seems that the maximum yield stress does not change
with grain size (Jones and Chew 1981).

To sum up, there is no convincing evidence that strength or deforma-
tion rate vary with grain size for the ductile (creep) range of behavior.
For the brittle range, one might expect strength to decrease as grain size
increases, but substantial experimental proof has not yet appeared.

SIZE EFFECTS FOR STRENGTH AND DEFORMATION RESISTANCE

In general, the measured strength of a brittle material decreases as
the size of the specimen increases, or as the critically stressed volume of
material increases. The accepted explanation is that bigger samples con-
tain bigger flaws and, as shown by fracture mechanics, strength decreases
as flaw size increases. Sophisticated statistical theory has been
developed for consideration of the distribution of flaw sizes within a
given specimen, for estimation of the probability of encountering larger
flaws in larger volumes, and for the effects on strength through a "weakest
link" theory.

A simple relation can be derived from rather involved theoretical
arguments (see Hawkes and Mellor 1970). If the most probable (modal)
strength is S_{V_1} for a specimen of volume V_1, and S_{V_2} and V_2 are modal
strength and volume for a geometrically similar specimen subjected to the
same strain rate, then

$$\frac{S_{V_2}}{S_{V_1}} = \left(\frac{V_1}{V_2}\right)^{1/m}$$

where m is a characteristic constant.

Experiments on nonmetallic brittle solids indicate that m is of order 10, so that the volume effect is a weak one. In terms of a linear dimension L the effect is stronger, since $V \propto L^3$ and therefore $S \propto L^{-3/m}$. If $m \approx 10$, S is approximately inversely proportional to the cube root of L. Thus an increase in L by a factor of 10 would roughly halve the strength.

The creep resistance of homogeneous ice at low strain rates ($\dot{\varepsilon} < 10^{-6}$ s^{-1}) is probably not much dependent on the volume of material involved, provided that the minimum linear dimension of any test sample is greater than 10 grain diameters.

FAILURE OF ICE IN MULTIAXIAL STRESS RATES

When isotropic ice is subjected to triaxial compression at low strain rates, it is usually said that the bulk stress $\bar{\sigma}$ has no effect on the induced deviatoric strain rate $\dot{\varepsilon}'_{ij}$, provided that "allowance is made for depression of the melting point." A more straightforward interpretation is that creep rate increases slightly, and the ductile yield stress decreases slightly, when the confining pressure increases at constant temperature. If the pressure is increased sufficiently, for example to about 0.1 GPa at temperatures near $-10°C$, ice Ih transforms to water and its shear resistance drops to virtually zero. Thus the yield surface in principal stress space is a cone with its apex on the hydrostat line ($\sigma_1 = \sigma_2 = \sigma_3$) at the pressure for the phase transition to water (Fig. 51), at least for temperatures above $-20°C$.

The same ice under triaxial compression at high strain rates suffers internal cracking and dilatation when unconfined, but confining pressure subdues the cracking and the deviatoric yield stress is increased. A first approximation for the failure criterion under these conditions would be a linear Coulomb-Navier-Mohr criterion. In the compression quadrants of principal stress space, the yield surface corresponding to such a criterion would be a cone disposed symmetrically about the hydrostat line, with its diameter increasing indefinitely as pressure increases. Clearly such a surface contradicts the pressure melting effect which was just discussed in connection with yield for low strain rates, and the actual yield surface must account for both effects of pressure. Such an envelope is sketched in Figure 52, which shows "strength" increasing with confining pressure at first, and then decreasing as the pressure becomes very high. Triaxial tests by Jones (1978), at $-11.5°C$ and strain rates of order 10^{-4} s^{-1}, show the effects of confining pressure reversing at about 30 to 40 MPa (Fig. 53).

Conventional compressive triaxial tests ($\sigma_1 \neq \sigma_2 = \sigma_3$) were made on natural and artificial sea ice by Soviet investigators (Panov and Fokeev 1977). The axial stress σ_1 increased with σ_2, σ_3 (Fig. 54), and the maximum shear stress ($\sigma_1 - \sigma_2$)/2 increased nonlinearly with the normal stress on the plane of maximum shear. When σ_2 was approximately 4 MPa, the yield values of σ_1 were an order of magnitude higher than σ_c. Under confining pressures σ_2, the failure stress σ_1 decreased as salinity and temperature increased, i.e. salinity and temperature had effects similar to their effects on σ_c. Isotropic fine-grained ice behaved differently than

77
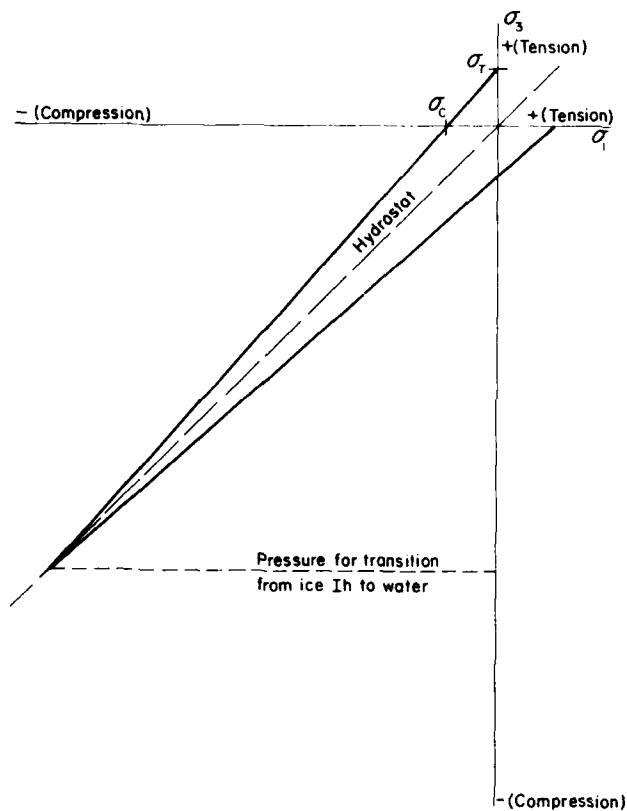
Figure 51. Two-dimensional representation of a simple yield criterion for low-rate ductile yield of isotropic freshwater ice at temperatures above $-20°C$.
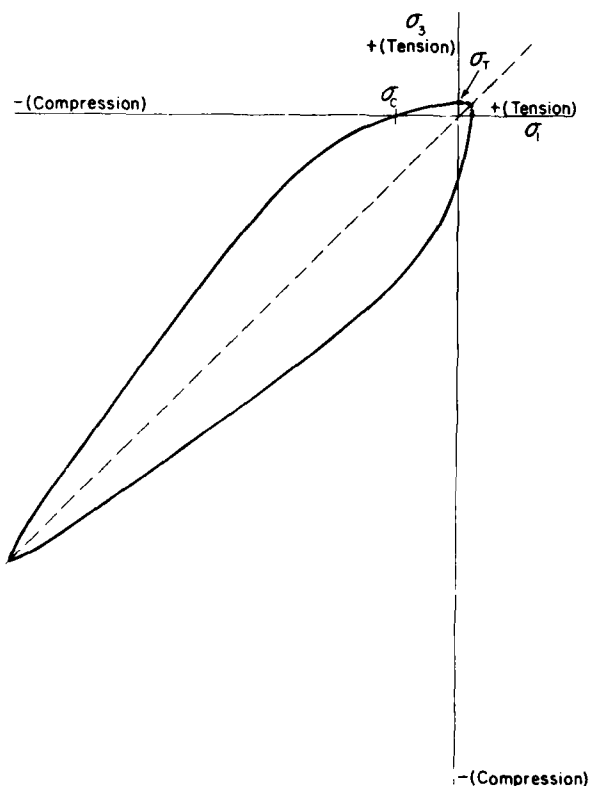
Figure 52. Two-dimensional representation of a yield criterion which accounts for crack suppression and melting point depression in isotropic freshwater ice under moderately high strain rates at temperatures in the vicinity of $-10°C$.

78
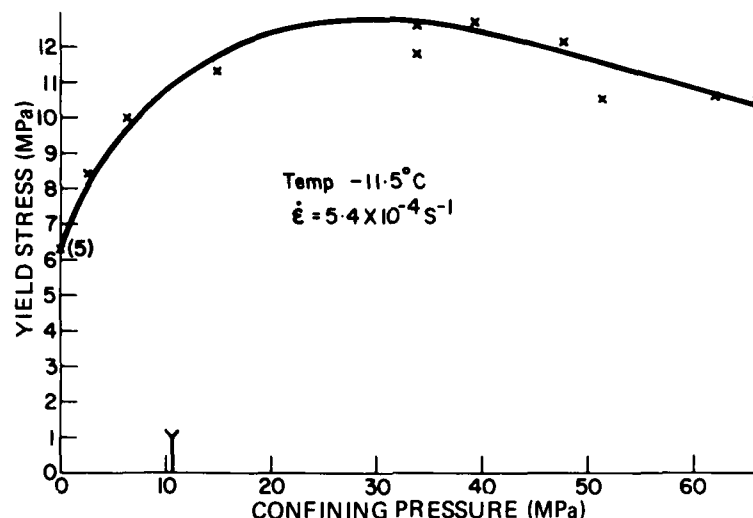
Figure 53. Variation of yield stress with confining pressure for conventional triaxial tests on non-saline ice at -11.5°C and a strain rate of 5.4 x 10⁻⁴ s⁻¹ (Jones 1978).
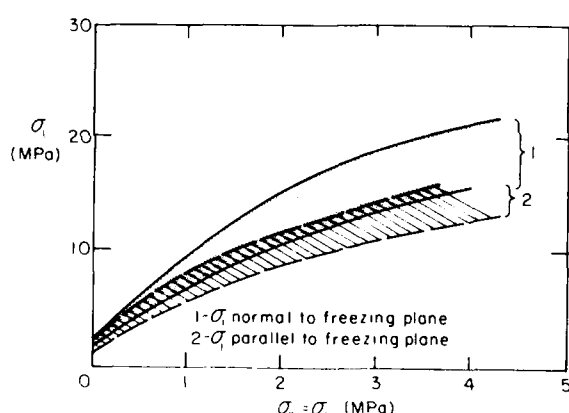
Figure 54. Variation of axial yield stress with confining pressure for sea ice at temperatures of -2° to -3°C and salinities of 0.16 to 3.54 °/oo (after Panov and Fokeev 1977).

anisotropic ice, and strength varied with the loading direction in aniso-tropic material. Values of ϕ for the Mohr envelope were mostly in the range 30° to 50°, with extreme values of 14° and 55°.

Triaxial tests to very high pressures (up to 350 MPa) and very low temperatures (-78° to -196°C) were made recently on non-saline polycrystal-line ice (Durham et al. 1982). Very high yield stresses were recorded, and phase transitions to higher density polymorphs were reached.

For the tension-compression quadrants of triaxial principal stress space there is little experimental information, and we have to rely largely on intelligent guesswork.

Under very low strain rates, σ_c is expected to equal σ_T, and experimental data support this idea. With $\sigma_c = \sigma_T$, the Tresca or von Mises envelope can be extended across the tension-compression quadrants
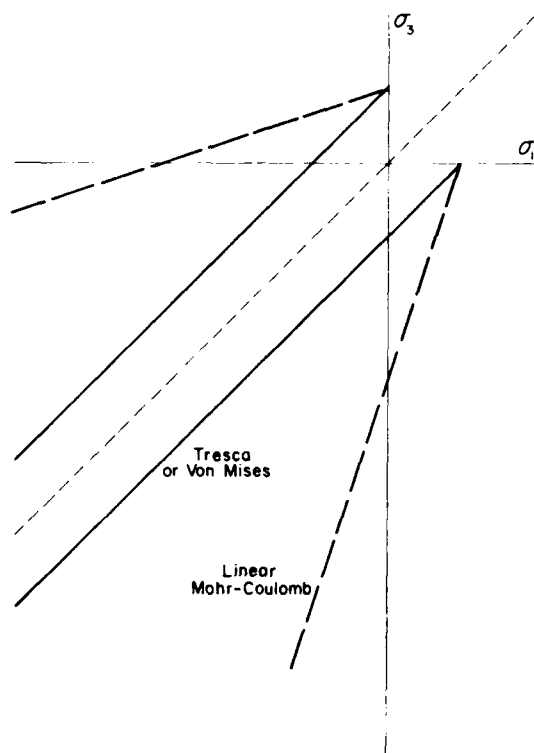
Figure 55. Two-dimensional repre-
sentation of the Tresca and von
Mises criteria, and the linear
Coulomb-Navier-Mohr criterion.

without conflict (Fig. 55). The pressure-melt version of these criteria
(Fig. 51) can similarly be extended *without significant conflict* for low
temperatures (-10°C), but for higher temperatures an extrapolation of such
an envelope would predict $\sigma_c < \sigma_T$, and there is no experimental evi-
dence for such an effect.

At high strain rates, where $\sigma_c \neq \sigma_T$, a straight line connection of
the σ_c and σ_T points is not likely to be far from the truth, especially
if an adjustment is made to assure continuity of slope as the envelope
passes into compression-compression where the linear Coulomb-Mohr envelope
is applicable for low pressures. Experimental data by Haynes (1978) are
not in conflict with this suggested trend.

The observed ratio of σ_c to σ_T gives useful insight into the fail-
ure criterion for low confining pressures and for the tension-compression
quadrant. At low strain rates in ice, $\sigma_c/\sigma_T = 1$, as already discussed,
which means that a von Mises or Tresca envelope is a good approximation for
low pressures and for tension-compression. At higher strain rates,
σ_c/σ_T increases from 1 to about 4 according to the data of Figure 40.
If the linear Coulomb-Navier-Mohr criterion is extended into the tension-
compression quadrant (where it is not strictly applicable), the predicted
value of σ_c/σ_T is 3 for $\phi = 30°$, and 4 for $\phi = 37°$. By contrast, the
simple Griffith criterion predicts $\sigma_c/\sigma_T = 8$, while the three-dimen-
sional version predicts $\sigma_c/\sigma_T = 12$. The Babel and Sines (1968)
generalization of the Griffith criterion predicts $\sigma_c/\sigma_T = 3$ if the
controlling flaws are circular holes, with the value increasing progres-
sively to 8 as the flaws change progressively from a circular cross section
to a completely flat ellipse.

80

For the tension-tension stress state there are no data for ice, and in view of formidable experimental difficulties it may be a long time before there are reliable data. Perhaps the most reasonable guess is that, for isotropic ice in biaxial or triaxial tension, failure will occur when one principal stress reaches the uniaxial strength σ_T. This gives the envelope as lines parallel to the principal stress axes, with intersection on the hydrostat line at $\sigma_1 = \sigma_2 = \sigma_3$.

In Figure 52 the preceding deductions about the behavior of isotropic ice are combined to form a complete failure envelope, slightly modifying the lines deduced for each individual quadrant so as to give continuity of slope across the axes.

The three diagrams discussed above are drawn in two dimensions because they are difficult to draw in three dimensions. They should not be confused with two-dimensional diagrams for biaxial stress states, i.e. for plane stress.

Biaxial tests were made by Frederking (1977), who pressed prismatic specimens between a pair of platens in one direction while rigidly restraining the ice in one of the other orthogonal directions, and leaving the remaining pair of faces stress-free. For isotropic ice the confinement had very little effect on the crushing strength, which remained approximately equal to the uniaxial compressive strength for strain rates of about 3×10^{-7} to 3×10^{-4} s^{-1}. This implies that, to a first approximation, the failure envelope in the compression-compression quadrant could be represented by lines parallel to the axes (Fig. 56). A similar effect was found when the lateral restraint was applied to columnar ice in a direction parallel to the long axes of the columns. However, if the restraint was applied perpendicular to the long axes of the columns, the failure stress in the loading direction was roughly double the uniaxial strength.
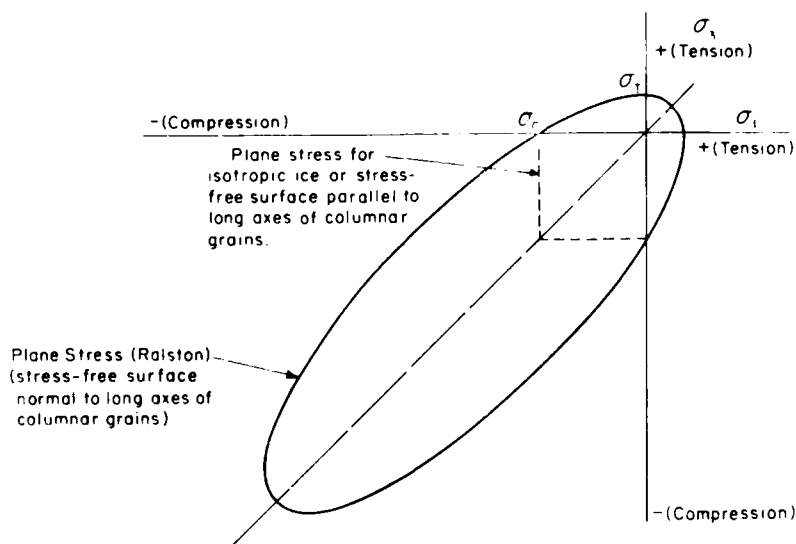

Figure 56. Failure envelopes for biaxial stress states ($\sigma_2 = 0$).

Ralston (1980) used the data of Frederking (1977), together with a parabolic Coulomb-Navier-Mohr criterion, in order to deduce the plane stress failure envelope shown in Figure 56. It should be noted that this plane stress envelope crosses the 45° line ($\sigma_1 = \sigma_3$) for a different reason than the triaxial envelope proposed by Mellor (1979), and shown in Figure 52.

THERMAL STRAINS IN ICE

At 0°C and atmospheric pressure, the density of pure water is 1.00 Mg/m^3 and the density of ice is 0.917 Mg/m^3, so that freezing involves a volumetric strain of -8% and thawing gives a volumetric strain of +9%. As ice is cooled at constant pressure its density increases, i.e. the ice contracts. The expansion coefficient varies with temperature, becoming negative below -200°C, but for most purposes the latter complication can be ignored.

For a single crystal of pure ice, the coefficient of linear expansion varies slightly with crystallographic direction, but at temperatures near 0°C the difference is only about 2% (greater parallel to the c-axis) and can be ignored for most practical purposes. Thus the coefficient of linear expansion α can be taken as $\alpha = \gamma/3$, where γ is the coefficient of cubical expansion given by density changes. At temperatures between 0°C and -40°C we can take $\alpha = +5 \times 10^{-5} \, C^{-1}$ (± 4%) for freshwater polycrystalline ice, noting that α decreases by approximately 10% as temperature drops from 0° to -40°C.

In sea ice, or other ice containing significant amounts of dissolved impurities, the situation is very different. At temperatures near the melting point, saline ice consists of solid ice, plus liquid inclusions which change in volume and salinity as the temperature changes. Although the ice crystals have a positive expansion coefficient, phase changes in closed brine cells could create freezing strains in a negative sense, i.e. volume increases as temperature drops. Above about -5°C, the freezing and thawing of brine inclusions is usually thought to be the dominant effect, implying that sea ice contracts as temperature increases in this range. At very low temperatures, when the brine is frozen and solid salts are precipitated, the behavior is almost identical to that of pure ice.

In the past, effective values of γ and α have been calculated as functions of temperature and salinity, using density values from the sea ice phase diagram. The usual source is a table and graph derived by Anderson (1960) on the assumption that air volume is zero and all brines remain trapped in place. Air volume was taken into account by Schwerdtfeger (1963) and by Cox and Weeks (in press), but of itself included air does little to change the variation of calculated density with temperature. While these calculations are sound in principle, they may not be very realistic, since at high temperatures brine can be expelled into air bubbles and even out through the ice boundaries. A reappraisal of the problem will be published soon by G.F.N. Cox of CRREL.

If ice is cooled or warmed very slowly, thermal strains can be accommodated by creep processes without any cracking, especially if the ice

temperature is above −10°C. However, if very rapid cooling occurs at low temperatures, high strain rates are induced in ice and it cracks. For strain in one direction, the strain rate $\dot{\varepsilon}$ produced by cooling of the ice at a rate $d\theta/dt$ is

$$\dot{\varepsilon} = \alpha(d\theta/dt)$$

assuming that α is invariant with temperature θ. Strain rates developed this way are likely to be much lower than the strain rates which are associated with brittle fracture in laboratory strength testing of ice. For example, extremely rapid cooling at 10°C/hr would give $\dot{\varepsilon} = 1.4 \times 10^{-7}$ s^{-1} in pure ice. However, fairly large tensile strains can develop if the temperature change is great enough. For example, in non-saline ice a temperature drop of 20°C gives a tensile strain of 10^{-3} (0.1%), which is at the top end of the range of tensile failure strains measured by Hawkes and Mellor (1972).

The most extreme cooling rates and temperature changes occur at the upper surface of an ice layer. Both the amplitudes and rates of temperature change decrease with increasing depth in the ice. Thus cracking initiates at the surface, and the depth of crack penetration is limited by the attenuation of temperature waves with depth.

The effect of cooling at the surface of sea ice has been analyzed in terms of elastic plate flexure, but because strain rates are likely to be low ($< 10^{-8}$ s^{-1}) and the bulk of the ice is likely to be "warm," the assumption of linear elasticity seems dubious.

PART III. SOME CHARACTERISTICS OF FRAGMENTED ICE

MECHANICAL PROPERTIES OF BRASH ICE AND ICE RUBBLE

When floating ice is fragmented, it can be regarded as a granular continuum if the dimensions of the volume under consideration are significantly greater than the block size of the broken ice. This interpretation is easiest to justify for brash ice, which can be regarded as a floating accumulation of more or less equant fragments in the size range 0.02 to 2.0 m. However, such an interpretation can perhaps be extended to heavily fragmented ice sheets when there has been rafting and ridging.

A number of research groups have treated fragmented floating ice as a granular material conforming to a linear Coulomb-Navier-Mohr yield criterion, and characterized largely by a friction angle ϕ. Measured values of ϕ have been summarized, together with additional values of ϕ deduced from crushing experiments (Mellor 1980). In this compilation, ϕ ranges from 42° to 58°, but some recent test results (Weiss et al. 1981) give values in the range 11° to 34° for ice of lower porosity.

Other important properties are the block density, and the porosity of the fragmented mass.

For bubble-free freshwater ice the block density is 0.917 Mg/m^3, but for bubbly ice or snow-ice the density may be as low as 0.89 Mg/m^3. For sea ice, block density varies with salinity, temperature and air content. The range for intact sea ice is approximately 0.89 to 0.93 Mg/m^3, but for fragments equilibrated with seawater the density is likely to be at the lower end of this range, say 0.9 Mg/m^3.

The porosity n of the ice mass varies with the degree of packing and the size gradation of the fragments. "Ice rubble" used in experiments has had porosity less than the 40% or so which is typical for uniform granular solids (e.g. sand, crushed stone). Keinonen and Nyman (1978) used ice with n from 0.32 to 0.37, Prodanovic (1979) had n = 0.38, and Weiss et al. (1981) used material with n ranging from 0.16 to 0.33. Sandkvist (1981) gives estimates of the water content of brash as a function of depth from actual field observations. His data suggest an almost linear decrease of porosity with depth, from virtually zero at the water surface level to 1.0 at the base of the brash layer. For fresh pressure ridges in sea ice there have been numerous inspired guesses at the overall porosity, but virtually no measurements. One might guess that porosity in a pressure ridge would vary from small values near the waterline (say about 0.05) to fairly high values (say about 0.3) near the crest and the keel, actual values varying to some extent with the mode of ridge formation and the amount of freeze-back.

When a wide layer of unbonded fragmented ice is floating in static equilibrium, the internal stresses are determined by gravity body forces, i.e. by the weight of the ice above water level and by the buoyancy below water level. If the total ice thickness t is significantly greater than the characteristic block size d, the layer can be treated as a continuum. Making the simplifying assumption that the porosity n and the friction angle ϕ were invariant with depth, Mellor (1980) gave the vertical (σ_z) and horizontal (σ_x, σ_y) components of normal stress.

$$\sigma_z = (1-n) \rho_i g \left(\frac{\rho_w}{\rho_i} - 1\right)(t-z)$$

$$= (1-n) \rho_i g \left[t_1 - \left(\frac{\rho_i}{\rho_w} - 1\right)(z-t_1)\right]$$

where ρ_i is the ice block density, ρ_w is the water density (≈ 1.026 Mg/m^3 for seawater), z is the depth below the top surface of the ice, t is the total ice thickness, t_1 is the thickness of ice above water level. The values of σ_x and σ_y depend on whether the ice layer has recently been compressed or extended horizontally. The limiting states of stress according to the Rankine theory of plastic yield give:

(a) for the passive state (compression) $\sigma_x = \left(\frac{1+\sin\phi}{1-\sin\phi}\right)\sigma_z$

(b) for the active state (extension) $\sigma_x = \left(\frac{1-\sin\phi}{1+\sin\phi}\right)\sigma_z$

(c) for the neutral state $\sigma_x = \left[\nu/(1-\nu)\right]\sigma_z$.

For a loose fragmented lay   of thickness t in which n and ϕ are invariant with depth, the crushing resistance per unit width, R, is

$$R = \frac{1}{2}\left(\frac{1+\sin\phi}{1-\sin\phi}\right)(1-n)\rho_i g\left(1 - \frac{\rho_i}{\rho_w}\right)t^2 .$$

Although this expression is oversimplified by the assumption of constant values for n and ϕ, it serves to illustrate that the average crushing pressure R/t is proportional to t. If there is some constant cohesion c between the ice fragments, the average crushing pressure includes a term which is independent of thickness:

$$\frac{R}{t} = \frac{1}{2}\left(\frac{1+\sin\phi}{1-\sin\phi}\right)(1-n)\rho_i g\left(1 - \frac{\rho_i}{\rho_w}\right)t + 2c\left(\frac{1+\sin\phi}{1-\sin\phi}\right)^{1/2} .$$

When c is large, the second term of the previous equation dominates, and the resistance is then similar to that of an intact ice sheet with a crushing stress of $2c\sqrt{(1+\sin\phi)/(1-\sin\phi)}$. With a two-dimensional Coulomb-Navier-Mohr failure criterion, uniaxial compressive strength is usually expressed as $2c\left[\cos\phi/(1-\sin\phi)\right]$, which is identical to the crushing stress just mentioned.

86

The way in which a uniform homogeneous brash layer responds locally to horizontal compression against a fixed barrier ought to depend on the displacement velocity (u) relative to the velocity of propagation for the front of a plastic disturbance (U). If u/U is very low a uniform thickening of the whole layer will occur, but if u/U > 1 there can be localized thickening, "plastic wave propagation," and pressure ridge formation. If there is a discontinuity where the layer thickness increases from h_1 to h_2, conservation of mass and momentum requires that

$$u/U = (h_2/h_1) - 1 .$$

For an increase from h_1 to h_2, an upper limit of h_2/h_1 can be estimated in various ways. From simple energy considerations the maximum value of h_2/h_1 is

$$\left(\frac{h_2}{h_1}\right)_{max} = \left(\frac{1+\sin\phi_1}{1-\sin\phi_1}\right)$$

where ϕ_1 is the friction angle for the original layer of thickness h_1. Different values ϕ_1 and ϕ_2 for the layer sections of thickness h_1 and h_2 can be accounted for by considering the thin section to develop a state of passive pressure, and the thick section a state of active pressure. Thus

$$\left[\left(\frac{1+\sin\phi_1}{1-\sin\phi_1}\right)\Big/\left(\frac{1+\sin\phi_2}{1-\sin\phi_2}\right)\right]^{1/2} \leq \frac{h_2}{h_1} \leq \left[\left(\frac{1+\sin\phi_1}{1-\sin\phi_1}\right)\left(\frac{1+\sin\phi_2}{1-\sin\phi_2}\right)\right]^{1/2} .$$

Another estimate can be made by applying the analogy of a retaining wall at both ends of the transition slope between the two sections of the ice layer (see Mellor 1980).

The foregoing ideas have been applied to the analysis of ship resistance in brash ice (Mellor 1980). While the assumption of a Coulomb-Navier-Mohr type of failure criterion seems reasonable for estimating stresses in the ice layer, forces against ship hulls and structures, and pressure ridge dimensions, it may not be appropriate for consideration of in-plane indentation. From comparison of the theoretical slip surfaces in front of an indenter (i.e. ship bow) with observed slip surfaces, it appears that a von Mises type of criterion might be a better assumption for problems of this type, in which the plane stress condition prohibits indefinite increase of shear strength with increase of confining pressure.

PRESSURE RIDGES AND LEADS

Pressure ridges and leads in sea ice are linear features representing compressive and tensile failures respectively. In the idealized forms, pressure ridges and leads are assumed to form in a band of uniform width, running at right angles to the direction of the major principal stress in the ice sheet.

The best known and most intricate model for pressure ridge formation is one by Parmerter and Coon (1972). An existing lead is assumed to close as compression develops, and ice rubble is assumed to disturb the isostatic

END

FILMED

DTIC
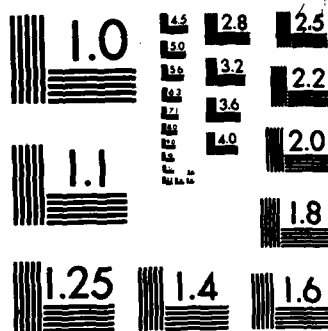
MICROCOPY RESOLUTION TEST CHART

NATIONAL BUREAU OF STANDARDS-1963-A

equilibrium of the ice sheet, leading to flexure and breakage. The ice fragments are pushed together and piled up, with horizontal thrust from the unbroken ice sheet supplying the potential energy for piling up the ice against gravity. Vertical dimensions of the ridge are limited by the available horizontal thrust, and ridge geometry is controlled partly by the angle of repose of the ice fragments. Development of a ridge is simulated by iterative calculations for the kinematics of the process.

The actual mechanical processes of pressure ridge formation are still not firmly established, and the following notes are intended to give an idea of the forces and stresses developed by some of the mechanical processes which might be involved in forming pressure ridges and leads. In general, they suggest that processes involving quasi-elastic deformation and quasi-brittle fracture call for horizontal thrust forces which are very high compared to the thrust likely to be developed by wind shear or current action.

Wind and current action

Sea ice is displaced and strained in the horizontal plane by wind shear on the upper surface or by water shear on the lower surface. In either case, the shear stress τ can be expressed as

$$\tau = C_D \rho u^2$$

where ρ is the fluid density, u is the "free stream" fluid velocity (relative to the ice), and C_D is a drag coefficient. For simple calculations, air density can be taken as 1.3 kg/m^3 and water density can be taken as

Figure 57. Surface shear stress as a function of fluid velocity for wind and water drag against sea ice.

88

1000 kg/m^3. A recent determination of C_D for water drag under first-year sea ice gives C_D = 1.32 x 10^{-3} (Langleben 1982), but for multiyear pack ice higher values have been measured, e.g. 2.2 x 10^{-3}, 4.14 x 10^{-3}, 6.6 x 10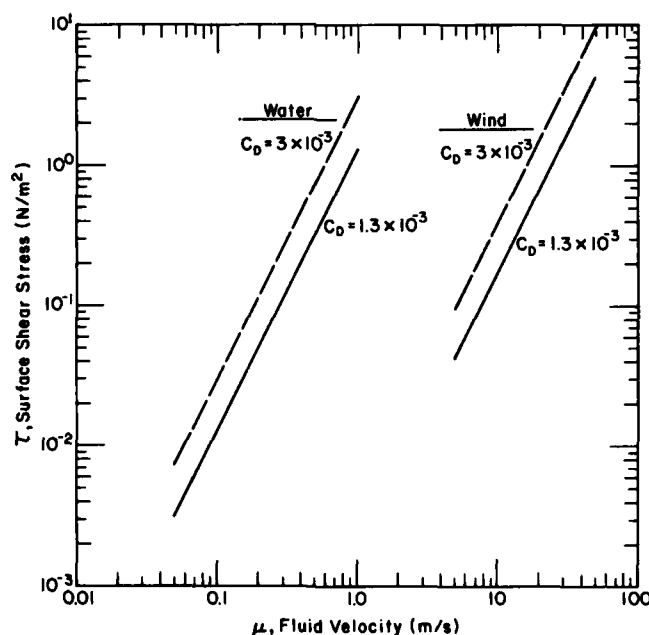$^{-3}$, 8.3 x 10^{-3} (see Langleben's paper for details). The value of C_D for air varies from 1.3 x 10^{-3} for strong winds over flat snowfields, to the range 1.6 x 10^{-3} - 3.2 x 10^{-3} for open sea ice, and perhaps to higher values for very rough pressured sea ice. For present purposes we can consider smooth first-year sea ice with C_D = 1.3 x 10^{-3} both on top and underneath, and calculate the shear stress as a function of fluid speed (Fig 57). For rougher ice, with C_D = 3 x 10^{-3}, values of τ are also shown in Figure 57. It might be noted that water shear and wind shear are of comparable magnitude for current velocities in the range 0.3 to 2 knots and wind speeds in the range 10 to 60 knots.

The shear stresses in Figure 57 are very low, so that they have to be integrated over large areas to produce significant forces. If F' is the force per unit width which is developed by integrating τ over an upstream distance L

$$F' = L\tau .$$

If τ = 1 N/m^2 is taken as a representative value for fairly fast currents (0.2 - 0.5 knot) or rather strong winds (40 - 45 knots), and it is then integrated over fetches of 10 km and 100 km, the resulting values of F' are:

L = 10 km	F' = 10 kN/m
L = 100 km	F' = 100 kN/m

Parmerter and Coon (1972) suggest that typical wind stresses on sea ice are of the order of 0.05 N/m^2. Such stresses lead to very small values of F', even with very large values of L, but they deduce that F' is only of order 1 kN/m during ridge formation (i.e. τ = 0.05 N/m^2, L = 20 km).

If the ice thickness t is of the order of 1 m, the average normal stress in the ice, F'/t, is very low, even with strong winds or strong currents acting over great distances. For example, a normal stress of 100 kN/m^2 (i.e. 1 bar) will cause ice to creep at a rate which is barely detectable over a period of days.

By contrast, if a fixed object of finite width projects through the ice sheet, or if a rigid body is embedded in the ice sheet, then wind and current shear is quite sufficient to produce very high local stresses.

Tensile and compressive failure of a wide ice sheet

When a wide sheet of ice is subject to simple unidirectional shear from wind or current, the ice is in a state of uniaxial strain in the horizontal plane, but the upper and lower surfaces of the ice are essentially free from normal stress or significant shear stress. In the ice, the mean normal stress in the direction of the wind or current, σ_{xx}, is

$$\sigma_{xx} = F'/t$$

where F' will rarely exceed 0.1 MN/m, and t is typically between 0.1 and 2 m in first-year ice. This suggests that, while σ_{xx} might reach 1 MPa in very thin ice, it is likely to be less than 0.1 MPa in ice of appreciable thickness.

The tensile fracture strength of unflawed ice is up to 2 MPa when measured in the laboratory, but large masses of natural ice without obvious cracks or gross flaws might have a tensile fracture strength closer to 1 MPa. The compressive strength of intact ice is up to 10 MPa when measured in the laboratory, but for bulk sea ice the compressive strength might be more like 3 MPa.

The fracture strength measured in tests of short duration is not necessarily of direct relevance to the formation of leads and pressure ridges, since the sea ice may be straining for days before it fails. Nevertheless, taking into account probable magnitudes of strain rate and failure strain, it is hard to imagine average failure stresses as low as 0.1 MPa, either for compression or tension.

If the ice sheet is in tension, the stress state is such that failure can be expected when the tensile principal stress reaches the uniaxial tensile strength ($\sigma_{xx} = \sigma_T$), assuming that the sheet is uncracked to start with. However, since σ_{xx} is only likely to approach 1 MPa in very thin ice, spontaneous tensile fracture must be a rare occurrence. Because there are always cracks of some kind in the ice, especially thermal cracks or cracks caused by wave flexure, it seems more likely that leads will form by the growth of existing cracks. Referring back to the calculated values of effective tensile strength σ_T as a function of flaw size 2c, and using the same values of Young's modulus and surface energy (p. 74-75),

$$\sigma_T = \frac{2.52 \times 10^4}{\sqrt{c}} = \text{Pa}$$

where c is in metres. Thus, if there are existing cracks only 2 m long at right angles to the principal stress, the effective value of σ_T for instantaneous tensile fracture is only 0.025 MPa.

If the ice sheet is in compression, the stress state is such that failure could occur when the major principal stress reaches the uniaxial compressive strength, taking due account of anisotropy in the ice (crushing occurs by displacement to the stress-free boundaries). However, it is unlikely that a wide ice sheet could undergo simultaneous crushing failure along a broad front, even in very thin ice, since the maximum compression values of σ_{xx} are expected to be well below σ_c.

Buckling of a wide ice sheet

For an ice sheet in compression, one possible mode of failure is crushing, as discussed above. Another possibility is buckling. From the usual analysis for an axially loaded infinite* elastic beam on an elastic

---

* The equation for the semiinfinite beam, used by some writers, gives half this value. The assumption of a semiinfinite beam seems to require that there be a hinge line where bending moments cannot be carried, and where there is no vertical force.

90

foundation (Hétenyi 1946), the critical force per unit width for buckling F' is

$$\frac{F'}{b} = \left[\frac{kEt^3}{3(1-\nu^2)}\right]^{1/2}$$

where k is the foundation modulus (in this case the unit weight of water), E is Young's modulus, ν is Poisson's ratio, and t is ice thickness. Sea ice is unlikely to buckle under truly elastic conditions, so that the value substituted for E should be less than the true Young's modulus. If we take $E = 3$ GPa, $\nu = 0.3$, and $k \approx 1$ Mgf/m^3 (or ≈ 10 kN/m^3)

$$F'_b = 3.3 \, t^{3/2} \text{ MN/m}$$

when t is in metres.

If $t = 1$ m, F'_b is 3.3 MN/m, i.e. well above any average value likely to be attained by F' under wind or water shear. If $t = 0.1$ m, F'_b is 0.1 MN/m, which is about the force level developed by strong wind or current acting over 100 km.

These estimates suggest that buckling by elastic instability across a broad front is unlikely to occur in any but the thinnest of ice covers, provided that the ice has uniform properties. However, an alternative analysis by Kerr (1980) introduces a new idea, and indicates that a semi-infinite plate of floating ice could buckle under a force smaller than F'_b as it is calculated from conventional theory. The magnitude of this effect cannot be assessed at present, as there is an undetermined coefficient in Kerr's result.

Another possibility is that the ice could buckle by creep, especially as the lower layers are likely to be warmer and softer than the top surface of the ice. If part of the ice sheet is depressed to the point where local flooding of the surface occurs, then there is no longer an elastic foundation in that area, and flexure is likely to accelerate.

Flexure of a wide ice sheet

Suppose that a state of compression develops, and that the ice sheet has a discontinuity, such as an old lead, at right angles to the thrust direction. If overthrusting can develop at the discontinuity, the ice will be flexed by the wedge action of the overthrust. An analysis for a semiinfinite elastic beam on an elastic foundation is given by Hétenyi (1946), and for the case which is of particular interest the bending moment M is

$$M = -\frac{P_1}{\lambda} B_{\lambda x}$$

where P_1 is the vertical force applied to the free end of the beam. The other symbols are defined by

$$\lambda = \left(\frac{k}{4EI}\right)^{1/4}$$

$$B_{\lambda x} = e^{-\lambda x} \sin \lambda x$$

where k is the foundation modulus, E is Young's modulus, and I is the moment of inertia of the beam section. Differentiation of M with respect to horizontal distance from the free end x gives

$$\frac{\partial M}{\partial x} = P_1 e^{-\lambda x}(\sin \lambda x - \cos \lambda x) .$$

M is a maximum or minimum with $\partial M/\partial x = 0$, i.e. when $x \to \infty$ or $x = \pi/2\lambda$. The required value of x for maximum bending moment in a wide plate is thus

$$x_* = \frac{\pi}{2}\left(\frac{4EI}{k}\right)^{1/4} = \frac{\pi}{2}\left[\frac{E t^3}{3k(1-\nu^2)}\right]^{1/4} .$$

This implies that, when the ice is flexed, it will tend to break first at a distance x_* from the free edge. Taking E = 3 GPa, k = 10 kN/m^3 and ν = 0.3, values of x_* are 5.1 m, 28.6 m, and 48.1 m for ice thicknesses of 0.1 m, 1.0 m and 2.0 m, respectively.

If there is no axial force being applied in the x-direction, the vertical force P_1 reaches a maximum value of

$$P_1 = -\frac{M_{max} \lambda}{B_{\lambda x_*}}$$

where the maximum "failure" value of the bending moment at distance x_* is

$$M_{max} = \frac{\sigma_{FT} I}{t/2}$$

in which σ_{FT} is the apparent tensile strength of the ice derived from beam flexure tests. Thus, the value of P_1 at failure is

$$P_1 = -\frac{2 \sigma_{FT} I}{t}\left(\frac{k}{4EI}\right)^{1/4}\frac{e^{\lambda x_*}}{\sin \lambda x_*} = -\frac{\sigma_{FT}}{6}\left[\frac{3kt^5}{E(1-\nu^2)^3}\right]^{1/4}\frac{e^{\pi/2}}{\sin \pi/2} .$$

From the discussion of beam flexure tests on ice, it can be seen that measured values of σ_{FT} vary widely, but for present purposes we assume σ_{FT} = 0.4 MPa. Taking E = 3 GPa, ν = 0.3, k = 10 kN/m^3,

$$P_1 = -0.706 t^{5/4} \quad \text{MN/m}$$

when t is in metres. For t = 1 m, $P_1 \approx 700$ kN/m. For t = 0.1 m, $P_1 \approx 40$ kN/m.

92

If P_1 is exerted by a wedge action as overthrusting occurs, the horizontal force F'_f that is needed to develop P_1 can be estimated in terms of an effective friction coefficient μ. For a small wedge angle,

$$F'_f \approx \mu\, P_1 \, .$$

Taking $\mu \approx 0.3$, F'_f is about 200 kN/m for 1-m-thick ice, but only about 12 kN/m for ice that is 0.1 m thick. Thus, if conditions are favorable for overthrusting, flexural breakage seems likely to occur at thrust forces lower than those needed for buckling according to standard theory.

The energetics of ridge formation

The energy needed to form a pressure ridge is assumed to be derived solely from the adjacent ice sheet, which thrusts with force F' per unit width in the x-direction. In order to build a ridge, potential energy has to be supplied to lift ice against gravity in the sail, and to push ice down against buoyancy in the keel. Energy is dissipated in the ice fracture process, and in overcoming frictional resistance between the ice fragments. For a lower limit estimate of the energy needed to build ridges, the energy dissipated in fracture and friction is neglected.

To illustrate the method, a pressure ridge can be idealized as shown in Figure 58, and the ridge and the formation process can be taken as symmetrical about the center line of the ridge, with horizontal displacements dx referred to that center line.

Work done by the ice sheet can be written as

$$dW = F' \, dx \, .$$

The mass per unit width M for half of the ridge is

$$M = M_s + M_k = \frac{1}{2}\,\bar{\rho}_s\, g\, h_s^2\, \cot \alpha_s + \frac{1}{2}\,\bar{\rho}_k\, h_k^2\, \cot \alpha_k$$
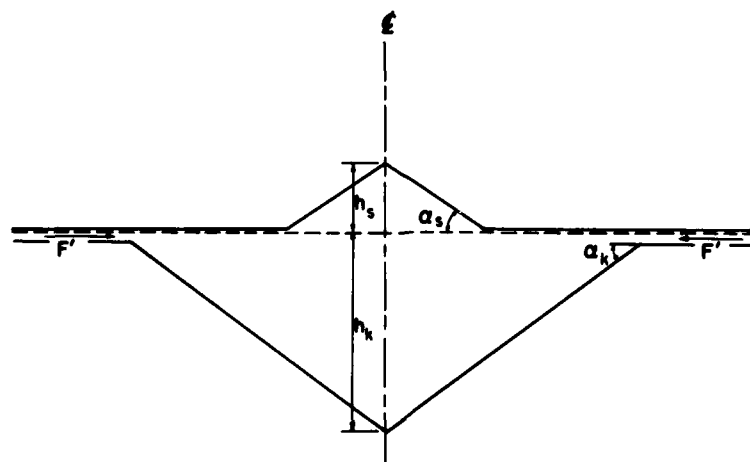

Figure 58. Idealized cross section of new pressure ridge.

93

where M_s and M_k are masses for sail and keel respectively, $\bar{\rho}_s$ and $\bar{\rho}_k$ are mean bulk densities, and α_s and α_k are the angles of repose for sail and keel.

The potential energy of the sail E_s is

$$E_s = M_s \, g \, h_s/3 \; = \; \frac{1}{6} \bar{\rho}_s \, g \, h_s^3 \, \cot \alpha_s$$

and the potential energy of the keel E_k is

$$E_k \; = \; M_k \, g_{eff} \, h_k/3$$

where g_{eff} is the effective value of g for submerged ice, i.e.

$$g_{eff} \; = \; \left(1 - \frac{\rho_w}{\rho_i}\right) g$$

in which ρ_i is the density of unbroken ice and ρ_w is water density. Thus,

$$E_k \; = \; M_k \left(\frac{\rho_w}{\rho_i} - 1\right) g \, \frac{h_k}{3}$$

$$= \; \frac{1}{6} \bar{\rho}_k \left(\frac{\rho_w}{\rho_i} - 1\right) g \, h_k^3 \, \cot \alpha_k \; .$$

The total potential energy of the ridge (E) is therefore

$$E \; = \; E_s + E_k \; = \; \frac{g}{6}\left[\bar{\rho}_s \, h_s^3 \, \cot\alpha_s + \bar{\rho}_k \left(\frac{\rho_w}{\rho_i} - 1\right) h_k^3 \, \cot\alpha_k \right] \; .$$

Equating work done by the ice sheet to energy gained by the ridge

$$dW/dx \; = \; dE/dx$$

or,

$$F' \; = \; dE/dx$$

$$= \; \frac{dE}{dh} \cdot \frac{dh}{dx} \; .$$

As the ice sheet of thickness t thrusts a distance dx, it contributes an increment of mass dM:

$$dM \; = \; \rho_i \, t \, dx$$

94

or,

$$\frac{dM}{dx} = \rho_i t \ .$$

Using this relation, dh/dx can be expressed as

$$\frac{dh}{dx} = \frac{dM}{dx} \cdot \frac{dh}{dM} \ .$$

In order to take the analysis further, additional assumptions have to be made. It is commonly assumed that the porosity of the ice rubble n is uniform, through both the sail and the keel. Thus

$$\overline{\rho}_s = \overline{\rho}_k = (1-n)\rho_i \ .$$

Some dubious assumptions have also been made about isostatic equilibrium. It has been assumed that the center of the ridge is in isostatic equili-brium, so that $h_s/h_k = (\rho_w/\rho_i)-1$. Taking $\rho_w = 1.026$ Mg/m^3, and $\rho_i = 0.9$ Mg/m^3 for sea ice fragments equilibrated with seawater, h_k/h_s would be about 7 according to this assumption. However, this is unrealistic, and it would be a bit closer to the mark to assume isostatic equilibrium for the complete sail against the complete keel, i.e.

$$h_s^2 \cot\alpha_s = h_k^2 \left(\frac{\rho_w}{\rho_i} - 1\right) \cot\alpha_k$$

or,

$$\frac{h_s}{h_k} = \left[\frac{\cot\alpha_k}{\cot\alpha_s} \left(\frac{\rho_w}{\rho_i} - 1\right)\right]^{1/2} \ .$$

If geometric similarity is somehow maintained during the ridge-building process, h_s/h_k is constant, i.e.

$$\frac{h_s}{h_k} = C \ .$$

Making these assumptions,

$$\frac{dM}{dh} = (1-n)\rho_i \, h_s \left(\cot\alpha_s + C^2 \cot\alpha_k\right)$$

$$\frac{dE}{dh} = \frac{(1-n)\rho_i g}{2} \, h_s^2 \left[\cot\alpha_s + \left(\frac{\rho_w}{\rho_i} - 1\right) C^3 \cot\alpha_k\right] \ .$$

95

Finally,

$$F' = \frac{dE}{dh} \cdot \frac{dh}{dx} = \frac{dE}{dh} \cdot \frac{dM}{dx} \cdot \frac{dh}{dM}$$

$$= \frac{\rho_i \, g \, t \, h_s}{2} \cdot \frac{\dfrac{\cot\alpha_s}{\cot\alpha_k} + \left(\dfrac{\rho_w}{\rho_i} - 1\right)C^3}{\dfrac{\cot\alpha_s}{\cot\alpha_k} + C^2} \quad .$$

To avoid algebraic nightmares, we can take numerical values for the dimensionless constants, e.g.

$$\left(\frac{\rho_w}{\rho_i} - 1\right) = 0.14 \; .$$

α_s or α_k might vary between about 20° and 33°, so that $\cot\alpha_s/\cot\alpha_k$ (or the inverse ratio) might be in the range 0.56 to 1.78. Corresponding values of C would then be in the range 0.5 to 0.28 (i.e. h_k/h_s in the range 2 to 3.6).

The expression for the thrust force F' can now be written

$$F' = \frac{A}{2} \, \rho_i \, g \, t \, h_s$$

where A might have values in the range 0.71 to 0.96 (A = 1 for a rubble field, for thickened brash ice, or for a "kite-shaped" pressure ridge).

For ice which is 1 m thick, this gives F' in the range 3.14 h_s kN/m to 4.22h_s kN/m when h_s is in metres. Taking realistic values of h_s, say 3 to 5 m, F' for t = 1 m is about 10 to 20 kN/m. This is the force level developed by a strong wind blowing over 10 to 20 km (see preceding notes on wind action). Parmerter and Coon (1972) considered that ridge-building forces were an order of magnitude lower than this, i.e. 1 kN/m.

Similar methods can be applied to brash ice using fewer assumptions. The limiting thickness of pressure ridges, including ridges formed against fixed structures and ship hulls, can be deduced by these methods, and by other methods derived from soil mechanics and plasticity theory (Mellor 1980). Some results were outlined in the foregoing section on mechanical properties of brash ice.

The mechanics of pressure ridge formation

Where floating ice thrusts against a fixed object of limited width, or where a rigid object is embedded in straining ice, wind or current forces can cause the ice to fail by flexure, buckling or crushing. However, the forces likely to be produced by moderate winds or currents seem insufficient to crush thick ice across a broad front, or to buckle it according to the generally accepted model. Flexural breaks seem more likely, provided

96

that local conditions favor the initiation of flexure. It is probably unrealistic to consider pressure ridge formation as a process of elastic deformation and brittle fracture. Sustained wind loads are likely to induce creep deformation and creep rupture, processes which can develop at stress levels well below those involved in elastic straining to failure. At present, the processes of pressure ridge formation are not well understood.

LITERATURE CITED

Abele, C. and G. Frankenstein (1967) Snow and ice properties as related to runways in Antarctica. USA Cold Regions Research and Engineering Laboratory, Technical Report 176, 37p.

Anderson, D.L. (1958) Preliminary results and review of sea ice elast⋅ ty and related studies. Transactions of the Engineering Institute ⸴ Canada, vol. 2, no. 3, p. 116-122.

Anderson, D.L. (1960) The physical constants of sea ice. Research, v⸴ 13, p. 310-318.

Babel, H.W. and G. Sines (1968) A triaxial fracture interior for porous brittle materials. Journal of Basic Engineering, Transactions of the ASME, June, p. 285-291.

Baker, R.W. (1978) The influence of ice crystal size on creep. Journal of Glaciology, vol. 21, no. 85, p. 485-500.

Brown, J.H. (1963) Elasticity and strength of sea ice. In Ice and Snow: Properties, Processes, and Applications (W.D. Kingery, Ed.), Cambridge, Mass.: MIT Press, p. 79-106.

Butkovich, T.R. (1954) Ultimate strength of ice. USA Snow, Ice and Permafrost Research Establishment, Research Report 11, 12p.

Butkovich, T.R. (1956) Strength studies of sea ice. USA Snow, Ice and Permafrost Research Establishment, Research Report 20, 15p.

Butkovich, T.R. (1959) On the mechanical properties of sea ice, Thule, Greenland, 1957. USA Snow, Ice and Permafrost Research Establishment, Research Report 54, 11p. and appendices.

Carter, D. (1970) Brittle fracture of snow ice. Proceedings, IAHR Symposium, Reyjavik, Iceland, 5.2.

Cox, G.F.N. and W.F. Weeks (in press) Equations for determining the gas and brine volumes in sea ice samples. USA Cold Regions Research and Engineering Laboratory, CRREL Report.

Cox, G.F.N., J. Richter, W.F. Weeks, M. Mellor and H. Bosworth (in press) The mechanical properties of multi-year sea ice, Phase I: Test results. U.S. Army Cold Regions Research and Engineering Laboratory, CRREL Report.

Currier, J.H. and E.M. Schulson (1982) The tensile strength of ice as a function of grain size, Acta Metallurgica, vol. 30, p. 1511-1514.

Durham, W.B., H.C. Heard and S.H. Kirby (1982) Deformation of ice at pressures to 350 MPa at 77 to 195 K. EOS, vol. 63, no. 45, p. 1094, T51B-01.

Duval, P. and H. LeGac (1980) Does the permanent creep-rate of polycrystalline ice increase with crystal size? Journal of Glaciology, vol. 25, no. 91, p. 151-157.

Dykins, J.E. (1970) Ice engineering-tensile properties of sea ice grown in a confined system. U.S. Naval Civil Engineering Laboratory, Technical Report R689.

Fletcher, N.H. (1970) The Chemical Physics of Ice. Cambridge University Press, 271 p.

Frederking, R. (1977) Plane-strain compressive strength of columnar-grained and granular-snow ice. Journal of Glaciology, vol. 18, no. 80, p. 505-516.

Frederking, R.M.W. and G.W. Timco (1980) NRC ice property measurements during the CANMAR KIGORIAK trials in the Beaufort Sea, Winter 1979-80. National Research Council of Canada, Division of Building Research, NRCC 18722, 63p.

Frederking, R.W. and G.W. Timco (1981) Mid-winter mechanical properties of ice in the southern Beaufort Sea. POAC, Quebec, Canada, Vol. 1, p. 225-234.

Gold, L.W. (1958) Some observations of the dependence of strain on stress for ice. Canadian Journal of Physics, vol. 36, no. 10, p. 1265-1275.

Gold, L.W. (1977) Engineering properties of fresh-water ice. Journal of Glaciology, vol. 19, no. 81, p. 197-212.

Goodman, D.J. (1979) Critical stress intensity (K_{IC}) measurements at high loading rates for polycrystalline ice. In Physics and Mechanics of Ice (P. Tryde, Ed.), Berlin: Springer-Verlag, p. 129-146.

Goodman, D.J. and D. Tabor (1978) Fracture toughness of ice: A preliminary account of some new experiments. Journal of Glaciology, vol. 21, p. 651-660.

Hamza, H. and D.B. Muggeridge (1979) Plain strain fracture toughness (K_{IC}) of fresh water ice. POAC 79, vol. 1, p. 697-707.

Häusler, F.V. (1981) Multiaxial compressive strength tests on saline ice with brush-type loading platens. Proceedings, International Symposium on Ice (Quebec), International Association for Hydraulic Research, Vol. II, p. 526-536.

Hawkes, I. and M. Mellor (1970) Uniaxial testing in rock mechanics laboratories. Engineering Geology, vol. 4, no. 3, p. 177-285.

Hawkes, I. and M. Mellor (1972) Deformation and fracture of ice under uniaxial stress. Journal of Glaciology, vol. 11, no. 61, p. 103-131.

100

Haynes, F.D. (1973) Tensile strength of ice under triaxial stresses. USA Cold Regions Research and Engineering Laboratory, Research Report 312.

Haynes, F.D. (1978) Effect of temperature on the strength of snow-ice. USA Cold Regions Research and Engineering Laboratory, CRREL Report 78-27, 18p.

Haynes, F.D. and M. Mellor (1977) Measuring the uniaxial compressive strength of ice. Journal of Glaciology, vol. 19, no. 81, p. 213-223.

Hétenyi, M. (1946) Beams on Elastic Foundation. University of Michigan Press, 255 p.

Hobbs, P.V. (1974) Ice Physics. Oxford: Clarendon Press, 837 p.

Jaeger, J.C. and N.G.W. Cook (1976) Fundamentals of Rock Mechanics. Chapman and Hall/John Wiley, 585 p.

Jones, S.J. (1978) Triaxial testing of polycrystalline ice. Third International Conference on Permafrost, Edmonton, p. 670-674.

Jones, S.J. and H.A.M. Chew (1981) On the grain size dependence of secondary creep. Journal of Glaciology, vol. 27, no. 97, p. 517-518.

Keinonen, A. and T. Nyman (1978) An experimental model-scale study of the compressible, frictional and cohesive behavior of broken ice mass. Part 2, IAHR Symposium on Ice Problems, Lulea, Sweden, p. 335-353.

Kerr, A.D. (1980) On the buckling force of floating ice plates. In Physics and Mechanics of Ice (P. Tryde, Ed.), Berlin: Springer-Verlag, p. 163-178.

Kohnen, H. (1972) Seismic and ultrasonic measurements on the sea ice of Eclipse Sound near Pond Inlet, N.W.T. in northern Baffin Island. Polarforschung, Jahrg. 44, Nr. 2, p. 66-74.

Kovacs, A., W.F. Weeks and F. Michitti (1969) Variation of some mechanical properties of polar snow, Camp Century, Greenland. USA Cold Regions Research and Engineering Laboratory, Research Report 276, 33 p.

Kovacs, A. and D.S. Sodhi (1980) Shore ice pile-up and ride-up: Field observations, models, theoretical analyses. Cold Regions Science and Technology, vol. 2, p. 209-288.

Lainey, L. and R. Tinawi (1981) Parametric studies of sea-ice beams under short and long term loading. International Symposium on Ice, IAHR, Quebec, Canada, p. 440-452.

Langleben, M.P. (1982) Water drag coefficient of first-year sea ice. Journal of Geophysical Research, vol. 87, no. 61. p. 573-578.

Langleben, M.P. and E.R. Pounder (1963) Elastic parameters of sea ice. In Ice and Snow; Properties, Processes and Applications, Cambridge, Mass.: MIT Press, p. 69-78.

Liu, H.W. and K.J. Miller (1979) Fracture toughness of fresh water ice. *Journal of Glaciology*, vol. 22, no. 68, p. 135-143.

Määttänen, M. (1976) On the flexural strength of brackish water ice by in-situ tests. In *Proceedings of the Third International Conference on Port and Ocean Engineering Under Arctic Conditions*, Fairbanks, Alaska, University of Alaska, 11-15 August 1975. Vol. 1. Fairbanks, Alaska, Institute of Marine Science, University of Alaska, p. 349-359.

Mellor, M. (1975) A review of basic snow mechanics. Symposium on Snow Mechanics, Grindelwald, International Commission on Snow and Ice, IAHR Publication no. 114, p. 251-291.

Mellor, M. (1979) Mechanical properties of polycrystalline ice. In *Physics and Mechanics of Ice* (P. Tryde, Ed), Berlin: Springer-Verlag, p. 217-245.

Mellor, M. (1980) Ship resistance in thick brash ice. *Cold Regions Science and Technology*, vol. 3, no. 4, p. 305-321.

Mellor, M. and R. Testa (1969) Effect of temperature on the creep of ice. *Journal of Glaciology*, vol. 8, no. 52, p. 131-145.

Mellor, M. and I. Hawkes (1971) Measurement of tensile strength by diametral compression of discs and annuli. *Engineering Geology*, vol. 5, p. 173-225.

Mellor, M. and D.M. Cole (1982) Deformation and failure of ice under constant stress or constant strain-rate. *Cold Regions Science and Technology*, vol. 5, no. 3, p. 201-219.

Mellor, M. and D.M. Cole (1983) Stress/strain/time relations for ice under uniaxial compression. *Cold Regions Science and Technology*, vol. 6, no. 3, p. 207.

Miller, K.J. (1979) The application of fracture mechanics to ice problems. In *Physics and Mechanics of Ice* (P. Tryde, Ed.), Berlin: Springer-Verlag, p. 265-277.

Murat, J.R. and L.M. Lainey (1982) Some experimental observations on the Poisson's ratio of sea ice. *Cold Regions Science and Technology*, vol. 6, no. 2, p. 105-113.

Murat, J-R. and R. Tinawi (1977) Sea ice testing in flexure. *Proceedings of POAC 77*, St. John's, Newfoundland, Vol. 2, p. 638-653.

Murrell, S.A.F. (1963) A criterion for brittle fracture of rocks and concrete under triaxial stress and the effect of pore pressure on the criterion. In *Rock Mechanics* (T. Fairhurst, Ed.), Proceedings, Fifth Symposium on Rock Mechanics, Pergamon Press, p. 563-577.

Nippon Kokan (NKK) (n.d.) Ice engineering, Part I. Study on ice force on offshore structure.

102

Nippon Kokan (NKK) (n.d.) Ice engineering. Printed technical document produced by NKK, Tokyo.

Paige, R.A. and C.W. Lee (1967) Preliminary studies on sea ice in McMurdo Sound, Antarctica, during "Deep Freeze 65." Journal of Glaciology, vol. 6, no. 46, p. 515-528.

Panov, V.V. and N.V. Fokeev (1977) Compression strength of sea ice specimens under complex loading. Problemy Arktiki i Antarktiki, vol. 49, p. 81-86 (English translation, p. 97-104).

Parmerter, R.R. and M.D. Coon (1972) Model of pressure ridge formation in sea ice. Journal of Geophysical Research, vol. 77, no. 33, p. 6565-6575.

Peyton, H.R. (1966) Sea ice strength. Geophysical Institute, University of Alaska, UAG R-182.

Prodanovic, A. (1979) Model tests of ice rubble strength. Proc. Fourth International Conference on Port and Ocean Engineering Under Arctic Conditions, Trondheim, Norway, Vol. I, p. 89-105.

Ralston, T.D. (1980) Yield and plastic deformation in ice crushing failure. In Sea Ice Processes and Models (R.S. Pritchard, Ed.), University of Washington Press, p. 234-245.

Saeki, H. and A. Ozaki (1981) Experimental study on flexural strength and elastic modulus of sea ice. POAC, Quebec, Canada, Vol. 1, p. 536-547.

Sandkvist, J. (1981) Conditions in brash ice covered channels with repeated passages. POAC, Quebec, Canada, Vol. 1, p. 244-252.

Schwarz, J. (1971) The pressure of floating ice-fields on piles. In International Association of Hydraulic Research Symposium: Ice and its Action on Hydraulic Structures, Reykjavik, Iceland, 8-10 September 1970. Delft, International Association of Hydraulic Research, paper 6.3.

Schwarz, J. (1975) On the flexural strength and elasticity of saline ice. In Proceedings, Third International Symposium on Ice Problems, 18-21 August 1975, Hanover, New Hampshire (G. Frankenstein, Ed.), International Association for Hydraulic Research, Committee on Ice Problems, p. 373-85.

Schwarz, J. and W.F. Weeks (1977) Engineering properties of sea ice. Journal of Glaciology, vol. 19, no. 81, p. 499-530.

Schwarz, J. et al. (1981) Standardized testing methods for measuring mechanical properties of ice. Cold Regions Science and Technology, vol. 4, no. 3, p. 245-253.

Schwerdtfeger, P. (1963) The thermal properties of sea ice. Journal of Glaciology, vol. 4, no. 36, p. 789-807.

Shapiro, L.H., R.C. Metzner and J.B. Johnson (1981) Fracture toughness of sea ice. Geophysical Institute, University of Alaska, for Shell Development Company.

Sinha, N.K. (1978a) Short-term rheology of polycrystalline ice. Journal of Glaciology, vol. 21, no. 85, p. 457-473.

Sinha, N.K. (1978b) Rheology of columnar-grained ice. Experimental Mechanics, vol. 18, no. 12, p. 464-470.

Sinha, N.K. (1981a) Rate sensitivity of compressive strength of columnar-grained ice. Experimental Mechanics, p. 209-218.

Sinha, N.K. (1981b) Constant stress rate deformation modulus of ice. POAC, Quebec, Canada, Vol. 1, p. 216-224.

Sinha, N.K. (1981c) Comparative study of ice strength data. International Symposium on Ice, IAHR, Quebec, Canada, p. 421-432.

Sinha, N.K. and R. Frederking (1979) Effect of test system stiffness on strength of ice. Proc. 5th International Conference on Port and Ocean Engineering Under Arctic Conditions, Trondheim, Norway, p. 708-717.

Tabata, T. (1958) Studies on the visco-elastic properties of sea ice. In Arctic Sea Ice, U.S. National Academy of Sciences, National Research Council, Publication 598, p. 139-147.

Tabata, T. (1960) Studies on mechanical properties of sea ice. V: Measurement of flexural strength. Low Temperature Science, ser. A, no. 19, p. 187-201.

Tabata, T. (1966) Studies of the mechanical properties of sea-ice. X: The flexural strength of small sea-ice beams. Institute of Low Temperature Science, Sapporo, Japan, Contribution 793.

Tabata, T. (1967) Studies of the mechanical properties of sea ice: The flexural strength of small sea ice beams. In Physics of Snow and Ice (H. Oura, Ed.), Institute of Low Temperature Science, Hokkaido University, p. 481-497.

Tabata, T., K. Fujino and M. Aota (1967) Studies of the mechanical properties of sea ice. XI: The flexural strength of sea ice in situ. In Physics of Snow and Ice (H. Oura, Ed.), International Conference on Low Temperature Science. Proceedings, Vol. I, Pt. 1. Sapporo, Institute of Low Temperature Science, Hokkaido University, p. 539-550.

Tabata, T., Y. Suzuki and M. Aota (1975) Ice study in the Gulf of Bothnia. II: Measurements of flexural strength. Low Temperature Science, ser. A., no. 33, p. 199-206.

Tabata, T., T. Kawamura and T. Takizawa (1976) Arctic sea ice research. I: Measurements of flexural strength of small sea ice beams. Low Temperature Science, ser. A, no. 34, p. 201-207.

Tinawi, R. and J.R. Murat (1978) Sea ice testing in flexure. Proceedings of the 4th International Conference, POAC, Memorial University of Newfoundland, p. 638-653.

Tratteberg, A., L.W. Gold and R. Frederking (1975) The strain rate and temperature dependence of Young's modulus of ice. International Symposium on Ice Problems, IAHR, Hanover, N.H., USA, p. 479-486.

Urabe, N., T. Iwasaki and A. Yoshitake (1980) Fracture toughness of sea ice. Cold Regions Science and Technology, vol. 3, no. 1, p. 29-37.

Urabe, N. and A. Yoshitake (1981a) Fracture toughness of sea ice: In-situ measurement and its application. POAC, Quebec, Canada, Vol. 1, p. 356-365.

Urabe, N. and A. Yoshitake (1981b) Strain rate dependent fracture toughness (K_{Ic}) of pure ice and sea ice. International Symposium on Ice, IAHR, Quebec, Canada, p. 410-420.

Vaudrey, K.D. (1977) Ice engineering: Study of related properties of floating sea-ice sheets and summary of elastic and viscoelastic analyses. U.S. Naval Civil Engineering Laboratory, Technical Report R860, 79p.

Wang, Y.S. (1979a) Crystallographic studies and strength tests of field ice in the Alaskan Beaufort Sea. Proceedings, POAC 79, Trondheim, Vol. 1, p. 651-665.

Wang, Y.S. (1979b) Sea ice properties. In Technical Seminar on Alaskan Beaufort Gravel Island Design, Exxon, U.S.A.

Wang, Y.S. (1981) Uniaxial compression testing of arctic sea ice. POAC, Quebec, Canada, Vol. 1, p. 346-355.

Weeks, W.F. and A. Assur (1967) The mechanical properties of sea ice. USA Cold Regions Research and Engineering Laboratory, Monograph II-C3.

Weeks, W.F. and A. Assur (1969) Fracture of lake and sea ice. USA Cold Regions Research and Engineering Laboratory, Research Report 269.

Weiss, R.T., A. Prodanovic and K.W. Wood (1981) Determination of the shear properties of ice rubble. International Symposium on Ice, IAHR, Quebec, Canada, p. 648-658.